Check for updates

Adsorptive removal of gaseous contaminants using biomass-based adsorbents

Kayode Adesina Adegoke, ID *ab Omolabake Abiodun Okon-Akan,†acd
Tosin Adewumi Adebusuyi, ID †e Oluwatobi Idowu Adewuyi,†f
Peter Oluwatosin Adu,†g Abayomi Bamisaye, ID †h Oyeladun Rhoda Adegoke,†a
Cecilia Opeyemi Babarinde†i and Olugbenga Solomon Bello*ab

Biomass-based adsorbents have emerged as attractive materials for the adsorptive removal of gaseous pollutants due to their abundance in nature, low cost, and environmental friendliness. The modification of the adsorbent surfaces has been regarded as an intriguing technique for improving and enhancing their adsorption capacity for efficient removal of pollutants. The present study investigates the most recent developments and applications of biomass-derived adsorbents for removing various gaseous contaminants from air and gas streams. The use of biomass materials such as agricultural waste and wood residue to synthesize adsorbents provides a long-term solution to environmental pollution. This is due to the fact that biomass-derived adsorbents can be designed to have a large surface area, porosity, and surface functionality, thereby increasing their adsorption capacity and selectivity for target pollutants using a variety of chemical processes such as carbonization, activation, and modification. This study presents a comprehensive report on the use of biomass-based adsorbents for the removal of various gaseous pollutants such as carbon dioxide (CO_2), volatile organic compounds (VOCs), nitrogen oxides (NO_x), sulfur dioxide (SO_2), hydrogen sulphide (H_2S) and multi-gas components. The surface chemistry of biomass adsorbents, in addition to their porous nature, is discussed. Multi-gas adsorption properties and the regeneration of biomass adsorbent are also discussed. The challenges and future prospects for developing biomass-based adsorbents for gaseous pollutant removal are also discussed, emphasizing the importance of a thorough understanding of adsorption mechanisms, scalability of manufacturing processes, and integration with existing air purification technologies. The findings of this study present biomass-derived adsorbents as a promising alternative for mitigating the challenges associated with the danger of gaseous pollutants, contributing to sustainable environmental management and public health protection.

aDepartment of Pure and Applied Chemistry, Ladoke Akintola University, P. M. B. 4000, Ogbomoso, Nigeria. E-mail: kwharyourday@gmail.com; osbello@lautech.edu.ng

bLAUTECH SDG 11 Sustainable Cities and Communities Research Group, Nigeria

cWood and Paper Technology Department, Federal College of Forestry Jericho, Ibadan, Nigeria

dForestry Research Institute of Nigeria, Nigeria

eDepartment of Chemical Sciences, Augustine University, Ilara-Epe, Lagos State, Nigeria

fDepartment of Agricultural and Environmental Engineering, University of Ibadan, Ibadan 200255, Nigeria

gDepartment of Chemistry, Obafemi Awolowo University, Ile-Ife, Osun State, Nigeria

hDepartment of Chemistry, Faculty of Natural and Applied Sciences, Lead City University, Ibadan, Oyo State, Nigeria

iDepartment of Biochemistry and Forensic Science, Abiola Ajumobi Technical University, Ibadan, Nigeria

† Shared the second authorship.

1. Introduction

Over the past few years, there has been a significant rise in public concern about air quality and environmental degradation. The combustion of fossil fuels and rising greenhouse gas emissions, particularly carbon dioxide (CO_2), have driven global warming. Human activities have increased CO_2 levels from 280 ppm to >400 ppm, primarily through electricity generation, transportation, and industrialization.[1–8] This increase in anthropogenic atmospheric pollutants is a significant challenge for humanity in the 21st century. The utilization of fossil fuels for diverse activities deteriorates urban air quality at an accelerated pace. Gaseous pollution damages both the physical and emotional health of metropolitan people. Studies reveal that by 2025, environmental contamination will generate irreversible environmental damage.[9,10] Air pollution, which is the marker of economic progress, is not a recent problem and is produced by

the existence of a diverse collection of gaseous and particulate components in the atmosphere.

Statistics on mortality attributable to air pollution originated in London in the 18th, 19th, and early 20th centuries. Since the 1990s, epidemiological research has shown the human health issues linked to air pollution, based on total hospital admissions and death data.[11–15] The World Health Organization (WHO) claimed that in 2012, one in nine fatalities was attributable to disorders related to air pollution.[16] According to the 2012 Census in India, the urban population of emerging nations rose from 1.5 million to 17 million. Concurrently, there has been an exponential increase of motorized vehicles throughout both the private and public sectors. Consequently, the proportion of gaseous pollutants in the air from traffic emissions significantly escalated. Furthermore, the utilization of coal, diesel, and similar fuels for *in situ* electrical production by diverse sectors contributes to the elevated concentration of atmospheric pollutants.[17] The principal gaseous pollutants comprise carbon monoxide (CO; kinetic diameter (K.D.) = 0.376 nm), nitrogen oxides (NO with K.D. = 0.320 nm and N_2O having a K.D. of 0.330 nm), sulfur dioxide (SO_2; K.D. = 0.360 nm), ozone (K.D. = 0.58 nm), and volatile organic compounds (VOCs) such as benzene (K.D. = 0.360 nm), ethylbenzene (K.D. = 0.6 nm), formaldehyde (K.D. = 0.4 nm), methyl ethyl ketone (K.D. = 0.52 nm), toluene (K.D. = 0.59 nm), and xylene (K.D. = 0.73 nm), among others. CO_2 is a greenhouse gas contributing to global warming and climate change. Exposure to these contaminants can negatively impact both people and other organisms.

The prevalent symptoms of gaseous pollutants encompass persistent headache, dizziness, cognitive impairment, fatigue, muscular spasms, irritation of the eyes, throat, and nasal passages, as well as discomfort in the joints, bones, and spinal column. However, exposure to gases such as carbon monoxide can result in severe symptoms, including disorientation, long-term neurological impairments, unconsciousness, cardiorespiratory failure, coma, and death.

Consequently, there has been substantial interest in the pursuit of scientific investigations on cutting-edge and eco-friendly technologies capable of eliminating gaseous and particulate matter pollutants.[18–21] Specialized materials with the inherent ability to selectively attract, collect, and retain gaseous and particulate matter pollutants under different design conditions are known as adsorbents. Adsorbent materials attract impurities onto their surfaces *via* chemical or physical interactions.[22–25] Adsorbent materials are used in various industries and applications for nano-purification purposes because of their capacity to adsorb molecules or particles onto their surfaces.[26–28]

Research into the discovery of efficient and sustainable adsorbents remains essential, and remarkable efforts in experiments using different materials for the adsorptive removal of contaminants have been reported in the literature.[29–34] Consequently, various adsorbents with unique characteristics and suitability for different pollutants have been experimented with and deployed to remove gaseous and particulate contaminants from air samples. Carbon-based materials are widely utilized adsorbents renowned for their porous structure and vast surface area, effectively capturing a diverse range of gaseous and particulate pollutants.[35,36] Activated carbon is widely used to remove contaminants and pollutants in multiple applications, including water treatment.[37] Also, activated carbon has been used in air purification, CO_2 capture, separation of gases, and removal of other gaseous contaminants from the atmosphere by pressure and temperature swing adsorption techniques.[38–41]

The previous reviews in this field are all incredibly beneficial for comprehending the benefits of biomass in adsorbing common gaseous and organic/inorganic substances that might potentially pose atmospheric risks. Nevertheless, these reviews are insufficient in explaining the precise mechanisms by which biomass functions as an efficient adsorbent for removing gaseous pollutants using adsorption technology. Unlike other reviews, which often include sorption from aqueous media, this review solely examines the adsorptive removal of gaseous pollutants onto biomass-based adsorbents of agricultural waste origin. This distinction is important to prevent confusion in describing the sorption of inorganic or other organic pollutants (*e.g.* dyes, pharmaceuticals, endocrine descriptor compounds, *etc.*). In this review, we carefully considered the choice of biomass, the derivative sources of porous carbon, and the surface chemistry of biomass-based adsorbents prior to evaluating the performance of biomass-based sorbents for different categories of gaseous pollutants, namely, CO_2, SO_2, H_2S, NO_x, volatile organic compounds (VOCs) and multi-gas components. The corresponding mechanism of adsorption is also discussed in each case. The present review, therefore, advances the technology and theory of gaseous adsorption onto biomass waste, which is not only green but sustainable. In addition, this review seeks to give comprehensive knowledge of the relationship between the biomass properties, adsorptive removal conditions, and the corresponding performance of various biomass-based adsorbents towards different types of gaseous pollutants. Regeneration studies of the spent biomass adsorbents are also discussed, which are essential for a successful adsorption–desorption process. Lastly, the knowledge gaps to foster the development of biomass-based sorbents and their applications for real-world implementation for gaseous pollutants removal are discussed.

2. Why biomass?

In the face of rising environmental challenges such as poor waste management, researchers are devising a multidisciplinary approach that leverages the circular economy concept toward identifying specific byproducts/waste materials with applicable adsorbent properties.[42,43] This innovative strategy addresses the increasing demand for effective pollution control while underscoring the importance of sustainable and environmentally friendly solutions, particularly by exploring biomass-derived materials as a basis for these adsorbents. In this regard, agricultural waste products such as rice husks and coconut shells have gained attention as sustainable biomass-derived adsorbents.[44–46] These biomass-based adsorbents

exhibit favourable adsorption characteristics and contribute to the utilization of agricultural byproducts and waste reduction. Thus, biomass-based adsorbents have emerged as a viable option because of their unique eco-friendliness, renewability, and outstanding adsorption characteristics.[47] Thus, investigating biomass-based adsorbents for the adsorptive removal of contaminants is a critical step toward developing environmentally sensitive technologies that solve the multiple issues linked with environmental pollution control and agricultural waste handling.

According to the waste data provided by the European Commission,[48] activities within the coal industry (including mining and energy activities), agricultural industry, water treatment, and home sector are responsible for producing and accumulating significant quantities of solid waste. In 2008, the EU-27 produced a total of 2.62 billion tonnes of waste. The construction sector contributed 32.9% of the total waste, the mining industry contributed 27.8%, the manufacturing industry contributed 13.1%, waste and water management contributed 7.3%, households contributed 8.5%, agriculture and forestry contributed 1.7%, and the energy sector contributed 3.5%. Current waste management techniques, namely the use of landfills, contribute to climate change and have the potential to contaminate water and soil, as well as cause local air pollution. To address the escalating environmental issues caused by the growing volume of waste being disposed of in landfills, numerous research initiatives are concentrating on creating novel waste management approaches. These efforts involve producing valuable products derived from readily available waste materials.[48]

According to the United Nations Environment Programme, the agricultural sector produces a total of 140 billion metric tons of biomass annually on a worldwide scale.[48] Prior studies have documented the use of biomass waste, namely agricultural leftovers, in the production of carbonaceous adsorbents.[49] Numerous studies have demonstrated the use of lignocellulosic materials such as soybean, bagasse, olive stones, shells, almond shells, rice husk, and coconut as precursors for carbon-based sorbents in the adsorption of various gaseous pollutants at low-medium temperatures.[50–55] For example, various byproducts derived from biomass, such as rice husk ash, have been utilized for manufacturing solid adsorbents for CO_2 capture at low temperatures.[56] A typical example is the annual global output of rice husk ash which is now around 20 million tons, accounting for approximately 20% of the total dry rice husk.[57]

3. Biomass-derived porous carbons

The process of converting biomass into porous carbons requires the use of carbonization (pyrolysis) and activation, which can be achieved by physical and/or chemical means. Physical activation is a two-step procedure. First, the raw material is heated to temperatures ranging from 400 to 850 °C in the absence of oxygen, causing it to undergo carbonization. Then, the resulting char is subjected to activation by exposing it to gases such as steam, air, nitrogen, oxygen, ammonia, carbon dioxide, or

a combination of these gases. This activation process occurs at temperatures around 600 to 1000 °C.[58,59] The utilization of CO_2 in the activation process results in the formation of porous carbons with a narrow distribution of micropores, which is ideal for achieving optimal pore size for separating CO_2 and CH_4. The steam activation produces carbons with a wider range of pore sizes and a smaller volume of micropores.[58] However, there is a less precise regulation of the porosity in the physical activation process. The reactions that occur during physical activation can form oxygen functional groups on the surface. On the other hand, activation with NH_3 introduces nitrogen-containing groups onto the carbon surface. This process is, however, typically combined with another gas to increase the porosity of the material.[60] The elevated temperatures often employed in physical activation pose an energy disadvantage.

Chemical activation can be performed in either one step or two steps. This involves impregnating the biomass or the resultant char from the initial carbonization stage with activating chemicals such as dehydrating agents and/or oxidants. Following impregnation, the combination of precursor and activation agent is subjected to elevated temperatures ranging from 400 to 800 °C under an inert environment.[58,59] Chemical activation, like physical activation, leads to the formation of porosity and functional groups on the surface of carbon. Chemical activations of biomass precursors often involve the use of acids, alkalis, and salts such as H_3PO_4, H_2SO_4, $ZnCl_2$, K_2CO_3, NaOH, and KOH.[59,61] Chemical activation is commonly used to create biomass-derived porous carbons with large surface areas and precise control over the porosity. However, the process becomes time-consuming and energy-intensive when the produced carbon needs to be washed to remove the residual activating agent in the carbon matrix. Additionally, this washing process is not environmentally friendly.

4. Surface chemistry of biomass-based adsorbents

The surface chemistry of biomass-based adsorbents is influenced by the presence of heteroatoms, such as oxygen, hydrogen, nitrogen, and sulfur, on its surface. These components can be supplied by the precursor, added during activation, or delivered by posttreatment. The presence of these heteroatoms on the surface of the carbon materials determines whether it is neutral, acidic, or basic and greatly affects its ability to adsorb substances. Fig. 1 provides an overview of the many surface functional complexes on the carbon surfaces, determining their basic or acidic properties.

Carboxylic acids, phenols, lactones, anhydrides, and lactols possess acidic properties, but ether and carbonyl groups are considered neutral. Quinone, pyrone, nitrogen, and chromene groups exhibit fundamental functions.[63,64] Different techniques are utilized to alter the surface chemistry of AC and generate acid or basic sites. These post-treatments impact both the characteristics and the amount of the surface functional groups. In general, oxidation processes are used to impart an
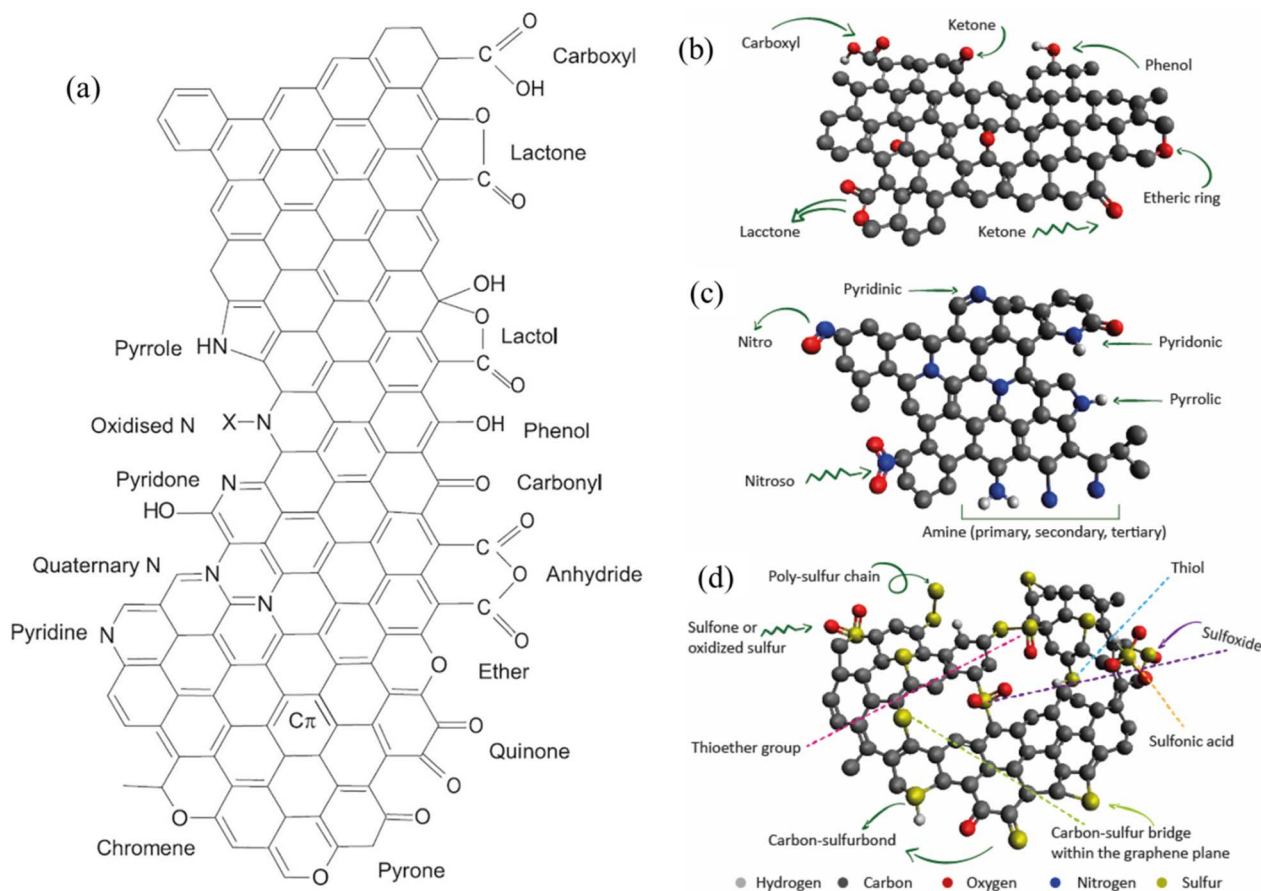
Fig. 1 (a) Nitrogen and oxygen surface functional groups on carbons.[62] Different surface functional groups on the surface biomass: (b) oxygenated functional groups (c) nitrogen functional groups (d) sulfur functional groups.

acidic nature to activated carbon.[65] Particularly, oxygen surface groups are introduced onto carbon materials by reactions conducted either in the gas phase (using reagents like oxygen or ozone) or in the liquid phase (utilizing nitric acid or hydrogen peroxide). Typically, the oxidation of carbon in a liquid phase is employed under mild reaction conditions (low temperature and short reaction time) to generate surface oxygen functionalities, such as carboxylic groups, without causing major changes to the textural qualities.[66]

In contrast, gas phase oxidation necessitates elevated temperatures and extended reaction durations resulting in a comparatively limited production of hydroxyl and carbonyl groups. This method is employed when there is a need to alter the porosity structure.[67,68]

The fundamental nature of activated carbon is determined by two types of structures: (i) the existence of basic surface functionalities such as chromene, pyrone, ketone, and basic amines. (ii) Oxygen-free Lewis basic sites on graphitic layers. The first method involves subjecting the material to high-temperature heat treatment in the presence of inert gases such as H_2, He, and N_2. This process selectively removes the acidic surface groups. The second technique involves nitrogenation, which refers to the addition of nitrogen to the surface of the activated carbon. This type of treatment can enhance the

basicity of the activated carbon by promoting the development of amine bases. Elevated temperatures and prolonged treatments cause the conversion of nitrogen groups from amide and amine to imide and imine and ultimately to pyridine and nitrile.[69–71]

5. Biomass-based adsorbent for CO_2 removal

In recent times, the worldwide issue of global warming which is caused by the release of greenhouse gases, has generated significant alarm and apprehension.[72–74] The CO_2 capture and sequestration is a very efficient method for extracting and storing CO_2.[75–77] The utilization of solid materials as an adsorbent offers a more environmentally friendly and economically efficient alternative to the traditional CO_2 capture technique which involves aqueous amine adsorption methods. This is mostly owing to the energy-intensive regeneration phase included in the current method.[78] Various adsorbents have been employed for the purpose of CO_2 adsorption. These include porous carbons,[79–82] carbon nanotubes,[83,84] zeolitic imidazole frameworks (ZIFs),[85] metal–organic frameworks (MOFs),[86,87] zeolites,[88,89] and mesoporous silica.[90] Porous carbon is considered a very promising material for adsorbing CO_2 due to its

Table 1 Biomass-derived adsorbents for CO_2 removal

Adsorbents	Initial conditions	Isotherm models	Kinetic models	q_{max} (mg g^{-1})	Adsorption mechanism	Findings	Ref.
Microporous carbons obtained from hydrothermally treated biomass waste tobacco stem by KOH activation with analogous textural properties and oxygen functional groups	0.5 g of pretreated sample/hydrochar and 1.0 g of KOH dissolved in 50 mL water. Initial PH: 7. Temperature: 500–800 °C at 3 °C min^{-1} for 1 h	BET (Brunauer–Emmett–Teller)	Non-local density functional theory	8.0 mmol g^{-1} (at 0 °C, 1 bar); 4.8 mmol g^{-1} (at 25 °C, 1 bar)	Electrostatic interactions; Physical sorption, intraparticle diffusion	Oxygen-containing functional groups on porous carbons are critically sensitive to CO_2 uptake, especially with carboxyl and hydroxyl groups	137
Nitrogen-doped porous carbons are obtained from biomass lotus stalks	Powdery lotus stalks with sizes of 74–150 nm blended with melamine; the mixture pyrolysis at 500 °C for 2 h to yield sample/LSM KOH/LSM mass ratio of 1, 2, and 3 at 500, 550, and 600 °C, respectively	BET (Brunauer–Emmett–Teller) at 25 °C; D-R (Dubinin–Radushkevich) at 0 °C		4.25 mmol g^{-1} (at 25 °C, 1 bar); 6.59 mmol g^{-1} (at 0 °C, 1 bar)	Physical sorption, intraparticle diffusion	The narrow microporosity of the N-doped carbonaceous adsorbent influences the CO_2 adsorption positively. Specific features of the Lotus stalk-derived adsorbents are high CO_2/N_2 selectivity, recyclability, adequate heat of adsorption, quick kinetics, excellent stability, and good dynamic adsorption capacity, which make them suitable for supercapacitor electrodes	154
Activated carbon from corn cobs (CC), date seeds (DS), peanut shells (PS), pomegranate peels (PP), and rice husk (RH), in powder form – with KOH and H_3PO_4 activating agents	150 g CC + 85% KOH at 800 °C and 35 min, 100 g DS + 85% H_3PO_4 at 800 °C and 45 min, 200 g PS + 85% KOH at 680 °C and 30 min, 300 g PP + 85% KOH at 700 °C and 35 min, 250 g RH + 90% H_3PO_4 at 800 °C and 45 min						

affordability, lightweight, extensive surface area, strong chemical and thermal stability, and rapid adsorption kinetics.[91,92]

Recently, biomass-derived carbon has gained attention as a cost-effective and ecologically benign substitute for synthetic adsorbents.[93,94] These carbon compounds may be synthesized from abundant sources such as foods, animals, and agricultural wastes.[95] Several studies have shown a significant focus on biomass-derived porous carbons for capturing CO_2 in order to mitigate global warming (Table 1). This attention is primarily due to their well-developed textural properties, relatively easy synthesis methods, and outstanding ability to adsorb CO_2.[96–100] When compared to other earliest substances, biomass has various advantageous qualities for creating CO_2 adsorbents, including pores, inexpensive nature, sustainability, renewable, and readily available.[101] Additionally, the utilization of biomass-derived porous carbon for capturing CO_2 is advantageous in addressing climate change and environmental pollution resulting from insufficient biomass management concurrently. Due to its carbon-neutral properties, biomass-derived porous carbon may be used to trap CO_2 and help emission-intensive companies and sectors reduce their carbon footprint. Additionally, it can contribute to negative emissions technologies for mitigating climate change.[102]

Although the initial CO_2 adsorption capacity of pyrolyzed biomass is rather poor (<0.5 mmol g^{-1} at 298 K and 1 bar), several changes are recognized to improve its capacity and selectivity, specifically for CO_2.[95] For example, the addition of basic groups or heteroatoms, such as nitrogen, increases the alkalinity and ability of carbon to adsorb CO_2.[103] Nitrogen doping is mostly accomplished by subjecting carbon to a nitrogen-rich component or gas with basic properties, which results in the introduction of nitrogen atoms onto the surface of the carbon.[104] Additionally, biomass precursors that are rich in nitrogen provide an easy and consistent approach for introducing nitrogen heteroatoms.

Furthermore, augmenting the microporosity of carbon using several physical and chemical activation methods proves to be a successful approach in expanding its ability to adsorb CO_2. Specifically, micropores with a diameter of less than 1 nm are extremely efficient in enhancing the CO_2 capacity. This is because they are similar in size to the kinetic diameter of CO_2 and may interact with it through overlapping adsorption forces and potential fields generated by nearby pore walls.[105] Previous studies have employed a post-synthesis activation method to enhance the microporosity of carbon derived from biomass. This process entailed using CO_2 or steam as activating agents at temperatures ranging from 500 to 900 °C to increase the development of micropores and enhance the ability of CO_2 to be adsorbed.[94] Nevertheless, the processes of carbon synthesis and activation are time-consuming and energy-intensive due to their two-step nature. Furthermore, the ultimate porosity can be influenced by factors such as temperature, flow rate, and the type of synthesis equipment used. Thus, a more streamlined and effective method is necessary.[96] The process of transforming biomass to porous carbon materials for CO_2 capture commonly involves carbonization (pyrolysis, gasification, and hydrothermal),[106–112] activation (physical and chemical)[113–124] and surface modification (N, S, Mg, etc.)[125–135] as illustrated in Fig. 2.
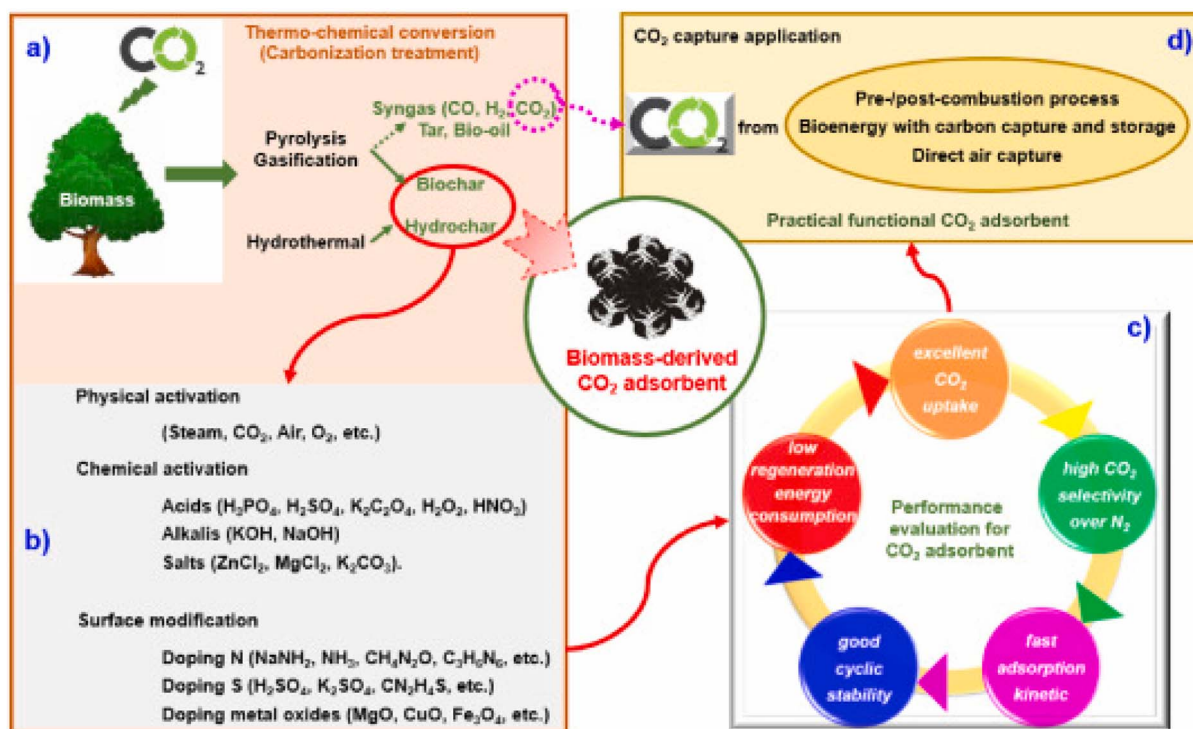

Fig. 2 (a–d) Schematic diagram of practical functional biomass-derived porous carbon for CO_2 capture.

The majority of activated carbon has a CO_2 uptake that is less than 3–4 mmol g^{-1} at 25 °C and 1 bar pressure.[136,137] The biomass-derived porous carbon composites nevertheless have a value higher than 4 mmol g^{-1} at 25 °C and 1 bar, as reported in the literature.[136,138,139] Particularly, several studies have proposed that a limited micropore volume in porous carbons improves their ability to adsorb CO_2. For example, the biomass-derived porous carbon produced by Coromina et al.[118] demonstrated outstanding CO_2 adsorption capacity of 5.0 mmol g^{-1} at a pressure of 1 bar and a temperature of 25 °C. In their study, Haffner-Staton et al.[139] reported that pre-carbonized wood, which was used to produce microporous carbon via KOH activation, gave a maximum CO_2 capture of 5.0 mmol g^{-1} under 1 bar at 25 °C. Similarly, Sevilla et al.[138] produced an effective microporous surface area of activated carbon by using KOH activation on biomass via hydrothermal method. This activated carbon had a CO_2 adsorption capacity of 4.8 mmol g^{-1} at 25 °C under 1 bar of pressure. Nevertheless, these investigations just ascribed the exceptional absorption of CO_2 by porous carbon to the presence of many small micropores that were less than 0.7 nm. However, the information about the impact of oxygen-containing functional groups on biomass-based porous carbons has been rarely reported.

Parshetti investigated carbon-based adsorbents with microporous architecture and high specific surface area (up to 2511 m^2 g^{-1}), which were produced from lignocellulosic feedstock using hydrothermal carbonization and chemical activation enabling CO_2 adsorption.[81] These adsorbents underwent extensive microscopic and spectroscopic investigations to determine their morphological, textural, and structural properties. Microporous carbons have a remarkable CO_2 absorption capacity of 3.71 mmol g^{-1} at 25 °C and 1 atm pressure. These materials exhibit high selectivity for CO_2 over NO gas and a hydrophobic core, making them ideal for CO_2 capture. The Freundlich equilibrium model correlated well with the experimental adsorption isotherm data, while the traditional micropore diffusion model well characterized the adsorption kinetics. The Virial model was used to compute Henry's law constant and indicated substantial electrostatic interactions and dispersion forces between CO_2 and porous carbons. These carbon-based adsorbents maintained their adsorption capacity for up to 10 reuse cycles for CO_2 capture. The study found that microporous adsorbents are a cost-effective and environmentally friendly method for trapping CO_2 from post-fossil fuel combustion processes.

Singh et al. found that the most effective adsorbent materials for CO_2 adsorption have outstanding textural features, tunable porosity, and low cost.[140] These materials are efficient adsorbents for CO_2 capture due to their shape and physicochemical features, which are created through various activation procedures, including solid-state activation. Another group provided a full overview of the pyrolysis mechanisms for cellulose, hemicellulose, and lignin.[141]

Sher et al. investigated the comparative screening of three groups of biomasses: soft or non-woody (peanut shell), intermediate woody (walnut shell), and hard woody (pine wood) for the development of adsorbents/activated carbons for post-

combustion CO_2 capture (over N_2 balance).[142] Three different groups of biomass residues are selected to study the role and nature of the material in adsorption and selection of the raw material for CO_2 adsorbent synthesis for future research, because of the hot issue of anthropogenic CO_2 emissions. The adsorption isotherms studied by the thermal gravimetric analyzer (TGA) revealed that CO_2 adsorption capabilities are in the range of 2.53–3.92 mmol g^{-1} (over N_2 balance) at 25 °C. The newly synthesized activated carbons (ACs) exhibited a fast adsorption rate at 41–94% in the initial 2 min. Porous surface development with catalytic KOH activation is seen clearly through SEM surface morphological analyses and mathematically confirmed from SBET ranges from 146.86 to 944.05 m^2 g^{-1}. FTIR and XRD peaks verify the generation of basic or inorganic O_2-rich moieties that help in acidic CO_2 capture. It has also been observed from adsorption isotherms that the order of higher adsorption groups is; peanut shell > pine wood > walnut shell, while the best activation mass ratio (sample/KOH) is 1 : 3. The synthesized low-cost ACs with an amount of 1.93 US\$ per kg production could help to overcome the environmental hazards and problems caused by CO_2 and biomass waste.

According to Bade et al.,[143] large-scale applications of activated carbon from a single substrate of agricultural waste have been found inefficient in the adsorption of CO_2. Thus, a composite activated carbon (CAC) was prepared using the chemical activation properties of four different agricultural waste substrates. The developed CAC exhibited the highest CO_2 removal efficiency compared to other activated carbon-based single substrate-derived adsorbents at a capacity of 8.86 wt%. The study conducted by Lui et al.[125] showed that beyond the inherent potential of biomass-based porous carbon materials for efficient CO_2 adsorption due to the abundance of narrow pores of less than 0.7 nm, the oxygen-containing functional groups on the porous carbons are established to be critically crucial for CO_2 uptake. Based on the density functional theory, the proliferation of oxygen-functional groups within the porous carbon material firmly grasps CO_2 through electrostatic interactions. The study reported by Valdebenito et al.[144] considered modifying a cellulose nanofibril (CNF) film to produce CO_2-adsorbent materials. The produced absorbent materials were assessed and found to be thermally stable with remarkable CO_2 adsorption when subjected to 99.9% CO_2 flow at 25 °C.

In the study reported by Yuan et al.,[101] a machine-learning approach was deployed to systematically map out gathered datasets on the CO_2 adsorption properties of biomass waste-derived porous carbon adsorbent materials as a function of the textural and compositional properties, as well as the adsorption parameters. From the results, the machine learning model revealed the significance of the adsorption parameter, textural properties, and compositional properties (in that order of superiority) for the considered biomass waste-derived porous carbon-based CO_2 adsorption materials. The study conducted by Khosrowshahi et al.[145] investigated the effects of external adsorption parameters such as time, temperature, and pressure on CO_2 adsorption properties of carbonaceous wastes from celery biomass. The effects of the presence of carboxyl, hydroxyl, and nitrogenous functional groups on CO_2 adsorption were

studied using molecular dynamics. It was observed that pyridinic nitrogen absorbs more CO_2 than graphitic nitrogen, and the study also revealed that increasing the simulation increases the optimality of the CO_2 adsorption rates.

The research by Hanif et al.[93] studied the use of nitrogen-rich *Albizia procera* leaves as the substrate for activated carbon adsorbent materials utilizing single-stage pyrolysis at high temperatures in the presence of $NaHCO_3$ as the activating agent. The study shows the subtle relationship between the surface characteristics and the resulting nitrogen content, which affects the CO_2 adsorption performance of the resultant adsorbent.

The study by Nguyen et al.[146] revealed a revolutionary way to generate energy and develop CO_2-adsorbent materials from agricultural byproducts. *Macadamia* nut shells, bagasse, and rice straw were gasified for energy, and the leftovers were collected and analyzed for CO_2 adsorption. The study found residual char from *Macadamia* nut shells absorbed CO_2 the best, followed by bagasse and rice straw. It also shows better CO_2 and N_2 recyclability than advanced CO_2 adsorbents reported in prior studies. The authors posited that the ultra-microporous volumes and aromatic functional groups on the char surface of *Macadamia* nut shells accounted for the excellent performances.
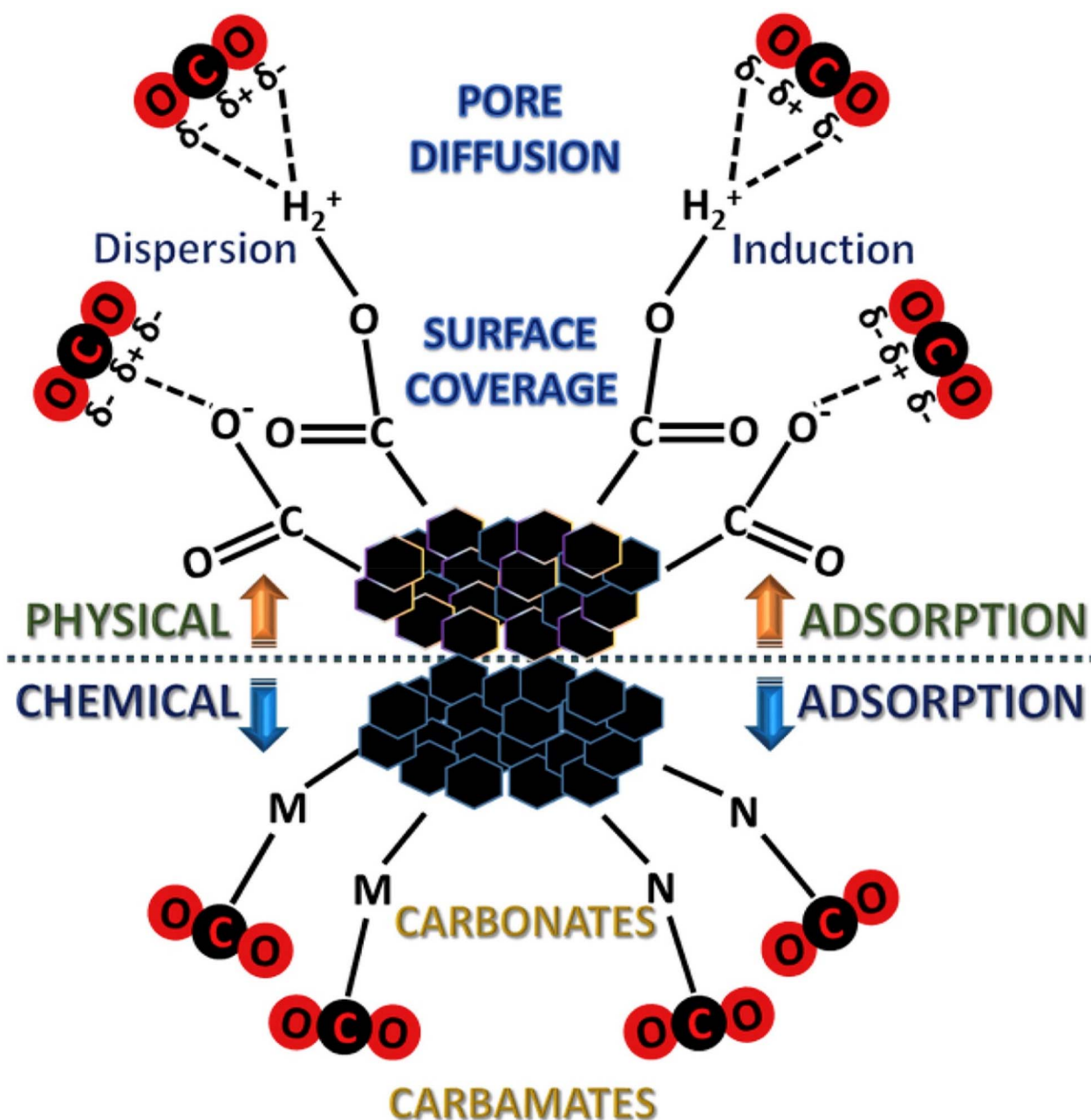

Fig. 3 Physisorption and chemisorption mechanistic process of CO_2 onto the surface of the biomass.[140]

Fig. 3 illustrates the potential mechanisms of CO_2 sequestration onto the surface of a sorbent by physical and chemical adsorption. Creamer *et al.* reported the sorption of CO_2 on non-activated porous carbons derived from sugarcane bagasse and hickory wood. It was noted that the primary sorption mechanism is physisorption, which is driven by weak van der Waals forces.[147] The CO_2 molecule's quadrupole nature was proposed as a valuable characteristic for establishing the surface interactions with adsorbent through the induction and dispersion processes. The author further suggested that the surface areas remain the primary determinant of the physisorption process of CO_2 onto the adsorbent. Martín-Martínez *et al.* synthesized a range of physically activated carbons from anthracite and investigated the process of CO_2 sorption, focusing on the morphology and dimensions of the pores.[140,148] Based on their observations, tiny micropores (1σ) were filled through physical sorption and exhibited a curved sorption isotherm, whereas larger micropores (2σ) were filled through a surface sorption and displayed rectilinear isotherm.

The process of impregnating porous carbon with metal oxide has been observed to enhance surface chemistry and increase the capacity for pollutant adsorption.[149] ACs derived from biomass can be impregnated with metal compounds such as silver, aluminum, copper, and iron, owing to their markedly higher adsorption capabilities. The impact of the impregnation ratio must be understood. This is the weight ratio of the activation agents to the precursor. The ratio is paramount in the activation process *via* chemical methods, as an increasing ratio is anticipated to enhance the biomass sorbent surface area.

In contrast to N- and/or S-doping treatments, the incorporation of metal oxides onto biomass-derived porous carbon has garnered relatively little attention.[114,150] In this context, further research has been conducted on metal oxide-doped CO_2 adsorbents derived from biomass. Lahijani *et al.* formulated a magnesium-doped CO_2 sorbent exhibiting a capacity of 1.86 mmol g^{-1} at 25 °C and 1 bar, achieving adsorption equilibrium within 30 minutes.[134] MgO-doped porous carbon sourced from biomass has been formulated by employing $MgCl_2$ (4500 ppm) present in seawater.[151] The q_{max} of 5.45 mmol g^{-1} was recorded for CO_2 adsorption and attained equilibrium within a span of 30 minutes. Another study detailed the development of biocarbon-supported MgO nanoparticles *via* the $MgCl_2$ decomposition method,[152] which demonstrated effective CO_2 capture through physisorption and the formation of magnesium carbonate, achieving a maximum CO_2 uptake of 5.34 mmol g^{-1}. Nonetheless, achieving adsorption equilibrium requires over 90 minutes for this adsorbent, indicating that the sorption kinetic rate diminishes as the MgO/biomass ratio increases.[96,134,151–153]

6. Biomass-based adsorbents for the removal of sulfur dioxide (SO_2)

The use of fossil fuels as energy sources is increasing due to their high energy production capability despite ongoing efforts of green and renewable technology.[155] Sulfur dioxide (SO_2) and other obnoxious gases such as hydrocarbons, CO_2, NO_x, and CO generate VOCs and particulate matter during the combustion of fossil fuels.[156] These emitted gases are transported over long distances for 3–5 days, depending on the meteorological conditions of the environment causing environmental pollution effects such as photochemical smog, ozone depletion, greenhouse effect, and global warming.[157] Sulfur dioxide, which is an established precursor of acid rain, causes acidification of water bodies, corrosion of buildings, damage of agricultural crops, *etc.*[158] The adverse effects of SO_2 on the health of animals and humans such as pulmonary, cardiovascular, and respiratory diseases due to its high toxicity.[159] Air pollution caused by SO_2 is becoming a serious environmental issue driven by an increase in urban migration, energy consumption, industrialization, transportation, and urbanization.[160] The release of SO_2 into the atmosphere can be *via* natural and anthropogenic activities. The major contributor to the release of SO_2 into the environment is the burning of fossil fuels such as coal, natural gas, and oil.[161] According to a report by the World Energy Council (2013), 82% of the primary energy supply in 2011 was from the burning of fossil fuel.[161] Urban air quality monitoring database obtained from low- and middle-income earning countries revealed that 98% of cities with an average of one hundred thousand inhabitants do not meet the World Health Organization (WHO) air quality guidelines, whereas only 56% of cities in high-income countries meet with the guidelines.[161] Fossil fuel consumption per capita in the twenty-largest world population is shown in Fig. 4.

A viable means of decontaminating the environment of SO_2 is by adsorption because of its simplicity, efficiency, economics, and possible regeneration of adsorbent.[163] Biomass-based activated carbon (AC) is commonly utilized for the adsorption of SO_2 to simultaneously solve two environmental problems: the adsorption of released SO_2 in the environment and the disposal of plant and animal organic wastes. Activated carbon has been widely utilized for adsorption of pollutants from air, liquids, and soil.[99] They are porous substances with high mechanical strength, large surface area, and high adsorption capacity.[164] Adsorption of pollutants on them does occur mainly on the pores on the surface of the particles. ACs used for commercial purposes are generally produced from coal, which is a non-renewable source of carbon, but it is relatively expensive. As a viable alternative, ACs are now derived from biomass such as palm, bamboo, and coconut shell.[165] Carbonization is the first step used in producing AC which leads to char production. This first step removes moisture and all volatile compounds present in the AC before subjecting the char to physical or chemical activation. Activating agents such as air, CO_2, steam, or a combination of these gases at temperatures of 800–1250 K are employed for physical activation, while acids and alkali metal hydroxides are used for chemical activation. AC is a commonly used adsorbent for water and gas treatments.[99] However, the adsorption capacity of AC decreases with an increase in temperature, making AC suitable for low-temperature applications.[166] The industrial application of AC as an acid gas adsorbent is restricted due to its low selectivity at high
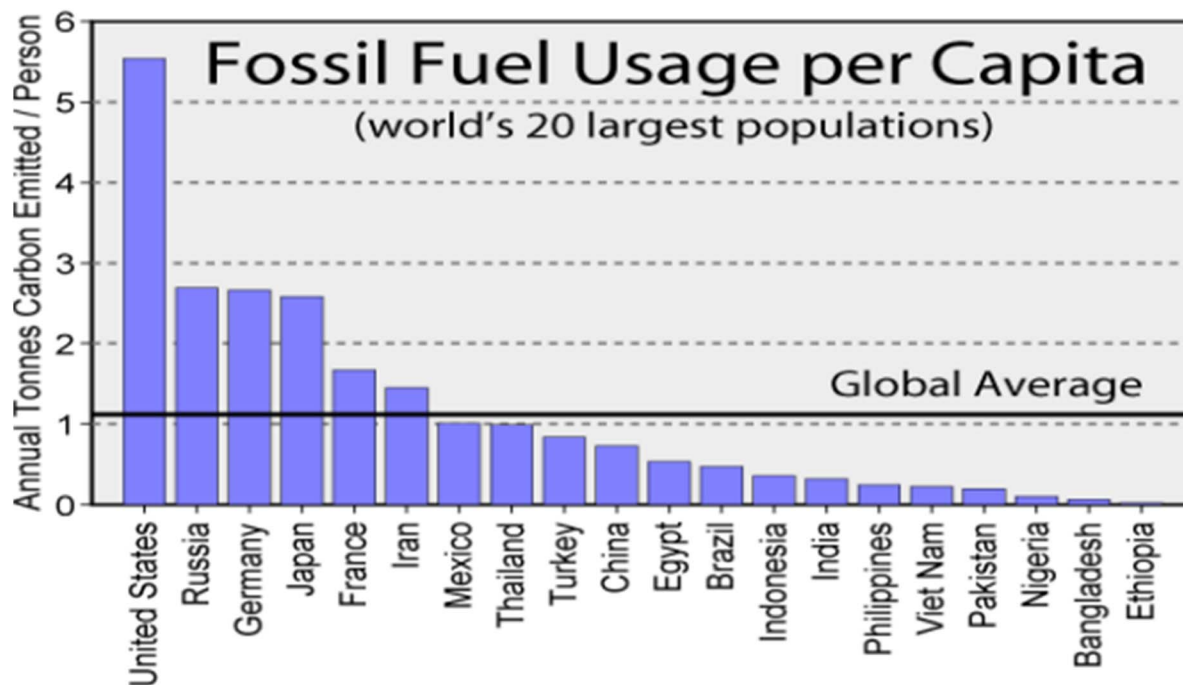
© 2025 The Author(s). Published by the Royal Society of Chemistry

Fig. 4 Fossil fuel usage per capita in the top 20 countries with the largest populations.[162]

temperatures, high regeneration cost, and poor adsorption in the presence of water vapor. The regeneration of AC usually occurs at a temperature range of 400–500 °C.[167]

6.1. Adsorption of SO_2 using activated carbon and carbonized biomass-based adsorbents

Lignocellulosic biomass is a widely recognized source of low-cost biomass materials for the effective production of activated carbons used in the adsorption of SO_2.[168] Various carbonaceous materials have been utilized in the production of ACs and applied for various purposes such as water purification, medical application, sewage treatment, gold purification, filter masks, gas purification, and filters in compressed air among other similar uses. They have also been widely used in removing gaseous pollutants such as sulphur dioxide, hydrogen sulphide, carbon dioxide, volatile organic compounds, and nitrogen oxides.[169] ACs of commercial value are produced from various carbonaceous precursors such as wood (∼33%), lignite and coal (∼42%), peat (∼10%), and coconut shells. However, agricultural wastes are preferred in ACs production because of their commercial availability, low cost, abundance, low inorganic and high carbon contents. A report by Daud and Ali[170] showed that at any level of burn-off, palm shell biomass-based AC had higher microspore volume than coconut-based AC due to properties of palm shell biomass-based AC such as lignocellulosic composition, botanical family, and texture. Palm shell activated carbon (PSAC) obtained from oil palm biomass wastes has been successfully used in the removal of SO_2, as reported by Guo and Lua[171] and the results obtained show that the AC gave better adsorptive capacity than commercial AC. Furthermore, the textural characterization of prepared PSAC gave higher

values of solid density, total porosity, BET surface area, and micropore surface area of 2.03 g cm^{-3}, 66%, 1366 m^2 g^{-1}, and 985 m^2 g^{-1}, respectively, compared with raw palm shell which gave values of 1.53 g cm^{-3}, 3.9%, 1.6 m^2 g^{-1}, and 0.2 m^2 g^{-1} respectively while char gave values of 1.63 g cm^{-3}, 17.2%, 176 m^2 g^{-1}, 108 m^2 g^{-1}, respectively for the measured parameters. Oil palm empty fruit bunch (EFB) was used in making AC for adsorptive removal of SO_2. At optimized parameters of 70 °C, 1 g of prepared AC, and 2000 ppm of SO_2, using Box-Behnken Design (BBD); approximately 1101 mg SO_2 per g activated carbon was observed. The results obtained show significant agreement between predicted and experimental values obtained. Inlet SO_2 concentration and adsorbent dosage were found to be the most significant factors which affected SO_2 adsorption with adsorbent dosage being the most significant.[155] Shukor et al.[172] studied the adsorption rate of SO_2 using ACs prepared from different biomass, namely coconut shell (CS-AC), rubber seed pericarp (RSP-AC), and their blends (CSRSP-AC). The prepared activated carbons were tested for their adsorption capacity for SO_2 using an evolved gas analyzer. The results obtained show that the single CS-AC and RSP-AC samples gave breakthrough time for SO_2 adsorption at 14 min and 23 min respectively. Meanwhile, the longest breakthrough time of 15 min was observed for the blended AC (CSRSP-AC) with a 20 : 80. It was observed that the more the amount of microporous RSP in the blend, the better the SO_2 adsorption capacity of the blend. This is an indication that a high ratio of RSP over CS in the blend (CSRSP-AC) increased adsorption capacity for SO_2. Furthermore, the presence of fly ash/Ca(OH)$_2$ catalyst in the 20 : 80 ratio of the blended CSRSP-AC improved its SO_2 adsorption capacity and gave a breakthrough time of 36 min at 35 °C

adsorption temperature. The use of adsorbent prepared from banana peels for the removal of SO_2 from motorcycle emissions was studied by Viena et al..[157] The banana peel AC was activated thermally and then used for the SO_2 adsorption experiment. The results obtained show that SO_2 emission of 24 523 ppm from motorcycle emission was totally removed to 0 ppm. This indicates 100% efficiency of banana peels AC in the removal of SO_2 from motorcycle emission. Sumathi et al.[156] investigated the effectiveness of using palm shell activated carbon (PSAC) for adsorptive removal of SO_2. The results obtained show that the breakthrough time for the removal of SO_2 was approximately 120 min for PSAC, which was higher than the reported for PSAC impregnated with Fe, Ni, and V but less than what was reported for Ce. A walnut shell was used in the preparation of AC for the removal of SO_2 from a simulated gaseous mixture obtained from coal combustion by Guo et al.[173] The results obtained show that prepared AC from walnut had a surface area of 401.2 m^2 g^{-1} which was less than what was reported for the AC prepared by impregnation with TiO, TiO_2, and Fe_2O_3 with values 937.1, 661.8, and 791.0 m^2 g^{-1} respectively. Furthermore, the breakthrough time and breakthrough sulphur capacity of raw AC were reported to have the lowest values when compared with AC impregnated with metals. Guo and Lua,[174] reported that the adsorption of SO_2 using AC prepared from oil palm shell and activated using CO_2 gave a better breakthrough time of 181.4 min when compared with the ones prepared via impregnation with 40% KOH (147.3 min) and 40% H_3PO_4 (155.2 min) but gave a lesser breakthrough time compared with 10% KOH impregnation (190.5 min). However, it gave a lower adsorption capacity (14.55 mg g^{-1}) for the adsorption of SO_2 when compared with other prepared adsorbents except for 40% KOH, which gave an adsorption capacity of 11.37 mg g^{-1}. The adsorption of SO_2 onto activated carbon prepared from pistachio nut shells by physical activation with CO_2 was studied theoretically and experimentally in a fixed-bed column. The experimental results showed that 89.6 mg g^{-1} was the adsorption capacity of the AC towards SO_2 while the breakthrough time was 380 min. Furthermore, there was a very good level of agreement between the results obtained experimentally and theoretically.[175] The summary of the adsorption of SO_2 by physical activation is summarized in Table 2.

6.2. Adsorption of SO_2 using chemically modified biomass-based adsorbents

The surface chemistry of an adsorbent determines its efficiency. Surface modification of adsorbents can be achieved through two major means which are: physical and chemical methods.[176] Surface modification by chemical means is highly preferred to physical methods because it has a direct influence on the surface of the adsorbent.[177] It is a viable means of transforming inexpensive materials from different precursors into highly valuable products with high adsorptive capacities. Chemical surface modifications give the material new surface properties that are not dependent on those of the bulk polymer.[178] Acid, alkaline, and neutral solutions have been employed as chemical agents in modifying the surface of adsorbent to achieve better adsorption

capacity.[179] Acid modification can be done using mineral acids and oxidants such as H_2SO_4, HCl, HNO_3, $HClO$, H_3PO_4, and H_2O_2.[180] Organic acids are seldom used for surface chemical modification because they have low strength and, therefore, produce a weaker effect.[181] Similarly, the surface functional groups of adsorbents can be influenced by using reducing agents. Alkali modification of the adsorbent's surface can improve the non-polar surface and hence enhance the adsorption capacity of the adsorbent for non-polar substances.[180] Alkali treatment of an adsorbent leads to the adsorption of a positive charge on the surface and hence leads to the adsorption of negatively charged species.[182] Alkali surface modification can be achieved using chemical agents such as NaOH, Na_2CO_3, KOH, Na_2SiO_3, LiOH, and oxides. Other chemical agents, which are oxidizing agents such as H_2O_2, and $KMnO_4$; metal impregnation such as cerium, zirconium, ferric chloride, hydroxides, carbonates, nitrates, or chromates; and organic agents such as ethanol have also been employed for chemical modification. Surface modification of AC-based adsorbents has been reported to improve their adsorption capacities for the removal of various contaminants, as reported.[176] Adsorption of SO_2 on oil palm-activated carbon in a fixed bed was carried out with and without pre-impregnation. SO_2 adsorption capacity on AC from oil palm shells pre-impregnated with KOH and H_3PO_4 of various concentrations was carried out. The results obtained show that AC pre-impregnated with 10% KOH gave a better adsorption capacity for the adsorption of SO_2 (Breakthrough time) (BTT) of 190.5 min and 15.34 mg g^{-1} adsorption capacity (W) compared with AC activated with CO_2 (BTT = 181.4 min and W = 14.55 mg g^{-1}) and 40% H_3PO_4 (BTT = 155.2 min and W = 16.08) pre-impregnation. However, the AC with 40% KOH (BTT = 147.3 min and W = 11.37 mg g^{-1}) pre-impregnation did not give a better adsorption capacity than 10% KOH sample, as likely expected. Over-gasification during preparation might be responsible for this, resulting in a reduction in pore surface area. Furthermore, pre-impregnation with 40% H_3PO_4 gave a better adsorption capacity but lesser breakthrough time when compared with AC without impregnation and the one pre-impregnated with 10% KOH.[174] Kraft lignin from Eucalyptus was used to make AC for the adsorption of SO_2 by impregnating it with $ZnCl_2$, acting as an activating agent. The results obtained show that the presence of oxygen and water vapour in the inlet stream increased the adsorption of SO_2 by the prepared AC due to the oxidation of SO_2 to SO_3 on the surface of the AC and subsequent hydration of the produced SO_3 to H_2SO_4.[183] Lee et al.[184] studied the adsorption of NO_x and SO_2 on coconut shell-prepared granulated activated carbon individually and simultaneously impregnated with KOH (KOH-IAC). The results obtained for individual adsorption experiments show that KOH-IAC gave a higher adsorption capacity for NO_x (0.734 mmol g^{-1}) than for SO_2 (0.6243 mmol g^{-1}). Meanwhile, simultaneous adsorption of NO_x and SO_2 using KOH-IAC showed that SO_2 adsorption was higher than NO_x. The report confirmed that the impregnation of the AC with KOH is a determining factor in the adsorption of NO_x and SO_2, thus establishing the surface chemical behaviour. Adsorbents prepared from wood and activated with phosphoric acid and impregnated with various calcium compounds ($CaCO_3$,

CaO, $Ca(CH_3COO)_2$, $Ca(OH)_2$, and $Ca(C_2H_5COO)_2$ were used as calcium precursors for the adsorption of SO_2 at low temperature. The CaO/AC adsorbents were prepared by various methods such as wet impregnation, rotary evaporator impregnation, physical mixing, ion exchange, and complex formation. The results showed that SO_2 adsorption on prepared adsorbents depended on calcium loading and dispersion. The adsorption capacity obtained for AC without impregnation was 26 mg g^{-1}, while the highest adsorption capacity recorded for impregnated AC (calcium acetate impregnation) was 120 mg g^{-1}. Other impregnated adsorbents gave adsorption capacities within the range of 30 mg g^{-1}–80 mg g^{-1} for SO_2 adsorption. Furthermore, it was observed that the physical mixing method gave the best calcium loading but low calcium dispersion. However, high calcium dispersion was obtained with samples prepared by complex formation method.[185]

The interaction between carbon on the surface of AC and metallic oxides increases SO_2 adsorption through the formation of basic oxygen-containing functional groups such as pyridine oxide, pyrones, quinones, or the deposition of metals on the pores of the AC surface. Oxides of various metals such as iron,[186] nickel,[187] magnesium,[188] cerium,[189] *etc.* have been doped on AC. Palm kernel shell doped with cerium oxide gave a maximum breakthrough time of 455 min and a minimum breakthrough time of 245 min for SO_2 adsorption;[156] rice husk ash doped with a blend of calcium and cerium oxides gave a breakthrough time of 52 min;[190] walnut shell doped with iron(III) oxide, titanium(IV) oxide, and a mixture of iron(III) oxide and titanium(IV) oxide gave breakthrough times of 1080 min, 1429.8 min, and 1321.8 min, respectively;[173] while coconut shell doped with copper gave a breakthrough time of 42 min for SO_2 adsorption.[191] The summary of the adsorptive removal of SO_2 using impregnated activated carbons is presented in Table 3.

To demonstrate the influence of impregnating various materials onto biomass/biochar sorbent on the adsorption of SO_2, CO_2 activation and impregnation with methyl diethanol-amine (MDEA) were simultaneously utilized to enhance the SO_2 adsorption capacity of biochar and increase its physicochemical properties.[159] The influence of pore shape and nitrogen functionality on SO_2 adsorption was also investigated. The results indicate that following CO_2 activation, the specific surface area of biochar rose from 56.91 m^2 g^{-1} to 755.35 m^2 g^{-1}, but this value decreased to 25.54 m^2 g^{-1} or lower after MDEA impregnation. Despite the degradation of the pore structure in activated biochar, the surface nitrogen content of the nitrogen-enriched biochar (with 10% MDEA impregnation) rose from 1.46% to a peak of 7.20%. Following 10% MDEA impregnation, the highest SO_2 sorption capacity rose from 57.8 mg g^{-1} to 156.2 mg g^{-1}.[159] Zhang *et al.* also reported the methyl diethanolamine-methanol impregnation method to prepare precursors for nitrogen-enriched biochar from peanut shells, corn stalks, and corncobs under different activation conditions to study the influence of precursors (raw biochar) on SO_2 sorption,[192] demonstrating an improved sorption capacity of 216.19 mg g^{-1} at 120 °C with O_2 and 500 ppm NO.

Wang *et al.*[193] discovered that the biochar impregnated with NH_3 has an enhanced specific surface area of 453 m^2 g^{-1}, following steam activation but diminished to a minimum of 4.81 m^2 g^{-1} subsequent to ammonia impregnation. Prior research also validated that the impregnation of amines might obstruct the surface pores of biochar, particularly the micropores.[192] The co-pyrolysis/activation modification approach utilizing nitrogen-containing compounds can streamline production and yield nitrogen-doped biochar with superior pore structure characteristics. The thermal reactivity of nitrogen-containing compounds and activators complicates

Table 2 Adsorption of SO_2 using activated carbons prepared by physical activation

Carbon source	Activation condition	Inlet SO_2 concentration (ppm)	Breakthrough time (min)	Adsorption capacity (mg g^{-1})	Reference
Palm shell	Gas inlet flow rate of 30–90 cm^3 min^{-1} at 298 K, 1 atm, on 20 mg AC	1000	203.8	35.2	171
Oil palm empty fruit	Temperature of 70 °C on 1 g AC	2000	—	1101	155
Pistachio nut shell	Gas inlet flow rate of 345 cm^3 min^{-1} at 25 °C, and 1 atm	1000	380	89.6	175
Oil palm shell	Gas inlet flow rate of 30–90 cm^3 min^{-1} at 25 °C, and 1 bar	2000	181.4	14.55	174
Coconut shell	Gas inlet flow rate of 500 mL min^{-1} at 35 °C, 1 atm, on 5 g AC	1000	14	—	172
Rubber seed pericarp	Gas inlet flow rate of 500 mL min^{-1} at 35 °C, 1 atm, on 5 g AC	1000	23	—	
Coconut and rubber seed blend	Gas inlet flow rate of 500 mL min^{-1} at 5 °C, 1 atm, on 5 g AC	1000	29	—	
Without fly ash and $Ca(OH)_2$ With fly ash and $Ca(OH)_2$	Gas inlet flow rate of 500 mL min^{-1} at 25 °C, 1 atm, on 5 g AC	1000	36	—	
Banana peels	Motorcycle emission	24 523	—	—	157
Palm shell activated carbon	Gas inlet flow rate of 0.15 L min^{-1} at 150 °C, 1 atm, on 1 g AC	2000	~120	—	156
Walnut shell activated carbon	Gas inlet flow rate of 0.12 L min^{-1} at 90 °C, space velocity of 600 h^{-1}, on fixed mass of AC	—	5	63	173

nitrogen stabilization in the solid phase, leading to a low nitrogen concentration in nitrogen-doped biochar. When carbon precursors were co-pyrolyzed with urea (a nitrogen source) and KOH (an activator), the highest nitrogen content of nitrogen-doped porous carbon was found to be just 1.52%.[194] Consequently, the one-step modification of biochar, premised on a well-developed pore structure and efficient nitrogen doping, is essential for creating a cost-effective material with superior SO_2 adsorption capabilities.[195] In another research,[196] CO_2 activation and high-temperature ammonia (nitrogen doping) have demonstrated efficacy in altering biochar, with the SO_2 adsorption capabilities of the changed biochar achieving 191.1 and 199.8 mg g^{-1}, respectively.

7. Biomass-based adsorbents for the removal of hydrogen sulfide (H$_2$S)

Gaseous pollutants are not easy to control because of their high mobility and difficulty in visualizing them. Some gaseous pollutants such as H_2S, which are contained in ambient air or biogas, are said to have high levels of toxicity and, therefore, pose health risks.[197] The production of biogas, which is a renewable source of energy, has been growing in recent decades.[198] However, H_2S, which is one of the constituents of biogas with a concentration range of 100–10 000 ppm, is a poisonous acidic gas.[198,199] Thus, burning of H_2S-containing biogas would cause serious corrosion of the combustion engine, boiler, and various parts of the system.[197,200] Furthermore, SO_2 generated during the combustion of H_2S-containing biogas could pose serious human health challenges.[197] In order to overcome this problem, several means have been used to mitigate air pollution caused by H_2S emissions. Ambient temperature catalytic oxidation of H_2S into

sulfur in a solid state is one of the most promising methods used for removing H_2S air pollutants with low concentration, i.e., <50 000 ppm, due to being secondary pollution-free and having moderate operating conditions.[201,202] Various adsorbent materials, such as porous natural and synthetic zeolites, metal oxides, and activated carbons, have been used to remove H_2S. The materials can either be amorphous or crystalline, which can be porous or non-porous with the ability to be modified to improve their H_2S affinity. Interfering compounds present in feedstock can be a determining factor in choosing the material to be used as an adsorbent for H_2S removal. A polar adsorbent surface helps to separate a polar H_2S from a non-polar molecule like CH_4 in a fuel gas mixture. However, separation based on polarity alone can be difficult in the presence of other polar compounds, such as CO_2 and water molecules. Water molecules present in the gas mixture may improve or hinder H_2S adsorption depending on the amount of water in the mixture and the strength of interaction between the adsorbent and the water molecules. The presence of CO_2 in the feed mixture poses further problems since both are acidic.[203] Several categories of adsorbents have been synthesized in the last two decades, which possess the capability to remove acid gases such as H_2S, and they are: carbon-based adsorbents, microporous and mesoporous silica, and MOFs. A good adsorbing material must possess high adsorption capacity, low rate of friction, fast adsorption kinetics, stability in a redox environment, regenerability, and ability to withstand high temperature.[204] Adsorption using carbon-based materials such as activated carbon[205] has been widely utilized for H_2S removal at room temperature due to their large pore size, high surface area and good surface chemistry.[206] The pore size of activated carbon is sufficient for gaseous adsorption to take place, and it has a large enough surface area that enables rapid reactions to occur, thus controlling air pollution.[207] The average size of H_2S pollutants is <2 nm, and this

Table 3 Adsorptive removal of SO_2 using impregnated activated carbon

Carbon source	Activation condition	Inlet SO_2 concentration (ppm)	Breakthrough time (min)	Adsorption capacity (mg g^{-1})	Reference
Oil palm shell impregnated with KOH	Gas inlet flow rate of 30–90 cm^3 min^{-1} at 25 °C, and 1 bar	2000	190.5	13.34	174
Oil palm shell impregnated with H_3PO_4	Gas inlet flow rate of 30–90 cm^3 min^{-1} at 25 °C, and 1 bar	2000	155.2	16.08	174
Kraft lignin from eucalyptus impregnated with $ZnCl_2$	Gas inlet flow rate of 200 cm^3 min^{-1} at 25 °C, 1 atm, on 0.2 g AC	2500	12	94.8	183
Coconut shell impregnated with KOH	Adsorption temperature of 403 K and pressure of 1 atm on 10.67 g AC	1006	69	40	184
Wood impregnated with H_3PO_4	Gas inlet flow rate of 60 mL min^{-1} at 573 K on 0.2 g AC	—	—	120	185
Rice husk ash AC modified with calcium and cerium oxides	Gas inlet flow rate of 0.15 L min^{-1} at 150 °C, 1 atm, on 0.7 g AC	2000	52	46.33	190
Walnut shell AC modified with iron(III) oxides	Gas inlet space velocity of 600 h^{-1} at 90 °C, 1 atm, on 0.5 g AC	2000	1080	—	173
Walnut shell AC modified with iron(III) oxides	Gas inlet space velocity of 600 h^{-1} at 90 °C, 1 atm, on 0.5 g AC	2000	~1430	—	173
Mixture of iron(III) and titanium(IV) oxides		2000	~1322	—	173
Coconut shell and copper nitrate modified AC	Gas inlet flow rate of 0.40 L min^{-1} at 50 °C, 1 atm	2000	42	—	191

makes the filtration method alone not sufficient to remove them completely.[135] One of the major factors that affect the desulfurization performance of carbon-based materials is their porous structure.[208] Microporous and mesoporous carbon-based materials are quite suitable for the removal of H_2S. Micropores provide the adsorption site for the removal of H_2S,[209] while mesopores are suitable for deposition of desulfurization products *i.e.*, sulfur, along with rapid mass transfer of H_2S gas molecules.[208] Chemical activation is the most common activating method for the pore structure development of carbon materials.[114] However, chemical activation develops micropores into carbon-based materials with the generation of fewer mesopores.[114] The traditional means of preparing mesoporous carbon is by using a sacrificial template method such as the use of SiO_2. Another major factor that affects the efficiency of H_2S removal by carbon-based materials is surface composition.[208,210,211] A means of improving the surface composition of carbon materials is the use of N-doped carbon which increases catalytic activity towards H_2S at room temperature. The introduction of nitrogen could lead to an increase in redox chemistry and chemical reactivity for acid–base reaction through improved basic catalytic sites.[135,212] Furthermore, it can increase the rate of dissociation and oxidation of H_2S in the presence of water molecules.

7.1. Adsorption of H_2S using activated carbon and carbonized biomass-based adsorbents

The use of ACs and other carbon-based materials as absorbents, as presented in Table 4, is very common for low-temperature desulfurization material due to their properties such as large surface area, which is usually greater than 1000 m² g⁻¹, high thermal stability, controllable surface chemistry, and high pore volume. Production of AC is generally cheaper than other types of adsorbents because they are obtained from easily available carbon materials such as wood, agricultural wastes, peat, coal, *etc.* The surface chemistry of ACs is highly controlled by modification of the functional groups on their surfaces.[209,219] The functionalization determines the extent of adsorbate–adsorbent interactions and consequently affects the chemical and physical adsorption rate. This has led to a variety of functionalized carbon-based sorbents produced by impregnation, deposition–precipitation, or doping with heteroatoms.[202,220,221] The direct integration method was recently proposed as a better alternative to the impregnation method.[222]

Ou *et al.*[213] investigated using granular activated carbon (GAC) for the adsorption of H_2S from the biogas generated by small to medium-sized cattle or pig farms. The GAC sorbent performance was conducted on a long-term basis for biogas generated from treating wastewater. Various adsorption parameters, such as adsorbent masses, volumes, and inlet H_2S concentrations, were analyzed to ascertain the impact of the different factors. The results obtained show that at H_2S inlet concentrations of 932–1560 ppm and 100 ppm breakthrough concentration, GAC gave breakthrough capacities of 745–1293 mg g⁻¹ at 20–25 °C. The comparison of these values to other types of adsorbents shows that it is high. The choice of GAC as an acceptable adsorbent for the removal of H_2S is due to

its low cost and high adsorption capacities. Further studies have shown that cellulose and lignin contents of the waste biomass have positive impacts on the yield and microporous surface area of the resulting biochar.[223] Yang *et al.*[221] carried out an adsorption experiment of H_2S using wood-based AC, and the results obtained show that at an H_2S concentration of 1000 ppm and inlet flow rate of 500 mL min⁻¹ on a 2 cm³ of sample packed into a column with particle size of 30–40 mesh, the H_2S breakthrough capacity was 5.6 mg g⁻¹. The breakthrough capacity obtained is higher than the value obtained when $ZnFe_2O_4$ was used alone as a sorbent for H_2S (1.6 mg g⁻¹) but lower than the values obtained when wood-based AC was impregnated with various masses of $ZnFe_2O_4$. In a related study carried out by Chen *et al.*[214] using cypress Sawdust to produce activated carbon, which was used for the adsorption of H_2S at an initial concentration of 1000 ppm, gave a breakthrough capacity of 12.5 mg g⁻¹, which was less than the value obtained for N-doped cypress sawdust without K_2CO_3 activation. Nowicki *et al.*[212] carried out a series of adsorption studies using various biomass-based materials, which are coffee, tobacco, corn cobs, and cherry stones. The sample materials were crushed, sieved, and subjected to pyrolysis at 700 °C before physical activation using CO_2 at 800 °C. The products obtained were code-named CP7PA, TP7PA, CCP7PA, and CSP7PA for coffee, tobacco, corn cobs, and cherry stones, respectively. They were then used for the adsorption of H_2S under dry and wet conditions with/without moisture. The results obtained show that CP7PA gave the highest H_2S breakthrough capacity of 149.6 mg g⁻¹ under wet conditions without moisture. In comparison, CSP7PA gave the lowest H_2S breakthrough capacity of 1.3 mg g⁻¹ under wet conditions with 70% moisture. Furthermore, the adsorbent obtained by directly activating coffee using CO_2 at 800C gave the highest H_2S breakthrough capacity of 215.6 mg g⁻¹ under moist wet conditions. In contrast, direct activation of coffee (CDA) adsorbent for adsorption under dry conditions gave the lowest value of 6.0 mg g⁻¹ among adsorbents prepared by direct activation. Adsorption of H_2S under wet conditions gave better adsorption breakthrough capacities of H_2S. A study carried out by Kazmierczak-Razna and Pietrzak,[216] used low-quality hay that was subjected to pyrolysis at different temperatures and times in a muffle chamber in a microwave furnace. The physical activation was done using CO_2, which was done after pyrolysis or by direct activation. The two temperatures used for pyrolysis were 700C and 800C in a muffle furnace for either 15 min or 30 min. The adsorbents obtained after pyrolysis and physical activation were code-named HPA7-15, HPA7-30, HPA8-15, and HPA8-30, while those obtained by direct activation were code-named HDA7-15, HDA7-30, HDA8-15, and HDA-30. The prepared adsorbents were used for the adsorption of H_2S under dry and wet conditions and the results obtained show that HPA7-15 gave the highest H_2S breakthrough capacity of 39.0 mg g⁻¹ under wet conditions. The HDA7-30 gave the lowest H_2S breakthrough capacity of 5.2 mg g⁻¹ under dry conditions. Furthermore, the lowest H_2S breakthrough capacity of 12.3 mg g⁻¹ was the lowest under wet conditions. This is an indication that the adsorption of H_2S under wet conditions gave a better result than under dry conditions. Another similar study by

Kazmierczak-Razna *et al.*[215] used low-quality hay for the synthesis of activated carbon using a microwave oven for the pyrolysis of the material at three different temperatures of 500 °C, 600 °C, and 700 °C. The prepared char was then subjected to physical activation in a microwave oven at 500 °C under a stream of CO_2. The synthesized adsorbents prepared at 500 °C, 600 °C, and 700 °C with CO_2 activation were code-named H5A, H6A, and H7A, respectively. They were then used for the adsorption of H_2S under dry and wet conditions, and the results obtained show that H7A under wet conditions gave the highest H_2S breakthrough capacity of 40.5 mg g^{-1} while H5A under dry conditions gave the lowest H_2S breakthrough capacity of 1.0 mg g^{-1}. The highest H_2S breakthrough capacity of 40.5 mg g^{-1} obtained for H7A is comparable to the value of 39.0 mg g^{-1} obtained under similar conditions in an earlier study by Kazmierczak-Razna and Pietrzak.[216] Hervey *et al.*[217] carried out a study on the adsorption of H_2S with activated carbon prepared from used wood pallets (UWP). The results from the study show that AC obtained from the pyrolysis of UWP *via* steam activation gave H_2S a breakthrough capacity of 12.92 mg g^{-1}. Meanwhile, c.UWP prepared by pyrolysis of UWP without steam activation gave H_2S breakthrough capacity of 0.04 mg g^{-1} while ox.UWP, which was produced from c.UWP by oxygenation gave H_2S a breakthrough capacity of 1.81 mg g^{-1}. Shang *et al.*[218] carried out a study on the adsorption of H_2S using adsorbent prepared

from the pyrolysis of rice hull and bamboo and compared their adsorption capacity towards H_2S with shell-derived commercial AC. The results obtained show that SR gave the highest H_2S breakthrough capacity of 382.7 mg g^{-1} while bamboo and AC gave H_2S breakthrough capacity of 109.3 mg g^{-1} and 35.6 mg g^{-1}, respectively. Activated carbon of wood origin without thermal treatment was used for the adsorption of H_2S with the application of a custom-designed dynamic tester. The tests were carried out under dry and wet conditions, and the results obtained show that adsorption under dry conditions gave H_2S breakthrough capacity of 3.1 mg g^{-1} and 5.7 mg g^{-1} under dry and wet conditions respectively. Furthermore, AC with thermal treatment at 450 °C and 950 °C were also used for the adsorption of H_2S under dry and wet conditions. The results obtained show that the H_2S breakthrough capacities at 450 °C under dry and wet conditions are 0.6 mg g^{-1} and 2.6 mg g^{-1}, respectively, while the H_2S breakthrough capacities under wet conditions at 950 °C are 2.0 mg g^{-1} and 6.6 mg g^{-1} respectively. This further confirms that wet condition favours the adsorption of H_2S.[210]

7.2. Adsorption of H_2S using chemically modified biomass-based adsorbents

Modification of the surface of an adsorbent involves adjusting the surface of a material by biological, chemical, and physical

Table 4 Adsorption of H_2S using biomass-based adsorbents prepared by physical activation for H_2S removal[a]

Carbon source	Activation condition	Inlet SO_2 concentration (ppm)	Breakthrough time (min)	Adsorption capacity (mg g^{-1})	Reference
Granulated activated carbon	Gas inlet flow rate of approximately 22.3 m^3 h^{-1} at 20–25 °C	1350	124	1293	213
Cypress sawdust	Gas inlet flow rate of 150 mL min^{-1} at 25 °C on 0.2 g AC	1000	12	12.5	214
Coffee	Gas flow rate of 450 mL min^{-1} at 22 °C on 1.0 g AC	—			212
CP7PA				149.6^w	
CDA				215.6^{mw}	
Tobacco					
TP7PA				21^{mw}	
TDA				178.4^{mw}	
Corn cobs					
CCP7PA				119.1^w	
CCDA				159.4^w	
Cherry stones					
CSP7PA				1.3^{mw}	
CSDA				19.5^{mw}	
Hay	Gas flow rate of 450 mL min^{-1} on 1.0 g AC			39.0^w	215
HPA7-15					216
Hay	Gas flow rate of 450 mL min^{-1} on 1.0 g AC	2000			217
H5A				1.1^w	218
H6A				10.8^w	
H7A				40.5^w	
Used wood pallets	Gas flow rate of 180 mL min^{-1} at 22 °C on 1.0 g AC			12.92	
Rice hull	Gas flow rate of 40 mL min^{-1}	—	620	382.7	
Bamboo			360	109.3	
Shell-derived AC			120	35.6	
Wood based AC	Gas flow rate of 150 mL min^{-1} on 1.0 g AC	1000	—	6.6^w	210

[a] Key: superscript w = wet, mw = moisture and wet.

means to form new material with different forms that can be used for the desired purpose. It involves physical and chemical changes to remove surface impurities on the adsorbent. Surface modification of an adsorbent usually leads to alteration in the functional groups on the surface. Surface modification of adsorbents can be done through thermal, mechanical, or chemical means.[224] Chemical modification involves the use of alkali, acid, or salt to improve the functional group on the surface of the adsorbent (Table 5). Meanwhile, the physical process improves the physical properties of the adsorbent such as surface area and pore sizes. Furthermore, surface modification can be achieved through the combination of methods, such as thermochemical and mechanochemical processes.[227]

Sawalha et al.[225] carried out an adsorption study using activated carbons synthesized from spent almond shells, coffee grains (COF), and eucalyptus barks, which were impregnated with potassium hydroxide and zinc chloride, respectively, to capture H_2S from biogas containing an average concentration of 970 ppm H_2S. The adsorption performance of eucalyptus barks impregnated with KOH for the removal of H_2S was the best among the three for a bed height of 2 cm and gas flow rate of 1.5 L min^{-1} at ambient conditions. It gave an adsorption capacity of 490 mg g^{-1} and a saturation time of 180 min, while COF gave a very poor adsorption capacity of 22 mg g^{-1} and a saturation time of 10 min. The results obtained further revealed that the more the lignin and cellulose contents of the prepared adsorbents, the better their adsorption capacity. Furthermore, they did a comparative study of the effect of an impregnation agent on the adsorption capacity of eucalyptus for the adsorption of H_2S. The results obtained show that eucalyptus barks impregnated with KOH gave H_2S a breakthrough time of 180 min, whereas the one impregnated with $ZnCl_2$ gave a breakthrough time of 70 min. This indicates that KOH is a better impregnation agent than $ZnCl_2$ for the adsorption of H_2S.

A similar study using spent coffee and zinc chloride as an impregnation agent at various ratios was carried out by Kante et al.[208] The ratio of dry coffee to $ZnCl_2$ was 1:0.5 (COFAC-0.5), 1:1 (COFAC-1), and 1:2 (COFAC-2). These prepared adsorbents were used for the adsorption of H_2S, and the results obtained show that COFAC-1 gave the highest H_2S breakthrough capacity of 127.0 mg g^{-1} while COFAC-2 gave the lowest H_2S breakthrough capacity of 18.3 mg g^{-1}. Another zinc compound ($ZnFe_2O_4$) was used as an impregnation agent in a study by Yang et al.[221] Wood-based carbon, which was activated with phosphoric acid, was used in the study. Various ratios of combinations between wood-based carbon and $ZnFe_2O_4$ were used. The synthesized adsorbents were referred to as ZFOB-x, where ZFO represents a combination of $ZnFe_2O_4$ and wood-based carbon, and x represents the amount of $ZnFe_2O_4$ in the composite. The synthesized adsorbents, along with wood-based carbon only, were used for the adsorption of H_2S, and the results obtained show that ZFOB-10 had the highest H_2S breakthrough capacity of 122.5 mg g^{-1} while ZFO had the lowest H_2S breakthrough capacity of 1.6 mg g^{-1}, a value which is lower than 5.6 mg g^{-1} which was obtained when wood-based carbon alone was used for the adsorption of H_2S.

In another study by Yuan et al.,[226] using $ZnFe_2O_4$ as an impregnation agent with leftover rice as biomass was carried out. The prepared adsorbents ($ZnFe_2O_4$)-loaded porous biochar (RZF) were code-named according to different activation temperatures and activation ratios as RZF-T-X:Y, where T is the activation temperature and X:Y is the mass ratio of leftover rice to $ZnFe_2O_4$. Among the various adsorbents prepared and used for the adsorption of H_2S, RZF-500-1:1 gave the highest H_2S breakthrough capacity of 228.29 mg g^{-1}, while the material prepared directly at the carbonization temperature of 500 °C without activator (RBC) that is adsorbent prepared from leftover rice alone without impregnation with $ZnFe_2O_4$ gave the lowest H_2S breakthrough capacity of 12.11 mg g^{-1}.

Alkaline chemical activation of coffee, tobacco, corn cobs, and cherry stones using KOH was carried out by Nowicki et al.,[212] The prepared adsorbents were coded CP7CA, TP7CA, CCP7CA, and CSP7CA for adsorbents prepared from coffee, tobacco, corn cobs, and cherry stones. The adsorbents were used for the adsorption of H_2S under dry and wet conditions with or without moisture. The results obtained show that TP7CA had the highest H_2S breakthrough capacity of 76.3 mg g^{-1} under wet conditions without moisture, while TP7CA under dry conditions without moisture had the lowest H_2S breakthrough capacity of 3.7 mg g^{-1}. Chen et al.,[214] used another potassium compound (K_2CO_3) to activate cypress sawdust doped with carbon nitride (CN) at various ratios. The produced adsorbents were coded as NPC-n, where n is the ratio of CN to CS. The H_2S breakthrough testing results showed that NPC-1 gave the highest breakthrough value of 426.2 mg g^{-1} while NPC-0.5 gave the lowest value of 119.1 mg g^{-1} among the NPC-n-prepared adsorbents. However, the H_2S breakthrough value obtained for NPC-0.5 is far higher than what was obtained for porous carbon without CN loading (PC), which gave a value of 12.5 mg g^{-1} and N-doped carbon without K_2CO_3 activation, which gave a value of 19.5 mg g^{-1}.

The effect of nitrogen doping of wood-based commercial activated carbon using urea or melamine at 450 °C or 950 °C was carried out by Seredych and Bandosz.[210] In all, a total of eleven different adsorbents were prepared with code-named BAX (raw activated carbon), CBAX-A (activated carbon heated at 450 °C), CBAX-AM (activated carbon heated at 450 °C and doped with melamine), CBAX-AMO (activated carbon heated at 450 °C, doped with melamine and preoxidized with HNO_3), CBAX-B (activated carbon heated at 950 °C), CBAX-BM (activated carbon heated at 950 °C and doped with melamine), CBAX-BMO (activated carbon heated at 950 °C, doped with melamine and preoxidized with HNO_3), CBAX-AU (activated carbon heated at 450 °C and doped with urea), CBAX-AUO (activated carbon heated at 450 °C, doped with urea and preoxidized with HNO_3), CBAX-BU (activated carbon heated at 950 °C and doped with urea), and CBAX-BUO (activated carbon heated at 950 °C, doped with urea and preoxidized with HNO_3). All the prepared adsorbents were used for the adsorption of H_2S under dry and wet conditions. The results obtained show that CBAX-BM under wet conditions gave the highest breakthrough capacity of 64.1 mg g^{-1}, while CBAX-BU gave the highest breakthrough capacity under dry conditions with a value of

Table 5 Summary of adsorptive removal of H_2S onto chemically modified biomass-based adsorbents[a]

Carbon source	Activation condition	Inlet SO_2 concentration (ppm)	Breakthrough time (min)	Adsorption capacity (mg g^{-1})	Reference
Almond impregnated with KOH	Gas flow rate of 1.5 L min^{-1} on 2 cm bed height at ambient temperature	970	10	230	225
Coffee impregnated with KOH			130	22	
Eucalyptus impregnated with KOH			180	490	
Coffee impregnated with ZnCl$_2$	Gas flow rate of 250 mL min^{-1} on 1 g AC	1000	~44	81.3	208
COFAC-0.5			~65	127.0	
COFAC-1			~1.0	18.3	
COFAC-2					
Wood impregnated with ZnFe$_2$O$_4$	Gas flow rate of 500 mL min^{-1} on 2 g AC at room temperature	1000	~108	122.5	221
Rice impregnated with ZnFe$_2$O$_4$	Gas flow rate of 100 mL min^{-1} on 0.2 g AC at 25 °C	300	~380	54.29	226
RZF-500-3 : 1			~960	117.06	
RZF-500-2 : 1			~1370	228.29	
RZF-500-1 : 1			~1100	153.8	
Coffee impregnated with KOH	Gas flow rate of 450 mL min^{-1} at room temperature on 1.0 g AC		~5	11.1^{mw}	212
CP7CA			~87	76.3^{w}	
Tobacco impregnated with KOH			~12	17.4^{w}	
TP7CA			~19	10.6^{md}	
Corn cobs impregnated with KOH					
CC7CA					
Cherry stones					
CS7CA					
Wood impregnated with melamine or urea	Gas flow rate of 150 mL min^{-1} on 1.0 g AC	1000	~370	51.6^{w}	210

[a] Key: superscript w = wet, mw = moisture and wet.

21.6 mg g^{-1}. The lowest H_2S breakthrough capacity under dry and wet conditions was observed with CBAX-A (0.6 mg g^{-1}) and CBAX-AM (2.5 mg g^{-1}), respectively. The value for CBAX-A under dry conditions is less than that obtained for BAX alone (3.1 mg g^{-1}) under dry conditions. Similarly, BAX alone, used as an H_2S adsorbent, gave a higher breakthrough capacity of 5.7 mg g^{-1} under wet conditions. The results showed that N-doping and wet adsorption conditions of H_2S gave better results.

Prior studies[228,229] on H_2S sorption utilizing copper sorbent-impregnated rice husk and cocoa AC. with NaOH as a substitute material for copper to assess its impact on the surface chemistry of AC. It was observed that NaOH significantly enhances the adsorption efficacy of AC by generating reactive functional groups, particularly the –OH functional group, following the modification of AC with NaOH. Impregnating of AC with KOH and KI to enhance the chemisorption of H_2S has been reported.[230] The H_2S sorption efficacy was evaluated within a temperature range of 30–550 °C employing the temperature-programmed sorption approach to ascertain the influence of sorption temperature on the material's sorption properties. At ambient temperature, the impregnation of AC with KOH enhances its H_2S sorption capacity, but impregnation with KI yields no noticeable advantage. At elevated adsorption temperatures (up to 550 °C), the impregnation of AC with KOH and KI significantly enhances its H_2S sorption performance, specifically regarding adsorption capacity and breakthrough time. N_2 adsorption, SEM, and EDS measurements indicated that the chemical interactions between H_2S and alkaline substances (KOH and KI) are enhanced at elevated temperatures. Utilizing all experimental data, the equilibrium adsorption model employing the linear isotherm was formulated to forecast the sorption behavior of these sorbents concerning the equilibrium isotherm constant and mass transfer coefficient for further scaling-up processes.

8. Biomass-based adsorbent for nitrogen dioxide removal

Nitrogen dioxide (NO_2) is an inorganic air pollutant that poses detrimental impacts on animal life, human health, and the environment. NO_x gas is emitted by natural occurrences including, volcanic eruptions, lightning strikes, and forest fires. In recent times, nanostructured metal oxides such as ZnO, TiO$_2$, and CuO have gained significant popularity as gas sensor

© 2025 The Author(s). Published by the Royal Society of Chemistry

components due to their distinct structure and surface-to-volume ratio, which sets them apart from layered materials.[231–234] Additionally, composites that incorporate MOFs in their structures are utilized for the purpose of adsorbing NO_2.[235,236]

Several studies have conducted comparisons of the adsorption capabilities of NO_2 at low temperatures using various activated carbons. The activated carbons for NO_2 removal were obtained either commercially or by chemical/physical activation of different precursors such as lignocellulosic biomasses or mineral coals. Many techniques were employed in the literature to alter the texture and surface chemistry of the material and enhance the efficacy of activated carbon for removing NO_2. Table 6 summarizes the performance of biomass-based materials for NO_2 removal under different operating environments.

Although previous studies were conducted on the interaction between NO_2 and carbonaceous materials in the early 1900s, the first study on the use of AC for NO_2 removal was published in 2007 by Pietrzak and Bandosz.[243] The efficacy of BAX-1500, a commercially available wood-based activated carbon, was assessed for adsorbing NO_2 using a custom-designed dynamic test. This experiment involved injecting either dry or wet air (with 70% humidity) that contained 0.1% volume/volume of NO_2. The air was injected at a flow rate of 0.45 L min^{-1} into a glass column that contained a packed activated carbon. The residence time was 0.4 s, which is consistent with the value commonly employed in industrial air filtering systems. It was observed that the adsorption and reduction of NO_2 took place on the surface of the activated carbon.

Similarly, Jeguirim et al. previously discovered this behavior when studying the interaction between NO_2 and black carbon.[244] The BAX-1500 exhibited adsorption capabilities of 42.7 and 63.8 mg g^{-1} under dry and wet conditions, respectively. The analysis of the AC's characteristics before and after adsorption testing using different analytical techniques revealed an enhancement in the acidity properties of the AC following NO_2 adsorption which was also evident in the colour change. The rise in acidity was ascribed to the surface oxidation and the generation of carboxylic groups during the reduction of NO_2, as well as the production of nitric acid during the interaction of NO_2 with hydroxyl groups. In addition, the application of NO_2 treatment resulted in a small reduction (10–15%) in the textural characteristics, such as the specific surface area and volume of micropores, due to surface oxidation. This suggests that both the physical characteristics and chemical composition of the adsorbent's surface are significant factors in the adsorption and interaction of NO_2 with activated carbon.

Nowicki et al. conducted a study to examine the impact of surface oxygen groups by comparing the effectiveness of activated carbons produced by chemical (KOH) and physical (CO_2) activations of coffee residues.[241] The adsorption capacity of 44.5 mg g^{-1} was achieved using activated carbon with a surface oxygen basic group concentration of 0.9 mmol g^{-1}. However, the physically activated carbon showed a reduced adsorption capacity for CO_2, despite the presence of a greater quantity of basic surface groups of 11.32 mmol g^{-1}. This behavior might be ascribed to the lack of micropores. In addition, both the

existence of micropores and the presence of surface oxygen basic groups are crucial for facilitating effective interactions between the NO_2 molecules and the carbon surface.

Similarly, Belhachemi et al. conducted a study to assess the effectiveness of several activated carbons. These carbons were made using chemical (C_{Zn}) and physical (C_{CO_2}) activation of date pits, as well as using commercial activated carbon (CAC). Modified activated carbons were also created through chemical oxidation (CAC-O) and thermal treatment (CAC-O-T). The experiments to measure the adsorption of NO_2 were conducted in a fixed-bed reactor, as seen in Fig. 5. The tests were carried out at normal room temperature and under dry circumstances.[245] For each test, a concentration of 500 parts per million by volume of NO_2 in nitrogen gas was introduced into the reactor. The flow rate of the gas was set at 20 NL h^{-1}, and the reactor included 100 mg of activated carbon. The experiment revealed NO_2 adsorption capabilities ranging from 78 to 136 mg g^{-1}, as seen in Fig. 5b. Furthermore, a substantial emission of nitrogen monoxide (NO) resulting from the reduction of NO_2 on the carbon surface was observed. The quantity of released NO exhibited a pattern that closely resembled the adsorption of NO_2. This behavior suggests that the conversion of NO_2 to NO is an essential process for the adsorption of NO_2, as previously proposed.[244] Moreover, examining the textural and surface characteristics revealed that the volume of micropores and the existence of stable oxygen groups were the primary factors that influenced the interaction between NO_2 and activated carbons. The quantity of strong acidic groups exhibits an inverse correlation with the quantity of remaining oxygen subsequent to the reduction of NO_2 to NO. thus, the presence of highly acidic groups hinders the reduction of NO_2 to NO and thus prevents the adsorption of NO_2 on the surface of adsorbent.

Ghouma et al.[246] discovered that the adsorption capacity of 131 mg g^{-1} which closely aligns with the findings of Belhachemi et al.[245] Nevertheless, the activated carbon derived from olive stone exhibited a smaller volume of micropores when compared to the activated carbon produced from date stone.[245] This increased capability was ascribed to the greater quantity of basic groups (1.86 mmol g^{-1}). The examination of the gases generated during Temperature Programmed Desorption (TPD) revealed that NO_2 can undergo either physisorption directly onto the activated carbon or chemisorption by interacting with the surface oxygen groups. Ghouma et al. conducted a study to determine the efficiency of activated carbon produced by water vapor activation. The performances of three distinct activated carbons made from the same precursor (olive stone) were examined.[246] The authors developed two physically activated carbons, one activated using CO_2 and the other using H_2O, as well as a chemically activated carbon using H_3PO_4. Their performance in breakthrough experiments was evaluated using a fixed-bed flow reactor setup.

Copper salt-impregnated carbon was subjected to a reductive atmosphere utilizing hydrazine hydrate or nitrogen heat treatment at 925 °C.[247] Impregnating copper increased NO_2 sorption and NO retention on carbon after NO_2 reduction. That enhancement is due to copper metal's strong surface dispersion. Both reduction techniques reduced copper, but the carbon

Table 6 Operating conditions used to prepare different activated carbons and their adsorption capacities of NO_2

Precursor	Activation conditions	S_{BET} ($m^2 g^{-1}$)	V_t ($cm^3 g^{-1}$)	V_{mic} ($cm^3 g^{-1}$)	Total content of surface oxides ($mmol g^{-1}$)	Adsorption test conditions	NO_2 sorption capacity ($mg g^{-1}$)	Ref.
Bituminous coal	Carbonisation at 700 °C KOH at 700 °C	1856	0.875	0.863	1.32	0.450 L min^{-1} 0.1% NO$_2$, moist air (70% humidity)	43.5	237
Walnut shell	Pyrolyzed at 400 °C KOH activation at 800 °C	2305	1.15	1.12	1.64	0.450 L min^{-1}	66.3	238
Plum stone	Direct CO$_2$ activation at 800 °C	697	0.37	0.34	1.09	0.1% NO$_2$, dry air 0.450 L min^{-1}	58.1	239
	Pyrolyzed at 400 °C KOH activation at 800 °C	2570	1.35	1.30	1.17	0.1% NO$_2$, dry air	67	
Pine sawdust pellets	CO$_2$ activation at 800 °C for 60 min	275	0.15	0.14	1.92	0.450 L min^{-1} 0.1% NO$_2$, moist air (70% humidity)	45.3	240
Coffee industry waste	Pyrolyzed at 800 °C KOH activation at 700 °C	1553	1.06	0.76	3.25	0.450 L min 0.1% NO$_2$, moist air (70% humidity)	44.5	241
Wood-based activated carbon BAX-1500	BAX150, impregnation with 5% Ag	1772	1.09	0.41	—	0.450 L min^{-1} 0.1% NO$_2$, dry air	66.0	242

surface reacted differently. Heat treatment increases metallic copper and reduces carbon matrix oxygen functional groups, whereas hydrazine reduces copper and incorporates nitrogen. The data indicates that NO_2 is mostly transformed into copper nitrates, while N_2 reduction is possible. Hydrazine-treated samples have high capacity due to metallic copper dispersion on carbon. Similarly, the impregnation of urea and heat-treated wood-based AC has been reported to positively impact NO_2 adsorption. In dry-air experiments, positively charged nitrogen centers may be involved in electron transfer for NO_2 chemisorption and superoxide ion oxidation to single-bond NO_3.[242]

9. Biomass-based adsorbent for volatile organic compounds removal activated carbon

Volatile organic compounds (VOCs) are a specific category of air contaminants that have garnered significant environmental concern. They are prominent aromatic compounds that are commonly found in industrial processes, including those in the paint and petroleum sectors.[248,249] They have significant biological toxicity resulting in respiratory tract infections, lung cancer, brain damage, and several other disorders.[250,251] Studies have demonstrated that adsorption is a cost-effective and efficient method for treating low levels of VOCs.[248,252,253] Currently, the development of adsorbent from biomass is considered a green strategy for obtaining carbon with functional properties (Table 7). For example, Shen et al.[262] synthesized rice husk-based porous carbon via ball milling and KOH activation. The resulting carbon material exhibited a toluene adsorption capacity of 250.6 mg g^{-1} at 20 °C, significantly higher than the original biochar's adsorption capacity of just 0.72 mg g^{-1}. Jin et al.[267] discovered that utilizing the air pre-oxidation technique in producing nitrogen-rich porous biochar enhanced the efficiency and augmented the toluene sorption capability from 296.4 mg g^{-1} to 437.8 mg g^{-1} at 30 °C.

Guo et al.[268] studied the impact of activated carbon characteristics on removing chlorobenzene. They found that the pore structure of the activated carbon was the primary influencing factor. It has been discovered that benzene and toluene prefer to be adsorbed in the confined micropores of activated carbon.[269] Regarding surface properties, several researchers have posited that certain carbonyl surface groups establish a bond with the aromatic ring of phenol based on a donor–acceptor hypothesis.[270] However, some individuals hypothesized that graphene layers interact with the π electrons of the aromatic ring of phenols, resulting in the presence of electron-rich areas (π–π argument).[271]

The surface acidity of biochar and its enhanced sorption of polar and hydrophilic VOCs are primarily attributed to the presence of oxygenic functional groups.[261] These functional groups, however, have a detrimental effect on the sorption of hydrophobic VOCs by inhibiting the interactions between the hydrophobic VOCs and electron-rich regions of biochar.[256] Chemical functional groups impact dispersive and electrostatic interactions between the biochar and VOCs, mostly through van
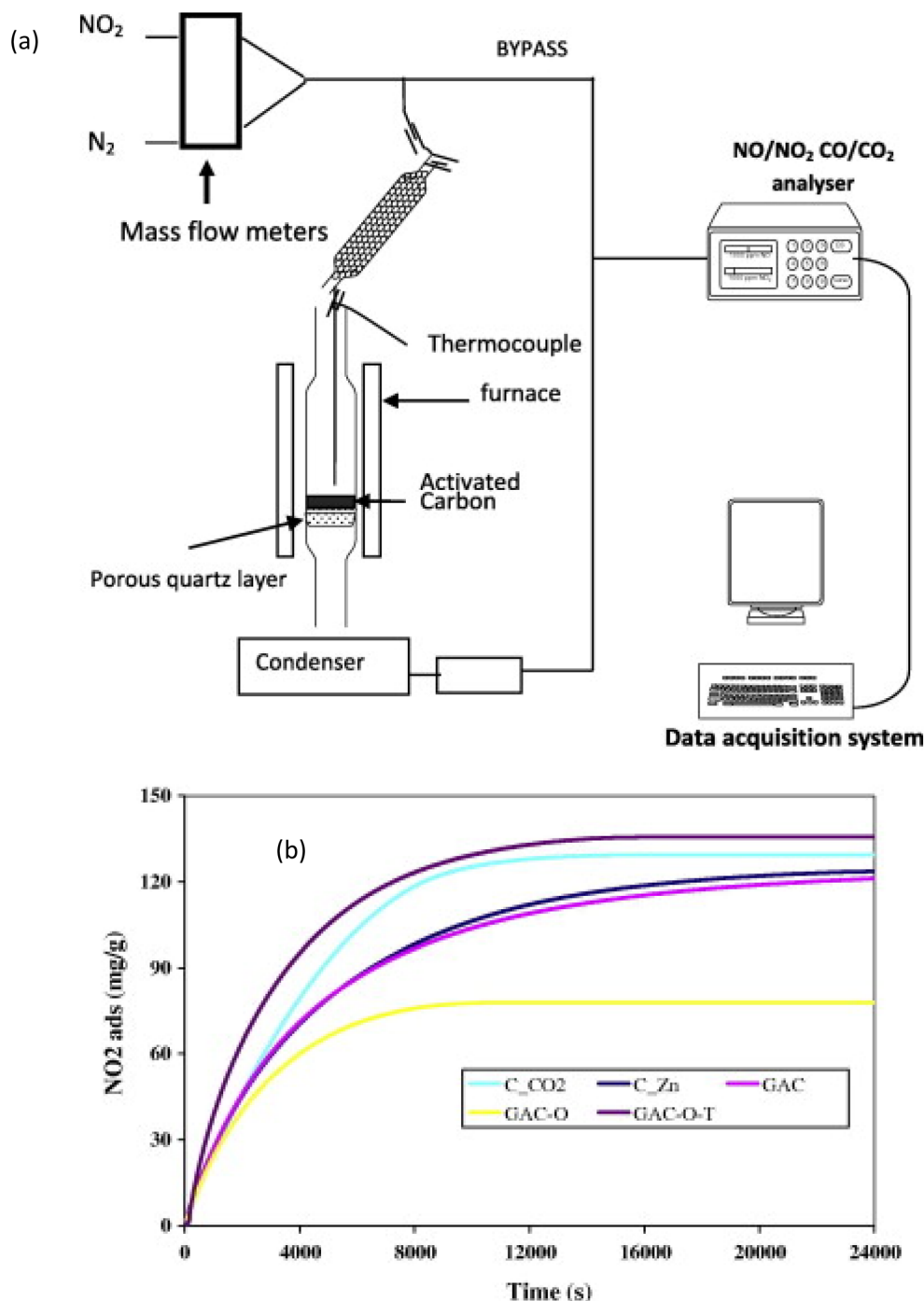
Fig. 5 (a) Scheme of the set-up for the NO_2 adsorption experiments. (b) NO_2 adsorption capacities at 25 °C for the different activated carbons.[245]

der Waals interaction.[272,273] The attractive forces that affect the sorption uptake include π–π dispersion interactions and hydrogen bonding. Hence, it is necessary to take into account the interplay between the pore property, chemical functional group of biomass-based materials, and characteristics of VOCs in order to assess the sorption efficiency of common VOCs.[257] Fig. 6 depicts the primary adsorption mechanism of VOC onto biomass-based materials. Therefore, understanding the sorption process and structural–functional relationship requires

a thorough understanding of the in-depth knowledge of adsorption equilibrium.

This involves physical sorption, which includes surface sorption, pore filling, and partitioning to noncarbonized organic matter. It also involves intermolecular forces such as π–π interaction, CH–π bonding and electrostatic attraction. The sorption characteristics of VOCs are influenced by their molecular sizes, molecular weights, and boiling points.

Table 7 Performance of biomass-based adsorbents for VOC removal

Biomass precursors	Activating conditions	Biochar preparation	Adsorption conditions	Adsorption capacity	Ref.
Bamboo-based biochar	Cu-BTC solvothermal synthesis with biochar of 0.3, 0.6, 0.9 g		FBR. Toluene 500, 1000, 1500, 2000 ppm, N_2; 60, 90, 120, 150 °C	Biochar$_{Cu-BTC}$: toluene: 501.8 mg g^{-1}, 60 °C, 1000 ppm	254
Pistachio Shells	Biomass + melamine, N_2: 700 °C		FBR. Toluene 110 ± 5 mg m^{-3}, 0, 40, 80% humidiy; N_2; 40 °C	88.8 mg g^{-1}, 150 °C, 1000 ppm Biochar$_{melamine}$: toluene: 233 mg g^{-1}, 40 °C	248
Gasification biochar	KOH 1 : 3, 850 °C	—	Gas chromatograph with a flame ionization detector. Benzene 50 ppm; 80 °C	Biochar$_{KOH}$: benzene: 144 mg g^{-1}, 80 °C	255
Hickory wood, peanut hull	H_3PO_4 or KOH : C = 1 : 1, 600 °C	HTC: 200 °C	TGA. VOC (50 mL min^{-1}), N_2; 20 °C	Biochar$_{H_3PO_4}$: acetone: 147.77 mg g^{-1}, 20 °C Cyclohexane: 159.66 mg g^{-1}, 20 °C	256
Milled hickory, wood chips, peanut shell	CO_2: 600, 700, 800, 900 °C	HTC: 200 °C	TGA. VOC (50 mL min^{-1}), N_2; 20, 40, 60 °C	Biochar$_{CO_2}$: acetone 121.74 mg g^{-1}, 20 °C Cyclohexane: 155.41 mg g^{-1}, 40 °C	257
Oxford Hardwood, wheat straw, corn straw, rice straw, rape straw	—	N_2: 300, 400, 500 °C	Bespoke testing system. Xylene isomer (100–400 ppm), N_2; 25, 35, 45 °C	P-Xylene: 50.88 mg g^{-1}, 25 °C M-Xylene: 36.82 mg g^{-1}, 25 °C O-Xylene: 45.37 mg g^{-1}, 25 °C	258
Bamboo, pepper wood, sugarcane	—	N_2: 300, 450, 600 °C	Mass = 5 mg. $T = 150$ °C flow rate = 10 °C min^{-1} under 50 mL min^{-1} N_2 atmosphere	Toluene: 62.91 mg g^{-1}, 20 °C Acetone: 91.16 mg g^{-1}, 20 °C Cyclohexane: 69.33 mg g^{-1}, 20 °C	259
Bagasse, hickory wood, sugar beet tailings					
Hickory wood	Ball milling, 1 : 100	N_2: 300, 450, 600 °C	TGA. VOC (50 mL min^{-1}), N_2; 20 °C	Toluene: ~70 mg g^{-1}, 20 °C. Acetone: 103.4 mg g^{-1}, 20 °C Cyclohexane: 72.5 mg g^{-1}, 20 °C Ethanol: ~65 mg g^{-1}, 20 °C Chloroform: 87.0 mg g^{-1}, 20 °C	260
Neem, sugarcane, bamboo	—	N_2: 350, 450, 550 °C	TGA. Benzene, toluene, methyl chloride, xylene, chloroform, carbon tetrachloride; 120 °C	Benzene: 54.6 mg g^{-1}, 120 °C Toluene: 65.5 mg g^{-1}, 120 °C Methyl chloride: 39.61 mg g^{-1}, 120 °C Xylene: 60.2 mg g^{-1}, 120 °C Chloroform: 30.81 mg g^{-1}, 120 °C Carbon tetrachloride: 40.99 mg g^{-1}, 120 °C	261
Rice husk	Ball-milling, 30 min KOH : C = 1, 3; 750 °C	N_2: 450 °C	FBR. Toluene 300 ppm, phenol 60 ppm; 20 °C	Biochar$_{KOH}$: toluene: 264 mg g^{-1}, 20 °C Phenol: 6.53 mg g^{-1}, 20 °C	262
Oil palm	—	N_2: 500, 600, 700, 800 °C	Batch equilibrium tests. Formaldehyde (0.5, 0.75, 0.9, 2.1 ppm), H_2O 50%; 25 °C	410 mg g^{-1}, 2.1 ppm, 25 °C	263

Table 7 (Contd.)

Biomass precursors	Activating conditions	Biochar preparation	Adsorption conditions	Adsorption capacity	Ref.
Wheat straw, bagasse	—	N_2: 500 °C	Bespoke testing system. Acetone, hexane, toluene, p-xylene (200–220 ppm), N_2; 25 °C	Acetone; 110.9 mg g⁻¹, 25 °C. Toluene: 45.2 mg g⁻¹, 25 °C. p-Xylene: 51.1 mg g⁻¹, 25 °C. Hexane: 36.8 mg g⁻¹, 25 °C. Multi-component: 109.1 mg g⁻¹, 25 °C	264
Corn stalk	Ball milling, 3:200; H_2O_2/NH_4OH	N_2: 600 °C	TGA. VOC (50 mL min⁻¹), N_2; 25 °C	$Biochar_{H_2O_2/NH_4OH}$: benzene: ~118 mg g⁻¹, 25 °C. M-Xylene: ~125 mg g⁻¹, 25 °C. O-Xylene: ~120 mg g⁻¹, 25 °C. P-Xylene: 130.21 mg g⁻¹, 25 °C	265
Coconut shell	Steam: 900 °C	N_2: 900 °C	FBR. Toluene 80 ppm, chlorobenzene, 80 ppm; 25, 30, 40 °C	$Biochar_{H_2O}$: toluene: 255 mg g⁻¹, 25 °C. Chlorobenzene: 272 mg g⁻¹, 25 °C	266

Li et al.[274] investigated five common straws as potential materials for preparing straw-based activated carbon (SAC) and characterized them using a scanning electron microscope, thermo-gravimetric analysis, and the Brunauer–Emmett–Teller method. Millet straw-derived activated carbon shows superior properties in S_{BET}, S_{mic} and adsorption capacities of both toluene and ethyl acetate. The preparation process of millet straw activated carbon was optimized via response surface methodology, using carbonization temperature, carbonization time, and impregnation ratio as variables and toluene adsorption capacity, ethyl acetate adsorption capacity, and activated carbon yield as responses. The optimal preparation conditions include a carbonization temperature of 572 °C, carbonization time of 1.56 h and impregnation ratio ($ZnCl_2$/PM, w/w) of 1.60, which was verified experimentally, resulting in millet straw activated carbon with a toluene adsorption capacity of 321.9 mg g⁻¹ and ethyl acetate adsorption capacity of 240.4 mg g⁻¹. Meanwhile, the adsorption isothermals and regeneration performance of millet straw-activated carbon prepared under the optimized conditions were evaluated. The descriptive ability of the isothermals via the Redlich–Peterson equation suggests a heterogeneous surface on millet straw-activated carbon. Recyclability testing has shown that millet straw-activated carbon maintained a stable adsorption capacity throughout the second to fifth cycles. The results of this work indicate that millet straw-activated carbon is a potential volatile organic compound adsorbent for industrial application.

Hierarchical porous carbons (HPCs) derived from biomass were produced using a cost-effective method that integrates pyrolysis and KOH impregnation.[275] The maximum surface area of HPCs reaches 3936 m² g⁻¹, demonstrating unprecedented acetone (26.1 mmol g⁻¹ at 18 kPa) and methanol (46.9 mmol g⁻¹ at 15 kPa) sorption capacities at 25 °C. Experimental and molecular modeling results indicate that the overall pore volume predominantly influences the sorption capacity of acetone and methanol at elevated pressures. Due to the electrostatic interactions between the gaseous molecules and carbon frameworks, the oxygen groups offer sorption sites for acetone and methanol at low pressure. The small micropore influences acetone/methanol selectivity at low pressure, but the oxygen groups do not enhance this selectivity. Kim et al. enhanced activated carbon by impregnating it with diverse acids or bases. The findings indicated that activated carbon modified with 1 wt% H_3PO_4 exhibited the highest adsorption capacity for toluene and benzene, representing a potential hybrid system sorbent for mitigating low-concentration VOC emissions.[276]

Shen et al. reported an exceptional carbon adsorbent developed from corncobs using KOH as an impregnating agent for the selective sorptive removal of VOCs in humid environments.[277] The carbon sorbent derived from corncobs demonstrated superior sorption capacities for volatile benzene (851.3 mg g⁻¹) and toluene (854.9 mg g⁻¹), significantly surpassing those obtained from KOH grinding methods, which are three times greater than commercial activated carbon (benzene 275 mg g⁻¹, toluene 310.5 mg g⁻¹). It was then established that the optimized structural characteristics of the

synthesized adsorbent exhibited a strong association with the sorption effectiveness of VOCs.

Coconut shell-based carbons were impregnated with phosphoric acid, ammonia, sulfuric acid, sodium hydroxide, and nitric acid to identify optimal modifications for enhancing the sorption capacity of hydrophobic VOCs on granular activated carbons (GAC).[278] The results indicated that alkali-impregnated GAC exhibited superior *o*-xylene adsorption ability. The uptake quantity increased by 26.5% and decreased by 21.6% following treatment with NH_3H_2O and H_2SO_4. In comparison to the original, acid-impregnated GAC exhibited reduced adsorption capability. Other authors have reported that the impregnation method modified and enhanced the sorption ability of adsorbent for removing VOCs.[279–283]

10. Biomass-based adsorbents for multi-gas removal

To date, there are limited studies on the adsorptive removal of multi-gas components using biomass-based adsorbents. Table 8 provides an overview of the preparation conditions of biomass sorbents and their corresponding performance for multigas removal. The palm shell-activated carbon coated with metal oxides was used to simultaneously remove SO_2 and NO_x. It demonstrated an increased in sorption capacity in the order $Fe_2O_3 < NiO < V_2O_5 < CeO_2$.[156] The metal oxides with strong oxidizing and oxygen retention capabilities added new oxygenic functional groups, such as C–O, COOH, and C=O, to the obtained adsorbent. This enhances the oxidation reaction of NO to NO_2, and SO_2 to SO_3, resulting in a highly effective removal of NO_x and SO_2.[156] It has been discovered that the biochar amine obtained from the feedstock of peanut shells, corn stalks, and corncobs had a significantly higher capacity for removing SO_2 in the presence of both NO and SO_2 compared to when NO was absent.[192] The SO_2 removal capacity initially increased and then decreased as the NO concentration increased. The maximum sorptive removal capacity was observed at 120 °C and 500 ppm NO, reaching 216.19 mg g^{-1}. The interaction between SO_2 and NO takes place, particularly at the N-containing sorption sites of biochar during the sorption process (Fig. 7). This interaction could potentially lead to creating $(SO_3)(NO_2)$ intermediates.[192]

Another study reported the competitive adsorptive removal of NO and SO_2 onto the active sites of biochar produced from palm shell activated carbon supported with cerium. It was demonstrated that molecules with a high boiling point have stronger intermolecular interactions and van der Waals attractive forces. Therefore, biochar efficiently adsorbs SO_2 relative to NO_x because SO_2 has a high boiling point than NO_x.[156,292] Elevating the concentration of SO_2 (up to 2500 ppm) could effectively displace and remove the NO from the active sites on the biochar thereby limiting the sorption of NO.[189] In addition, the flue gas exhibited a much greater concentration of NO (up to 700 ppm) compared to that of SO_2, resulting in a more pronounced catalytic bonding of NO on the active sites of biochar supported with cerium. Consequently, it decreased the number of active sites available for the removal of SO_2.[189]

The simultaneous adsorption of NO and SO_2 onto cerium-impregnated palm shell-activated carbon (Ce/PSAC) sorbent has been reported.[285] In the presence of 15% H_2O, the water layer contained a higher concentration of NO_2 molecules due to NO_2 being more soluble in water and having stronger oxidizing properties than O_2 and NO. As a result, the reactions between NO_2 and HSO_3^- and SO_3^{2-} to form SO_4^{2-} were enhanced. Consequently, more SO_2 molecules were captured into the water
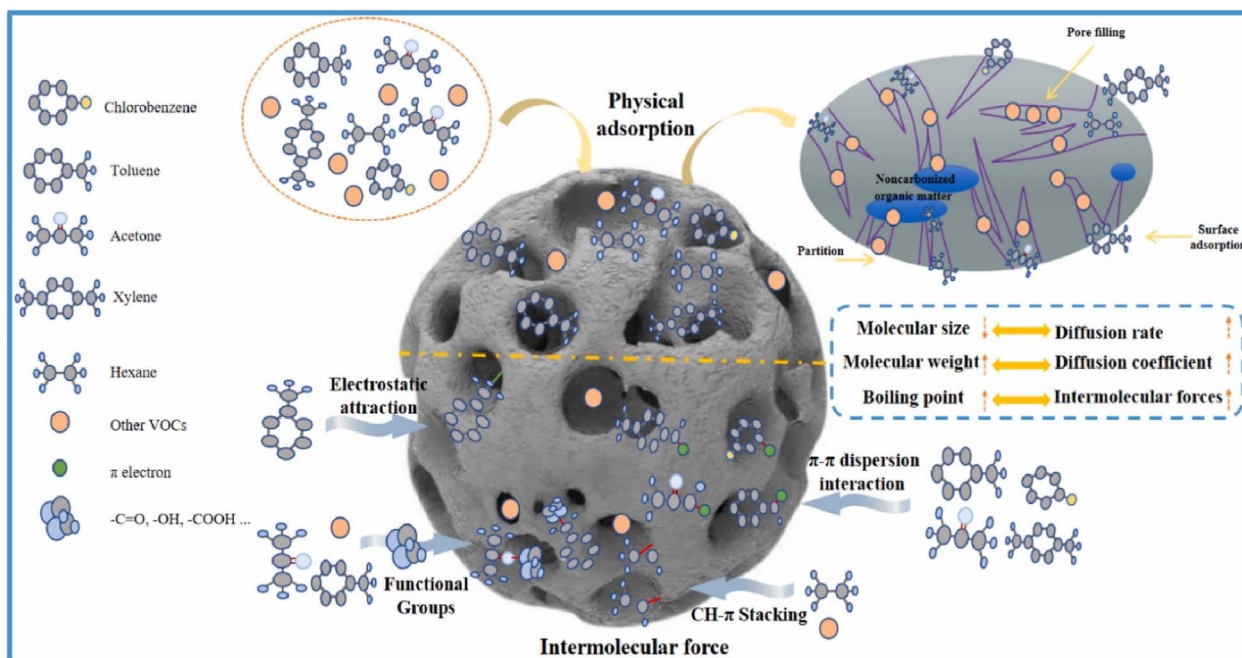

Fig. 6 Adsorption mechanism of VOCs onto biomass/biochar.

Table 8 Performance of biomass-based adsorbent for multi-gas removal

Biomass precursors	Biochar preparation	Activating conditions	Adsorption conditions	Typical adsorption capacity	Ref.
Palm shell	N_2; ~700 °C	CO_2; 1100 °C	FBR. SO_2 2000 ppm, NO 500 ppm, O_2 10%, N_2; 100, 200, 300 °C	SO_2: biochar$_{Ce}$, ~180 min (breakthrough time), 200 °C; NO_x: biochar$_{Ce}$, ~170 min, 200 °C	284
Palm shell	N_2; ~700 °C	Ni, Ce: 5%	FBR. SO_2 2000 ppm, NO 500 ppm, O_2 10%, N_2; 100 °C	SO_2: biochar$_{Ce}$, 155 min, 100 °C; NO_x: biochar$_{Ce}$, 65 min, 100 °C	156
Palm shell	N_2; ~700 °C	Ni, V, Ce, Fe: 10%; CO_2; 1100 °C	FBR. SO_2 (1000, 1500, 2000, 2500 ppm), NO (100, 300, 500, 700 ppm), O_2 10%, N_2; 150–300 °C; GHSV: 23 527 h^{-1}	Biochar$_{Ce}$: 2500 ppm SO_2/700 ppm NO: SO_2, 120.25 mg g^{-1}, 150 °C; NO, 3.52 mg g^{-1}, 150 °C	189
Palm shell	N_2; ~700 °C	Ce: 10%; CO_2; 1100 °C	FBR. SO_2 (500–2500 ppm), NO (100–700 ppm), H_2O (15, 30, 45, 60%), O_2 10%, N_2; 100–300 °C; GHSV: 14 000–36000 h^{-1}	Biochar$_{Ce}$: 2000 ppm SO_2/500 ppm NO: SO_2, 121.7 mg g^{-1}, 150 °C; NO, 3.46 mg g^{-1}, 150 °C	285
Rice husk	N_2; 600 °C	Ce: 10%; NH_4Cl, NH_4Br: 1%, 2%	FBR. Hg (33 μg m^{-3}), SO_2 1000 ppm, NO 200 ppm, O_2 10%, N_2; 150 °C; GHSV: 23 527 h^{-1}	Biochar$_{NH_4,Br}$: FBR. Hg 30 μg g^{-1}	286
Food waste	N_2; 500, 700 °C	CO_2; 900 °C; HNO_3: 1:10; melamine: N_2 450 °C	SVA. CO_2, 25 °C, 0–101 kPa. Gravimetric sorption. Benzene; 25, 35, 45 °C. Coal-fired flue gas, 150 °C	Flue gas (SO_2 1177 ppm, NO 254 ppm): Hg 80%, SO_2 ~35%, NO ~35%, 150 °C; Biochar$_{melamine}$: CO_2: 4.41 mmol g^{-1}, 25 °C	287
Maize straw	N_2; 750 °C	$ZnCl_2$; 1:1; Co/Ce:C = 5, 15, 25% (Co:Ce = 4:6, 5:5, 6:4); N_2 550 °C	FBR. Hg (100 μg m^{-3}), SO_2 1000 ppm, NO 600 ppm, NH_3 600 ppm, O_2 6%, N_2; 80–320 °C; GHSV: 100 000 h^{-1}	Benzene: 380.7 mg g^{-1}, 25 °C; Biochar$_{Co/Ce}$: NO: 84.7%, 230 °C	288
Pinecone	N_2; 500 °C	H_2O_2; 10:1; Cu/Mn:C = 8, 12, 14% (Cu/Mn = 1-3:1, 1:2-5); N_2 500 °C	FBR. Hg (700 μg m^{-3}), HCHO 100 ppm, SO_2 (400, 800 ppm), NO_x (300, 600 ppm), NH_3 300 ppm, O_2 5%, N_2; 100–300 °C; GHSV: 13 000 h^{-1}	Hg^0: 96.8%, 230 °C; Biochar$_{Cu,Mn}$: HCHO: 89%, 175 °C	289
Walnut shell	N_2; 500–900 °C	KOH: 2:1, N_2; 600 °C; Al, Cu, Fe, Mn: 5%	FBR. Hg (100 μg m^{-3}), SO_2 200 ppm, NO_x 300 ppm, NH_3 300 ppm, O_2 5%, N_2; 150 °C. GHSV: 10 000 h^{-1}	Hg: 83%, 175 °C; Biochar$_{Fe}$: SO_2 100%, 250 °C; NO_x ~90%, 300–400 °C; Hg ~90%, 250 °C	290
Rice straw	Ball milling; 1 (Fe/Mn = 1.1–2.0); N_2 800 °C	—	FBR: Hg (35 μg m^{-3}), o-Xylene 20 ppm, O_2 5%, N_2; 100–350 °C; GHSV: Xylene 30 000 h^{-1}, Hg^0 90 000 h^{-1}	Biochar$_{Fe/Mn}$: o-Xylene: ~88%, 100 °C; ~75%, 350 °C; Hg: ~96%, 100 °C; ~72%, 350 °C	291

layer, leading to an overall increase in the removal of SO_2 compared to the scenario where the simultaneous removal of NO was not considered.[285]

Recently, Qin *et al.* prepared a defective walnut shell-based carbon that was modified with transition metal (Fig. 8). The removal efficiencies of SO_2, NO_x, and Hg^0 onto the prepared adsorbent varied as the carbonization temperature increased. This change was due to the impact of the carbonization temperature on the porous characteristics and surface defects of the adsorbent (Fig. 8a–d). Carbonizing at 700 °C significantly increased the degree of graphitization, the presence of a rich pore structure, and the contents of surface defects in the adsorbent compared to other temperatures. This enhancement was advantageous for the loading and dispersion of the active constituents of Fe species, thereby affecting the adsorbent activity for the simultaneous removal process.[290] The DFT simulation demonstrated a significant sorption interaction between Mn and Fe species and NO_x, SO_2, and Hg^0 (Fig. 8f–i). This indicates that biochar Fe/Mn has a higher simultaneous removal effectiveness of about 80% at temperatures ranging from 300 to 350 °C.[290] When biochar sorbents were introduced into coal-fired flue gas at a temperature of 150 °C in an entrained-flow reactor, almost 80% of gaseous mercury was eliminated. Additionally, the SO_2 concentration was reduced by 35.6% while that of NO decreased by 36.0%.[290]

Similarly, the presence of 6% O_2 and 10% H_2O has been reported to have a beneficial effect on the oxidation reactions of SO_2 to SO_3 and H_2SO_4, as well as the oxidation of NO to NO_2.[286] An inconsistent impact of SO_2 was seen in the elimination of Hg^0. Specifically, low levels of SO_2 appeared to enhance its removal, whereas high levels of SO_2 (above about 700 ppm) had an inhibitory effect.[293] When both SO_2 and NO are present, SO_2 consumes the active oxygen and produces sulfate, which causes permanent damage to the active sites on the adsorbent. As a result, the interaction between Hg^0 and NO_2, which was generated from NO, becomes impeded by SO_2.[294] Gao *et al.* found that the presence of adsorbed SO_2 can hinder the adsorption of NO, NH_3, and Hg^0 through competitive inhibition.[288] The combined impact of SO_2 and H_2O had a more detrimental effect as their competing adsorption and the formation of ammonium sulfates led to the degradation of the porous structure and the obstruction of the active sites on the adsorbent.

Sumathi *et al.* simultaneously removed both NO_x and SO_2 by impregnating coconut shell-AC with KOH.[295] Moreover, the activated carbon may penetrate the pore structure with the addition of potassium, markedly improving the efficacy of NO_x and SO_2 reductions due to its surface's heightened reactivity. The simultaneous elimination of SO_2 and NO from simulated flue gas with cerium oxide supported on palm shell AC (Ce/PSAC) was investigated in a fixed bed adsorber.[285] The influences of adsorber temperature, humidity present, feed gas concentration, and space velocity were examined as process parameters. The experimental results indicated that increased space velocity decreased the sorption capacity of SO_2 and NO. Humidity increased the SO_2 sorption capacity but inhibited NO sorption at levels exceeding 15%. Temperature significantly influenced the simultaneous elimination of SO_2 and NO by cerium supported on PSAC. The q_{max} of SO_2 and NO were attained at a temperature of 150 °C, measuring 121.7 mg g^{-1} and 3.5 mg g^{-1}, respectively. This demonstrates that inexpensive biomass-derived AC may serve as an effective sorbent for the simultaneous removal of SO_2 and NO from flue gas.

A highly efficient porous carbon filter for indoor air pollutant removal was created utilizing NaOH-impregnated AC (NaOH/AC) for the sorption of H_2S and CH_3COOH.[296] The NaOH/AC filter was studied using several methods, demonstrating favorable physical and chemical features, particularly the presence of –OH functional groups, for the sorption of air contaminants. The NaOH/AC filter was subjected to various curing temperatures and dwell periods to analyze the impact of curing conditions on sorption efficacy. The optimal performances were achieved with the NaOH/AC filter cured at 100 °C for 20 min, effectively removing the starting concentration of 400 ppm of CH_3COOH within 15 min and H_2S within 30 min at 20 °C and 60% relative humidity. Isotherm and kinetic models were employed to examine the sorption process. Both the Langmuir isotherm and pseudo-second-order kinetic models exhibited
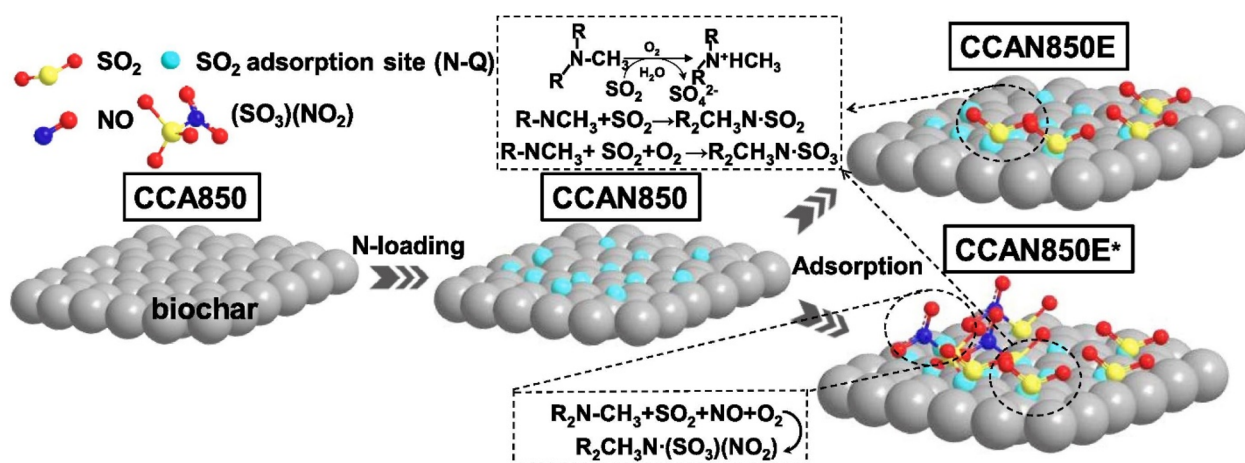

Fig. 7 Schematic representation of the adsorption of SO_2 onto nitrogen content of biochars.[192]

the most accurate fit for the sorption of CH_3COOH and H_2S on the NaOH/AC filter. The sorption process was governed by intraparticle diffusion in conjunction with film diffusion. The NaOH/AC filter exhibited a q_{max} of 473 mg g^{-1} for H_2S and 550 mg g^{-1} for CH_3COOH. The wasted NaOH/AC filter was regenerated for subsequent usage.

11. Regeneration studies

In an industrial application, regenerating used biomass adsorbent is essential for a successful adsorption–desorption process and it is important to strive for a lower regeneration temperature and a short cycle duration. The quick kinetics process is advantageous for reducing the duration of the adsorption cycle.
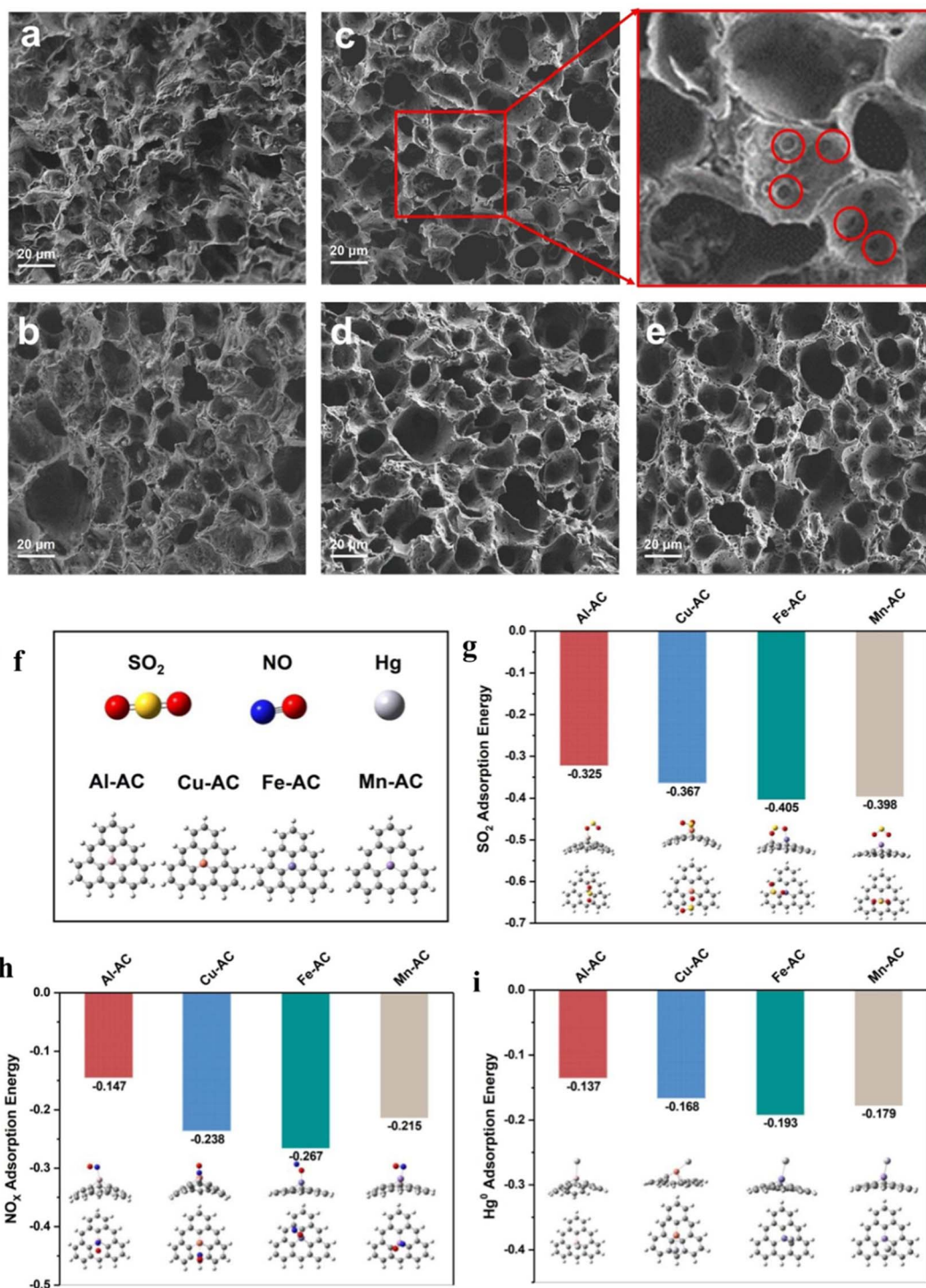

Fig. 8 SEM images at (a) 500 °C (b) 600 °C (c) 700 °C (d) 800 °C (e) 900 °C. (f–i) Molecular structures and energy states of SO_2, NO_x and Hg^0 adsorbed on walnut shell-based carbon.[290]

Increased chemisorption strength hinders the regeneration of biomass adsorbent, necessitating higher regeneration or desorption temperatures and resulting in greater energy consumption.[297]

Atanes and colleagues[298] discovered that the SO_2 removal onto acidic biomass adsorbents by physisorption may be easily regenerated for several sorption cycles. It has been observed that heat treatment mostly impacted the physical structure of the used adsorbent.[299] During this process, H_2SO_4 that had been adsorbed onto the biomass was eliminated, resulting in a reduction in carbon content. A comparison of the two different treatments has been experimented.[300] It was found that approximately half of the adsorbed SO_2 was regenerated after the first cycle. Additionally, low treatment temperatures resulted in greater levels of residual sulfur which led to a drop in SO_2 sorption. The efficacy of SO_2 sorption decreased as the number of regeneration cycles increases to the third time, due to the degradation of pore texture and active adsorption sites.[301]

The effectiveness of biomass H_2O regeneration during 6 cycles has been reported.[299] It was discovered that the pore structure of biomass changed after the regeneration cycles leading to a moderate increase in both micropore volumes and surface areas starting with the fourth cycle. In addition, the acid surface that resulted from SO_2 adsorption was broken down during the desorption test at 600 °C. This process creates new basic surfaces which may enhance the ability of the biomass to adsorb more SO_2 compared to its initial state. Surprisingly, these two factors resulted in increased SO_2 adsorption capabilities during the fourth–sixth cycles compared to the first-thirdcycles.

Two primary types of adsorption technology considered suitable for capturing CO_2 in post-combustion processes and can be used to effectively regenerate the adsorbents involve temperature swing adsorption (TSA) and pressure swing adsorption (PSA), or in certain cases, vacuum swing adsorption (VSA).[50] The biomass may be easily regenerated by either raising the temperature in the TSA process or lowering the system pressure in the PSA process.[302] Nevertheless, implementing a traditional PSA method to compress the flue gases with a higher flow rate would be impractical and challenging due to its lack of cost-effectiveness. A pressure level of 5 kPa was found to be a suitable lower pressure during the desorption stage of CO_2 to keep operation expenses low.[302] In contrast, the regeneration of adsorbent with a high concentration of CO_2 by increasing the temperature of the reactor in the TSA process has been reported.[50] This may be readily accomplished using the heat generated by an operating industrial facility through the addition of a heating exchanger.[50] Due to a weak interaction between the biomass and CO_2, the energy requirement for its regeneration is low. This process has been widely observed in various studies.[50,134,138]

Most reported biomass can be easily and quickly regenerated over multiple cycles without a significant decrease in their sorption capacity and these are achieved through the TSA process[81,134,303] or the PSA process.[151,303–305] The sorbent's excellent reusability indicates that the physisorption process was the main mechanism. The decrease in CO_2 capture efficiency *via* cyclic processes may be attributed to diminished surface activity, agglomeration, and insufficient regeneration of the adsorbent.[306] It is important to note that the CO_2 uptake in the spent biomass adsorbent may be used immediately for soil amendment and for carbon storage. Under normal soil and atmospheric temperature, the CO_2 will not escape (leak). Therefore, there is no need to regenerate the biomass for an extended period of time.[147]

A study by Zhang *et al.*[256] showed that the temperature of desorption of acetone on biomass was less than that of cyclohexane due to the higher porosity, numerous functional groups on the biomass, and the characteristics of VOCs. The VOCs that are absorbed in the small micropores typically necessitate a high temperature for desorption. Also, the hydrochar H_3PO_4 which has an excess of oxygenic functional groups could enhance the adhesion force with hydrophilic acetone. In addition, the adsorbate with a higher boiling point possesses a stronger attraction to the sorbent thereby explaining that cyclohexane has high boiling point than acetone and is more challenging to desorb. After the 5 cycles, about 90% of the acetone's adsorption capacity was retained, whereas cyclohexane had 83.30% of its capacity retained.[257] In another findings, there was a decrease of just 2.5% in cyclohexane and 0.9% in acetone throughout the past four cycles.[256] The significant reduction in the adsorption capacity of VOCs during the initial cycle might be ascribed to either the partial release of VOCs due to their strong affinity for biomass,[259] or the formation of persistent bonds that require higher temperatures to break them.[265,273]

Literature studies demonstrate that impregnation is not only an efficient option for viable adsorbents in gaseous adsorption but also cost-effective due to its superior regeneration capacity. Therefore, evaluating their influence on adsorbent regeneration cannot be overemphazied. For example, the research conducted by Creamer demonstrated that aluminium-impregnated cotton-wood AC has a 99% regeneration capacity, in contrast to magnesium at 96% and iron at 90%.[307] In another study,[151] X-ray Photoelectron Spectroscopy (XPS) was employed to determine the stability of the regenerated sorbent, and it was ascertained that the elemental and chemical composition of the regenerated sorbent remained mostly unaltered, having q_{max} of 5.45 mol kg^{-1}. It may, therefore, be inferred that after more than 20 cycles, the elevated desorption temperature (673 K) diminishes the number of active sites and compromises the adsorbent's surface integrity. On the other hand, a thin layer shape using SEM analysis on the surface of Mg-based biomass AC indicates surface degradation during several cyclic sorption processes.[308]

The use of dual adsorption sites on metal-impregnated biomass AC could further enhance CO_2 selectivity.[309] For instance, metal ions with hydroxyl groups were used to impregnate biomass,[310] demonstrating that the resultant sorption exceeded that of a singular site. Here, Metal–Organic Frameworks (MOFs) containing a hydroxyl group derived from Mg, Zn, and Cu were reported to exhibit remarkably rapid adsorption kinetics, with gravimetric CO_2 adsorption capacities of 0.08, 0.13, and 1.24 mmol g^{-1}, and CO_2/N_2 selectivity of 182, 1700, and 2000, respectively. The efficacy of CO_2 sorption was significantly enhanced by the integration of these two adsorption sites. The adsorption capacity of a nickel-based biomass sorbent has been developed[311] to exhibit 5.22 mmol g^{-1} at 25 °C,

surpassing the capacity of commercial AC (3.37 mmol g^{-1}) at ambient temperature. Mg-based MBAC has been used for post-combustion CO_2 collection in binary mixed conditions, achieving a CO_2 adsorption capacity of 5.87 mmol g^{-1} at 25 °C.[312] It has superior CO_2 selectivity compared to N_2 gas. Metal oxides exhibit significant sensitivity to certain gases and are more stable than other precursors.[313] However, investigations indicate that metal oxides alone exhibit poor selectivity for certain gases while possessing a greater surface area.[314] Nonetheless, the drawback of metal oxide can be mitigated by impregnating it with carbonaceous biomass materials.

12. Density function theory calculation and molecular dynamics studies

Density functional theory (DFT) is a renowned computational chemistry technique that can be used to investigate micro-mechanisms at the molecular level. This is useful for understanding the interaction between small molecules and the adsorbent surface in the process of gas adsorption.[315,316] For instance, Rafizah Rahamathullah et al.[317] conducted an integrated study combining DFT simulations and CO_2 adsorption experiments using biochar derived from desiccated coconut waste (amine-biochar@DCW). The study introduced a new class of amine-functionalized biochar as potential CO_2 adsorbents. Among the tested materials, triethylenetetramine (TETA)-biochar@DCW exhibited the highest CO_2 adsorption capacity at 61.78 mg g^{-1}. Before the experiments, DFT simulations were performed using the B3LYP/6-31G (d,p) level of theory to analyze the energy band gap, global chemical reactivity descriptors (GCRD), and molecular electrostatic potentials (MEP). The simulated data showed that TETA-biochar@DCW had the lowest HOMO–LUMO gap of 2.7890 eV before adsorption, which increased after CO_2 was adsorbed. The 3D MEP plots also highlighted TETA-biochar@DCW as a highly reactive adsorbent for CO_2. The combined theoretical and experimental results suggest that amine-biochar@DCW, particularly the TETA-functionalized variant, is a cost-effective and efficient material for CO_2 capture, demonstrating great potential as a sustainable adsorbent.

Marziyeh Ahmadi et al.[318] studied the improvement of CO_2 adsorption using activated carbon modified with lithium hydroxide (LiOH). Their research focused on how operating conditions and the properties of the adsorbent affect performance. Experimental findings suggest that the structure of activated carbon can be approximated as a fullerene made up of heptagonal and pentagonal rings.[319] A model fullerene containing 28 carbon atoms (C28) was designed and analyzed to represent this structure in simulations, as shown in Fig. 9a. Using DFT calculations, the study revealed that in its optimal configuration, the C_{28} structure adsorbs CO_2 molecules at a distance of 3.3 Å, with a binding energy of approximately 0.06 eV. The adsorption occurs mainly at the heptagonal faces on the top and bottom of the structure. In contrast, the pentagonal faces showed weaker CO_2 adsorption. The C_{28}

model is considered the smallest simulated structure for activated carbon, with a diameter of about 5.33 Å, and bond lengths ranging between 1.39 Å and 1.56 Å. Fig. 9b illustrates the distribution of electrical charges in the C_{28} structure using the Mulliken scale.[320] Further modeling indicated that applying pressure reduces the distance between CO_2 molecules and the C28 structure, thus enhancing adsorption. LiOH nano-structures were also introduced to improve CO_2 adsorption performance. Fig. 9c shows the periodic arrangement of LiOH crystals. To compare the effects of LiOH with the AC model, smaller LiOH structures of similar dimensions were designed. This approach avoided periodic boundary condition calculations as LiOH particles were modeled as free-standing structures, allowing for high-accuracy Gaussian functions.

The study concluded that combining AC and LiOH nano-structures significantly improves CO_2 adsorption. DFT simulations modeled the adsorption behaviour based on binding energy and evaluated the performance of hybrid systems composed of AC and LiOH structures. The findings highlight that LiOH nanoclusters enhance the surface interactions of materials, optimizing the adsorption process and increasing the overall efficiency of the hybrid system ($C_{28} + Li_4(OH)_5 + CO_2$) recorded 0.13 eV and 2.4 Å for binding energy (eV), distance of CO_2 from the adsorber (Å), respectively, exhibited superior CO_2 adsorption capabilities while $C_{28} + CO_2$ recorded 0.06 eV and 3.3 Å corroborating the experimental findings and highlighting the synergistic effects of combining AC with LiOH.

Furthermore, Lihua Deng et al.[321] investigated the CO_2 adsorption properties of straw-based biochar prepared through multi-step KOH activation, focusing on the structure-effect relationship under atmospheric and pressurized conditions. The study analyzed the CO_2 adsorption capacity of KOH-activated biochar, and the adsorption performance of different sites at atmospheric pressure is illustrated in Fig. 10c. At 0 °C, larger nanopores (0.7 nm) and nitrogen-containing functional groups were the primary contributors to CO_2 adsorption (Fig. 10(c1)). At 25 °C, smaller nanopores (0.5 nm) and oxygen-containing groups dominated adsorption (Fig. 10(c2)), though the oxygen-containing groups showed no significant difference in adsorption capacity at different temperatures. These findings are critical for designing high-performance CO_2 adsorbents with targeted properties.

A slit pore model was constructed with pore sizes ranging from 0.1 to 2.0 nm, and the equilibrium results of the system are shown in Fig. 10(d1–d9). At a pore size of $D_{eff} = 0.1$ nm, CO_2 diffusion into the pores was restricted, causing molecules to cluster around the pore openings. As pore size increased, CO_2 molecules showed a stronger tendency to adsorb on the carbon wall's surface, transitioning from monolayer adsorption to bilayer adsorption. At 0.5 nm, the transition between monolayer and multilayer adsorption was observed (Fig. 10(d9)). Additionally, as pore size increased, the mass density of CO_2 in the pores decreased (Fig. 10(d8)), which explains why ultramicro pores are the primary storage sites for CO_2 under atmospheric conditions.

To evaluate the adsorption energy of various carbon structures, the study created models of intrinsic carbon, defective

carbon, and structures incorporating hydroxyl and N-5 groups, as determined from earlier analyses. Simulation results revealed that CO_2 molecules tend to align either parallel or perpendicular to carbon surfaces for adsorption, as shown in Fig. 10a. Differential charge calculations (Fig. 10b) indicated that modifying the carbon structure with heteroatoms, such as nitrogen and oxygen, enhances CO_2 capture. Adsorption energy increased from[322] (pure carbon) to −0.215 eV, −0.260 eV, and −0.229 eV for carbon structures with heteroatoms. Adding heteroatoms improved the carbon surface's electronegativity, increasing CO_2 adsorption. Nitrogen-containing groups acted as Lewis bases, modifying the charge distribution to enhance adsorption, while oxygen-containing groups strengthened hydrogen bonding between the carbon surface and CO_2 molecules. Hydroxyl and N-5 groups showed greater electron transfer than pure carbon, further improving CO_2 capture efficiency, as shown in Fig. 10b. The doping of nitrogen (N) and oxygen (O)

atoms into the carbon substrate modifies the charge distribution, increases the polarity of carbon atoms, and enhances the local electron density in regions rich in N, O, and C. This creates more effective adsorption sites for CO_2. These findings provide valuable insights into optimizing biochar's pore structure and tailoring the carbon surface's chemical properties to enhance CO_2 adsorption capacity. Under pressurized conditions, the CO_2 adsorption capacity of biochar is positively correlated with its total pore volume. However, at atmospheric pressure, the optimal adsorption sites differ based on temperature. At 25 °C, ultramicro pores (0.5 nm) and oxygen-containing functional groups dominate adsorption, whereas, at 0 °C, ultramicro pores (0.7 nm) and N-5 functional groups play a key role. Simulation results further indicate that the transition from monolayer to bilayer adsorption occurs at a pore size of 0.5 nm. Both oxygen- and nitrogen-containing functional groups effectively enhance
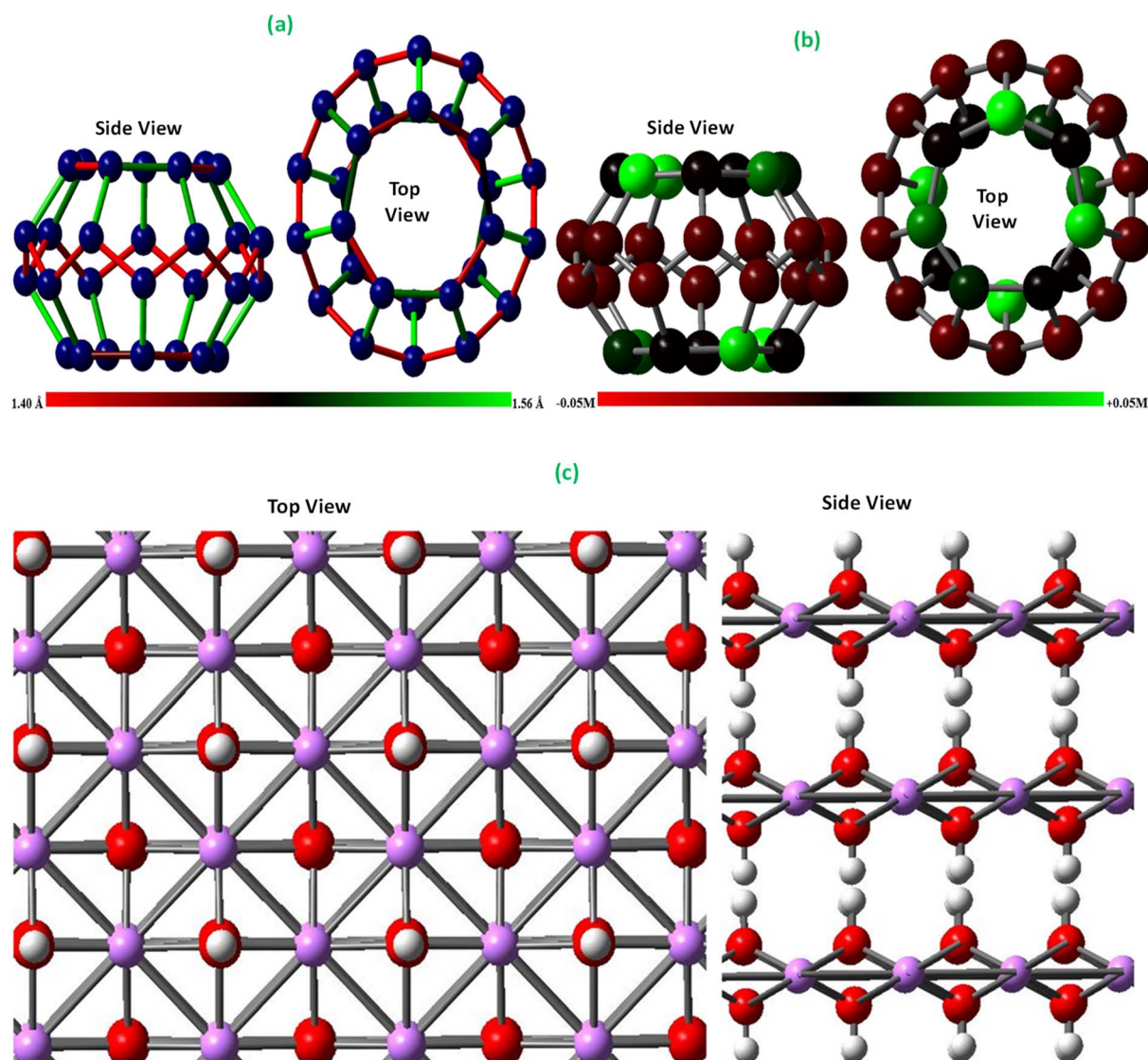

Fig. 9 (a): Modeled structure of AC with chemical formula C_{28}, which fullerene includes pentagonal and heptagonal rings; (b): the electric charge distribution of the C_{28} structure on the Mulliken scale; (c): LiOH crystal structure showing the top and side view.[318]

the CO_2 adsorption capacity of biochar, making them critical for improving adsorption performance.

Yang *et al.* studied the adsorption properties of seaweed-based biochar for greenhouse gases (CO_2, CH_4, N_2O) using DFT.[323] Different models of seaweed-based biochar were constructed and the interactions with greenhouse gases were analyzed through structural parameters, adsorption energy, charge transfer, and surface electronic properties. The study found that biochar doped with nitrogen (N) and oxygen (O) heteroatoms exhibited improved adsorption performance. By calculating the lowest energy configurations for various adsorption sites (*e.g.*, top site and side site) and molecular orientations of greenhouse gases, the most stable adsorption configuration of greenhouse gas molecules on biochar (BC) is presented in Fig. 11a. The results of multiple linear regression analysis are shown in Fig. 11b, where the red dots represent

adsorption energy data obtained from the analysis above. In contrast, the black dots represent adsorption energy data from a different N-doped biochar system calculated separately to validate the accuracy of the regression model. These findings suggest that parameters such as $V_{s,max}$, lowest occupied molecular orbital (E_{LOMO}), and ΔE_{gap} can serve as reliable descriptors for the preliminary screening of biochar material models with high greenhouse gas adsorption energy.

The results also showed that biochar was more sensitive to CO_2 and N_2O than CH_4. Specifically, the adsorption energies for CO_2 and N_2O on N-doped biochar increased by 58.1% and 21.4%, respectively. Additionally, quantitative structure–activity relationships were developed, linking the adsorption energy of greenhouse gases to key electronic properties of the biochar surface. The electrostatic potential, the energy of the E_{LOMO}, and the energy gap (ΔE_{gap}) of α orbitals showed a strong linear
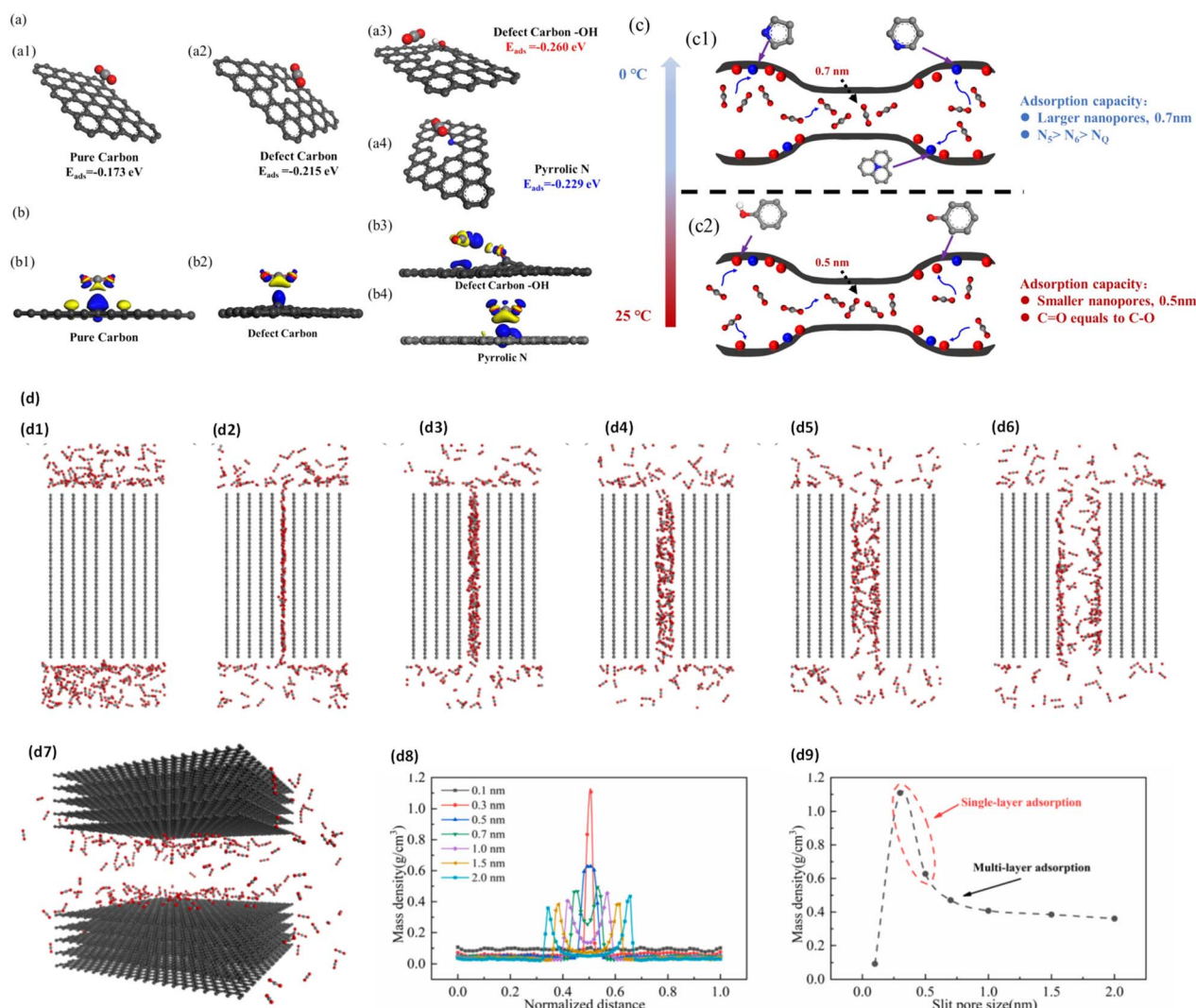

Fig. 10 Adsorption energies of CO_2 on (a1) pure carbon, (a2) defect carbon, (a3) defect carbon −OH, (a4) defect carbon + pyrrolic N; (b) differential charge density of CO_2 capture on (b1) pure carbon, (b2) defect carbon, (b3) defect carbon −OH, (b4) defect carbon + pyrrolic N (c): adsorption of CO_2 by adsorption sites at different temperatures: (d) diffusion of CO_2 in slit pore models with different effective pore sizes (d1) 0.1 nm, (d2) 0.3 nm, (d3) 0.5 nm, (d4) 0.7 nm, (d5) 1.0 nm, (d6) 1.5 nm, (d7) 2.0 nm, (d8) mass density distribution of CO_2 molecules (d9) the relationship between the mass density distribution and the effective pore size.[321]

correlation with the adsorption energy. These properties can be used as predictors for the preliminary screening of greenhouse gas adsorbents. This research provides molecular-level insights into the greenhouse gas adsorption mechanism and offers guidance for designing more effective materials for environmental remediation.

13. Concluding remarks

This review has presented significant advancements in the adsorption processes of various gaseous pollutants, highlighting biomass materials as attractive candidates for a green and sustainable ecosystem. The study has noted that while intensified research and awareness regarding the hazards of gaseous compounds are crucial, the substantial enhancement of global security and the quest for environmental sustainability should further inspire scientists and engineers to create innovative and unconventional sorbents derived from agricultural waste. Despite significant advancements, there are still challenges that must be addressed for the effective deployment of these

materials. This would enable them to exhibit superior adsorption capabilities relative to conventional benchmark materials.

The swift advancement of the social economy has increasingly brought environmental issues to light. The major focus of contemporary researchers involves the selection of clean and effective technologies for pollution removal in order to achieve a balance between development and environmental protection. The cost-effective and reusable properties of sorption materials derived from biomass should perfectly align with the sustainable development criteria. The conventional techniques employed in biochar production exhibit low efficiency, necessitating a substantial quantity of raw ingredients. When considering the application of biochar materials in engineering practices, it is important to consider the quality relationship between these materials and the raw materials. Therefore, continuous investigation into techniques for modifying and regenerating is still a research hotspot.

Currently, there have been few endeavours conducted on adsorbents for typical gaseous pollutants. For example, the current studies on CO_2 adsorption primarily depend on simulated gas mixtures, including only a few key gas components
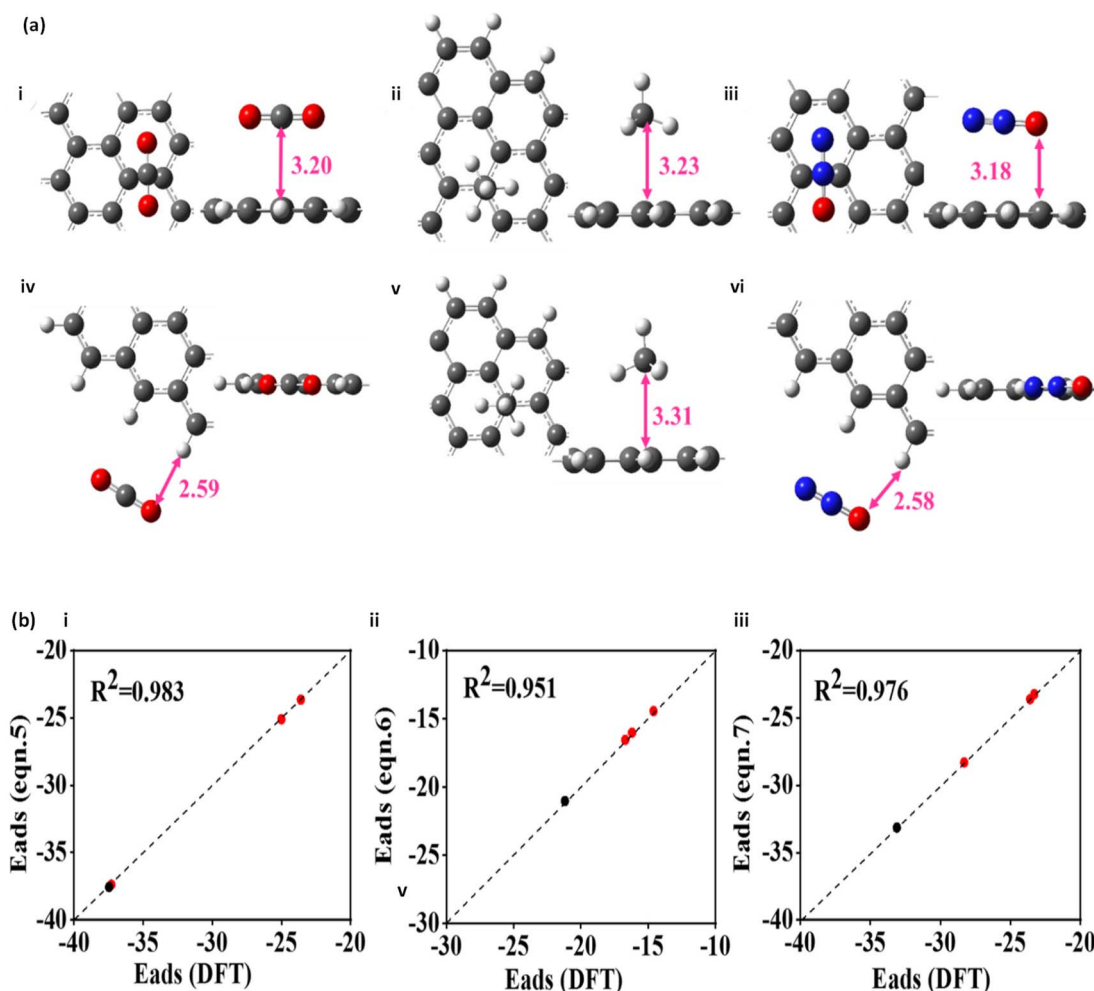

Fig. 11 (a) Optimized structures of the most stable configurations for the (i) CO_2-top, (ii) CH_4-top, (iii) N_2O-top, (iv) CO_2-side, (v) CH_4-side, and (vi) N_2O-side adsorbed on the BC and (b) Scatter plot showing Eads (i) CO_2, (ii) CH_4, (iii) N_2O.[323]

(such as N_2, CO_2, and H_2O) or even pure CO_2. Further research is required to investigate the competitive adsorption of biomass adsorbent in industrial flue gas that contains contaminants. The adsorption of VOCs onto solid sorbents often decreases as the adsorption temperature increases. This is mostly due to the physical exothermic interaction. Significantly, elevated temperatures enhance molecular diffusion and chemisorption, resulting in intricate impacts on the adsorption of VOCs, particularly when metal oxide-modified biochar is involved. In addition, humidity can impact the adsorption of VOCs onto carbon materials because the H_2O molecules can compete to occupy the pore sites. Nevertheless, there has been limited research on the impact of temperature and humidity on the sorption of VOCs onto biomass-based sorbents.

The use of advanced analytical techniques should be encouraged. Various characterization techniques have been utilized to quantify the pore textural characteristics and the presence of surface functional groups of the adsorbent before and after the adsorption process. For example, Abdulrasheed et al.[292] and Shafeeyan et al.[64] provided a comprehensive description of the common methods used, such as chemical titration, FTIR, X-ray photoelectron spectroscopy (XPS), temperature-programmed reduction (TPR), and temperature-programmed desorption (TPD). Typically, NH_3-TPD may be utilized to assess the surface acidity of biochar, whereas H_2-TPR measurement was employed to analyze the redox properties of metal oxides. Nevertheless, the assessment of biochar's functional groups was conducted using an offline method, which may undergo alterations throughout the cooling process of the used sorbent. Hence, it is imperative to develop in situ sophisticated techniques for quantitatively analyzing the adsorbents in order to accurately identify the sorption mechanism of the gaseous pollutants.

Current studies on multi-gaseous adsorption onto biomass adsorbent is quite limited. The previous studies did not attempt to simultaneously test more than three gaseous pollutants. Several suggestions may be considered to achieve an enhanced sorption of several gaseous components through synergistic adsorption. The oxygen-containing functional groups present in biomass materials are often acidic and positively impact the sorption of polar and hydrophilic VOCs. Moreover, these groups offer many active sites where NH_3 may be adsorbed, resulting in better efficiency in removing NO. Meanwhile, the oxygenation anchoring sites serve as a useful intermediary stage for introducing nitrogen functional groups. These functional groups are typically more successful than the pore characteristics in adsorbing acidic CO_2 and SO_2, particularly at temperatures over
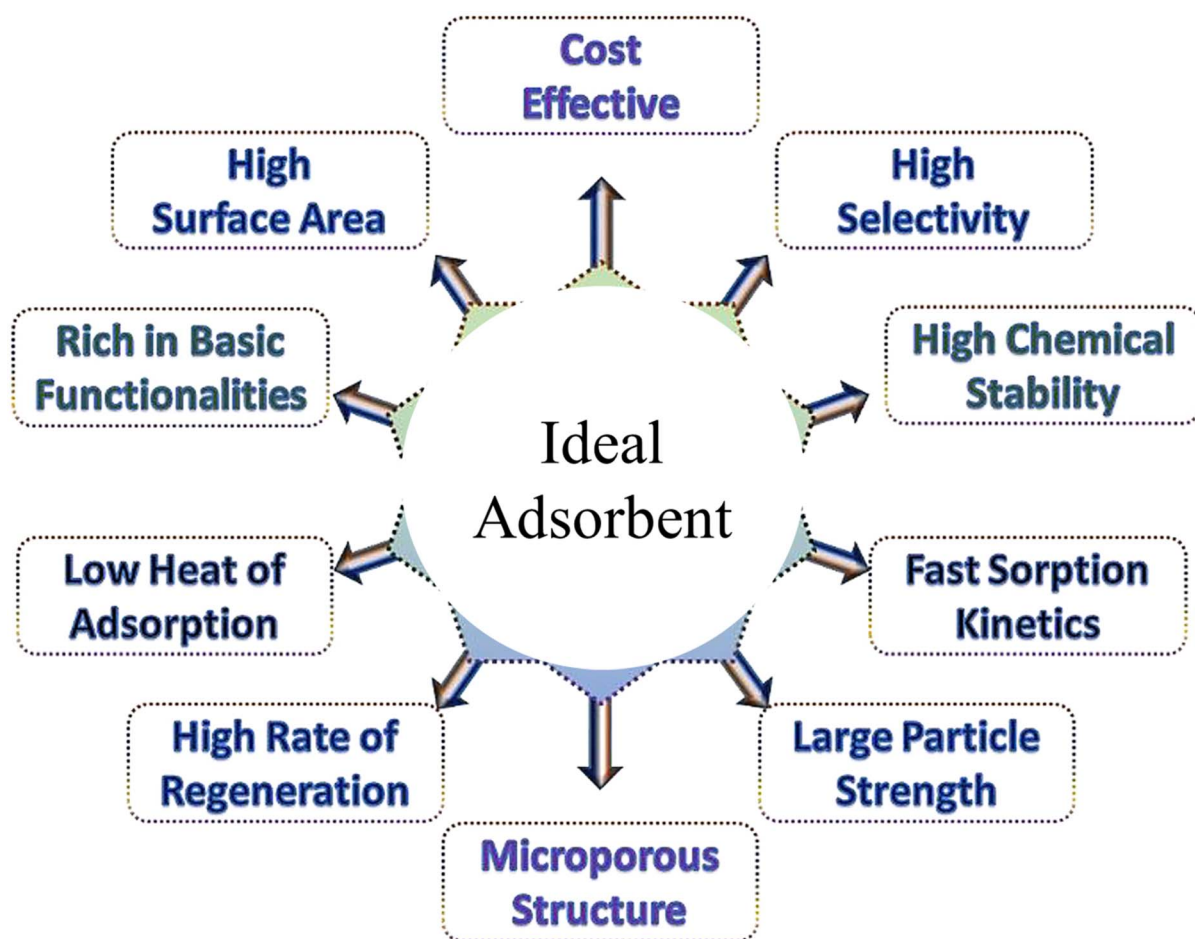

Fig. 12 Expected characteristics of an ideal sorbent for gaseous pollutant removal.

100 °C. Also, developing biochar that can efficiently remove several *gas* pollutants in a single-step procedure is currently challenging due to the unavoidable issue of competing adsorptions.

Furthermore, the majority of investigations on the adsorption of gaseous pollutants onto biomass sorbent have been conducted using a laboratory scale. However, it may be challenging to achieve the same level of adsorption capacity under complex industrial-relevant conditions as those observed in laboratory-scale platforms, primarily due to the unique particle properties of adsorbents and the necessity to consider reactor bed layouts. The potential configurations for integrating these sorbents with combustion flue gas streams include injection systems, fixed-bed, moving-bed, and fluidized-bed setups.[324] The multiphase reactor enhances the mass transfer and diffusion of gases, which are the primary rate-controlling stages in gaseous adsorption, thereby resulting in an improved sorption efficiency.[325]

The effectiveness of using biomass adsorbent in large-scale industrial applications will determine the practicality and cost-effectiveness of employing biomass-based adsorption technology for removing gaseous contaminants. This study recommends that an ideal adsorbent for gaseous pollutants decontamination should meet the following industrial criteria (Fig. 12): (i) produced using cost-effective and energy-efficient methods such as ultrasonic, microwave, template, and plasma techniques. (ii) Exhibit a higher adsorption capacity and selectivity for N_2, while also being able to tolerate other flue gas components such as SO_x, NO_x, H_2O, and light hydrocarbons, as it is preferable for them to be able to simultaneously remove multiple gaseous pollutants. (iii) Ensure long-term adsorption–desorption operation cycles, such adsorbent needs to have fast adsorption and desorption kinetics, lower energy requirements for desorption, and good mechanical regeneration stability.

The disposal approach for spent biomass-based sorbents needs to be revisited. The major focus of the industry is on regenerating and renewing the used adsorbents until their ability to remove gas pollutants becomes ineffective. This is mostly achieved by thermal regeneration at temperatures of about 200–300 °C, which can be facilitated by transferring heat with a flowing flue gas in industrial facilities. The desorbed gas pollutants, such as NO_x and SO_2, can be efficiently collected and used as chemical feedstock. Before returning the waste biomass to the boiler, it is essential to note that it has a higher heating value and energy density compared to its original biomass form, making it a more efficient fuel. Due to its higher concentration, CO_2 is in high demand for disposal compared to other types of gases. Biochar, which has the special ability to adsorb CO_2, could be buried as a form of carbon sequestration before it loses its effective adsorption capability. In this scenario, biomass functions as a soil supplement that sequesters carbon.

Data availability

All data and materials used in this study are available within this article.

Author contributions

Conflicts of interest

No conflicts of interest.

Acknowledgements

References

1 K. A. Adegoke and N. W. Maxakato, *J. CO₂ Util.*, 2023, **69**, 102412.
2 IEA, *Key World Energy Statistics 2009*, OECD Publishing, 2009, DOI: **10.1787/9789264039537-en**.
3 BP Energy, *BP Energy Outlook 2019 Edition*, 2019.
4 S. Solomon, G. K. Plattner, R. Knutti and P. Friedlingstein, *Proc. Natl. Acad. Sci. U. S. A.*, 2009, **106**, 1704–1709.
5 D. L. Hartmann, A. M. G. Klein Tank, M. Rusticucci, L. V. Alexander, S. Brönnimann, Y. A. R. Charabi, F. J. Dentener, E. J. Dlugokencky, D. R. Easterling, A. Kaplan, B. J. Soden, P. W. Thorne, M. Wild and P. Zhai, in *Climate Change 2013 the Physical Science Basis: Working Group I Contribution to the Fifth Assessment Report of the Intergovernmental Panel on Climate Change*, 2013, vol. 9781107057, pp. 159–254.
6 R. Lindsey, Climate Change: Atmospheric Carbon Dioxide, **https://www.climate.gov/news-features/understanding-climate/climate-change-atmospheric-carbon-dioxide**, accessed 20 February 2025.
7 K. A. Adegoke and N. W. Maxakato, *Coord. Chem. Rev.*, 2022, **457**, 214389.
8 K. A. Adegoke and N. W. Maxakato, *Mater. Today Chem.*, 2022, **24**, 100838.
9 A. Palliyarayil, H. Saini, K. Vinayakumar, P. Selvarajan, A. Vinu, N. S. Kumar and S. Sil, *Emerg. Mater.*, 2021, **4**, 607–643.

10 G. McGranahan and F. Murray, *Air Pollution and Health in Rapidly Developing Countries*, Routledge, 2012.

11 L. Filleul, A. Zeghnoun, C. Declercq, C. Le Goaster, A. Le Tertre, D. Eilstein, S. Medina, P. Saviuc, H. Prouvost and S. Cassadou, *Rev. Mal. Respir.*, 2001, **18**, 387–395.

12 F. Dominici, R. D. Peng, M. L. Bell, L. Pham, A. McDermott, S. L. Zeger and J. M. Samet, *JAMA*, 2006, **295**, 1127–1134.

13 R. D. Peng, H. H. Chang, M. L. Bell, A. McDermott, S. L. Zeger, J. M. Samet and F. Dominici, *JAMA*, 2008, **299**, 2172–2179.

14 K. Bhaskaran, S. Hajat, A. Haines, E. Herrett, P. Wilkinson and L. Smeeth, *Heart*, 2009, **95**, 1746–1759.

15 H. Mustafić, P. Jabre, C. Caussin, M. H. Murad, S. Escolano, M. Tafflet, M.-C. Périer, E. Marijon, D. Vernerey and J.-P. Empana, *Jama*, 2012, **307**, 713–721.

16 World Health Organization, *Ambient air pollution: A global assessment of exposure and burden of disease*, 2016.

17 S. K. Guttikunda, R. Goel and P. Pant, *Atmos. Environ.*, 2014, **95**, 501–510.

18 K. Sheoran, S. S. Siwal, D. Kapoor, N. Singh, A. K. Saini, W. F. Alsanie and V. K. Thakur, *ACS Eng. Au.*, 2022, **2**, 378–396.

19 T. Pettit, P. J. Irga and F. R. Torpy, *J. Hazard. Mater.*, 2018, **360**, 594–603.

20 K. Wróblewska and B. R. Jeong, *Environ. Sci. Eur.*, 2021, **33**, 110.

21 İ. A. Reşitoğlu, K. Altinişik and A. Keskin, *Clean Technol. Environ. Policy*, 2015, **17**, 15–27.

22 G. Crini, E. Lichtfouse, L. D. Wilson and N. Morin-Crini, *Environ. Chem. Lett.*, 2019, **17**, 195–213.

23 L. Pellenz, C. R. S. de Oliveira, A. H. da Silva Júnior, L. J. S. da Silva, L. da Silva, A. A. Ulson de Souza, S. M. de, A. G. U. de Souza, F. H. Borba and A. da Silva, *Sep. Purif. Technol.*, 2023, **305**, 122435.

24 K. A. Adegoke, O. O. Adesina, O. A. Okon-Akan, O. R. Adegoke, A. B. Olabintan, O. A. Ajala, H. Olagoke, N. W. Maxakato and O. S. Bello, *Curr. Res. Green Sustain. Chem.*, 2022, **5**, 100274.

25 K. A. Adegoke and O. S. Bello, *Water Resour. Ind.*, 2015, 8–24, DOI: 10.1016/j.wri.2015.09.002.

26 M. Hemalatha, G. S. Lakshmi, V. Megha and B. C. Kotibagar, Applications of Nanomaterials for Water Treatment: Current Trends and Future Scope, in *Modern Nanotechnology*, ed. J. A. Malik and M. J. Sadiq Mohamed, Springer, Cham, DOI: 10.1007/978-3-031-31111-6_7.

27 V. F. Gold, A. Bamisaye, M. O. Adesina, K. A. Adegoke, A. R. Ige, O. Adeleke, M. O. Bamidele, Y. A. Alli, A. K. Oyebamiji and O. O. Ogunlaja, *J. Dispers. Sci. Technol.*, 2024, 1–17.

28 A. A. Adaramaja, A. Bamisaye, S. M. Abati, K. A. Adegoke, M. O. Adesina, A. R. Ige, O. Adeleke, M. A. Idowu, A. K. Oyebamiji and O. S. Bello, *RSC Adv.*, 2024, **14**, 12703–12719.

29 Y. Dai, Q. Sun, W. Wang, L. Lu, M. Liu, J. Li, S. Yang, Y. Sun, K. Zhang, J. Xu, W. Zheng, Z. Hu, Y. Yang, Y. Gao, Y. Chen, X. Zhang, F. Gao and Y. Zhang, *Chemosphere*, 2018, **211**, 235–253.

30 Z. Ajmal, M. ul Haq, Y. Naciri, R. Djellabi, N. Hassan, S. Zaman, A. Murtaza, A. Kumar, A. G. Al-Sehemi, H. Algarni, O. A. Al-Hartomy, R. Dong, A. Hayat and A. Qadeer, *Chemosphere*, 2022, **308**, 136358.

31 A. Othmani, A. Kadier, R. Singh, C. A. Igwegbe, M. Bouzid, M. O. Aquatar, W. A. Khanday, M. E. Bote, F. Damiri, Ö. Gökkuş and F. Sher, *Environ. Res.*, 2022, **215**, 114294.

32 S. F. Ahmed, M. Mofijur, S. Nuzhat, A. T. Chowdhury, N. Rafa, M. A. Uddin, A. Inayat, T. M. I. Mahlia, H. C. Ong, W. Y. Chia and P. L. Show, *J. Hazard. Mater.*, 2021, **416**, 125912.

33 Z. Bano, N. Z. Ali, M. A. Khan, S. Mutahir, S. Zhu, F. Wang and M. Xia, *Ceram. Int.*, 2022, **48**, 8409–8416.

34 X. Wang, M. A. Khan, M. Xia, S. Zhu, W. Lei and F. Wang, *J. Mater. Sci. Mater. Electron.*, 2019, **30**, 5503–5515.

35 M. M. Sabzehmeidani, S. Mahnaee, M. Ghaedi, H. Heidari and V. A. L. Roy, *Adv. Mater.*, 2021, **2**, 598–627.

36 J. Zhou, X. Wang and W. Xing, in *Post-Combustion Carbon Dioxide Capture Materials*, ed. Q. Wang, The Royal Society of Chemistry, 2018, p. 0.

37 J. Jjagwe, P. W. Olupot, E. Menya and H. M. Kalibbala, *J. Bioresour. Bioprod.*, 2021, **6**, 292–322.

38 R. Ahmed, G. Liu, B. Yousaf, Q. Abbas, H. Ullah and M. U. Ali, *J. Clean. Prod.*, 2020, **242**, 118409.

39 Z. Zhang, Z. P. Cano, D. Luo, H. Dou, A. Yu and Z. Chen, *J. Mater. Chem. A*, 2019, **7**, 20985–21003.

40 L. Chen, S. Deng, R. Zhao, L. Zhao, S. Li, Z. Guo, Y. Lu, J. Zhao and K. Wu, *Energy Technol.*, 2021, **9**, 2000756.

41 K. A. Adegoke, K. G. Akpomie, E. S. Okeke, C. Olisah, A. Malloum, N. W. Maxakato, J. O. Ighalo, J. Conradie, C. R. Ohoro, J. F. Amaku and K. O. Oyedotun, *Sep. Purif. Technol.*, 2024, **331**, 125456.

42 F. O. Ochedi, Y. Liu and Y. G. Adewuyi, *Process Saf. Environ. Prot.*, 2020, **139**, 1–25.

43 V. Acevedo-García, E. Rosales, A. Puga, M. Pazos and M. A. Sanromán, *Sep. Purif. Technol.*, 2020, **242**, 116796.

44 H. Mumtaz, M. Farhan, M. Amjad, F. Riaz, A. H. Kazim, M. Sultan, M. Farooq, M. A. Mujtaba, I. Hussain, M. Imran, S. Anwar, A. M. El-Sherbeeny, F. A. Siddique, S. Armaković, Q. Ali, I. A. Chaudhry and A. Pettinau, *Sustain. Energy Technol. Assessments*, 2021, **46**, 101288.

45 D. Mallesh, J. Anbarasan, P. Mahesh Kumar, K. Upendar, P. Chandrashekar, B. V. S. K. Rao and N. Lingaiah, *Appl. Surf. Sci.*, 2020, **530**, 147226.

46 B. Aghel, S. Behaein and F. Alobaid, *Fuel*, 2022, **328**, 125276.

47 M. Karimi, M. Shirzad, J. A. C. Silva and A. E. Rodrigues, *J. CO_2 Util.*, 2022, **57**, 101890.

48 M. Olivares-Marín and M. M. Maroto-Valer, *Greenh. Gases: Sci. Technol.*, 2012, **2**, 20–35.

49 O. Ioannidou and A. Zabaniotou, *Renew. Sustain. Energy Rev.*, 2007, **11**, 1966–2005.

50 M. G. Plaza, S. García, F. Rubiera, J. J. Pis and C. Pevida, *Sep. Purif. Technol.*, 2011, **80**, 96–104.

51 M. G. Plaza, C. Pevida, C. F. Martín, J. Fermoso, J. J. Pis and F. Rubiera, *Sep. Purif. Technol.*, 2010, **71**, 102–106.

52 M. G. Plaza, C. Pevida, B. Arias, J. Fermoso, M. D. Casal, C. F. Martín, F. Rubiera and J. J. Pis, *Fuel*, 2009, **88**, 2442–2447.

53 A. Boonpoke, S. Chiarakorn, N. Laosiripojana, S. Towprayoon and A. Chidthaisong, *J. Environ. Sustain.*, 2013, **2**, 77–81.

54 S.-J. Son, J.-S. Choi, K.-Y. Choo, S.-D. Song, S. Vijayalakshmi and T.-H. Kim, *Korean J. Chem. Eng.*, 2005, **22**, 291–297.

55 J. A. Thote, K. S. Iyer, R. Chatti, N. K. Labhsetwar, R. B. Biniwale and S. S. Rayalu, *Carbon*, 2010, **48**, 396–402.

56 H. T. Jang, Y. Park, Y. S. Ko, J. Y. Lee and B. Margandan, *Int. J. Greenh. Gas Control*, 2009, **3**, 545–549.

57 S. A. Miller, P. R. Cunningham and J. T. Harvey, *Resour. Conserv. Recycl.*, 2019, **146**, 416–430.

58 H. Marsh and F. Rodríguez-Reinoso, *Activated Carbon*, 2006.

59 P. González-García, *Renew. Sustain. Energy Rev.*, 2018, **82**, 1393–1414.

60 X. Tan, S. Liu, Y. Liu, Y. Gu, G. Zeng, X. Hu, X. Wang, S. Liu and L. Jiang, *Bioresour. Technol.*, 2017, **227**, 359–372.

61 M. A. Yahya, Z. Al-Qodah and C. W. Z. Ngah, *Renew. Sustain. Energy Rev.*, 2015, **46**, 218–235.

62 J. L. Figueiredo and M. F. R. Pereira, *Catal. Today*, 2010, **150**, 2–7.

63 J. Rivera-Utrilla, M. Sánchez-Polo, V. Gómez-Serrano, P. M. Álvarez, M. C. M. Alvim-Ferraz and J. M. Dias, *J. Hazard. Mater.*, 2011, **187**, 1–23.

64 M. S. Shafeeyan, W. M. A. W. Daud, A. Houshmand and A. Shamiri, *J. Anal. Appl. Pyrolysis*, 2010, **89**, 143–151.

65 M. Jeguirim, M. Belhachemi, L. Limousy and S. Bennici, *Chem. Eng. J.*, 2018, **347**, 493–504.

66 M. I. S. Haider, G. Liu, B. Yousaf, M. Arif, K. Aziz, A. Ashraf, R. Safeer, S. Ijaz and K. Pikon, *Environ. Pollut.*, 2024, 124365.

67 J. L. Figueiredo, *J. Mater. Chem. A*, 2013, **1**, 9351–9364.

68 P. V Samant, F. Gonçalves, M. M. A. Freitas, M. F. R. Pereira and J. L. Figueiredo, *Carbon*, 2004, **42**, 1321–1325.

69 F. Kapteijn, J. A. Moulijn, S. Matzner and H.-P. Boehm, *Carbon*, 1999, **37**, 1143–1150.

70 C. L. Mangun, K. R. Benak, J. Economy and K. L. Foster, *Carbon*, 2001, **39**, 1809–1820.

71 R. Pietrzak, *Fuel*, 2009, **88**, 1871–1877.

72 J. Wang, L. Huang, R. Yang, Z. Zhang, J. Wu, Y. Gao, Q. Wang, D. O'Hare and Z. Zhong, *Energy Environ. Sci.*, 2014, **7**, 3478–3518.

73 R. Balasubramanian and S. Chowdhury, *J. Mater. Chem. A*, 2015, **3**, 21968–21989.

74 X. Ma, L. Li, R. Chen, C. Wang, K. Zhou and H. Li, *Fuel*, 2019, **236**, 942–948.

75 A. Ö. Yazaydın, A. I. Benin, S. A. Faheem, P. Jakubczak, J. J. Low, R. R. Willis and R. Q. Snurr, *Chem. Mater.*, 2009, **21**, 1425–1430.

76 Y. Xia, R. Mokaya, G. S. Walker and Y. Zhu, *Adv. Energy Mater.*, 2011, **1**, 678–683.

77 X. Ma, L. Li, R. Chen, C. Wang, H. Li and S. Wang, *Appl. Surf. Sci.*, 2018, **435**, 494–502.

78 K. Kim, D. Kim, Y.-K. Park and K. S. Lee, *Int. J. Greenh. Gas Control*, 2014, **26**, 135–146.

79 Z. Yang, Y. Xia and R. Mokaya, *J. Am. Chem. Soc.*, 2007, **129**, 1673–1679.

80 A. Aijaz, N. Fujiwara and Q. Xu, *J. Am. Chem. Soc.*, 2014, **136**, 6790–6793.

81 G. K. Parshetti, S. Chowdhury and R. Balasubramanian, *Fuel*, 2015, **148**, 246–254.

82 X. Ma, L. Li, Z. Zeng, R. Chen, C. Wang, K. Zhou and H. Li, *Appl. Surf. Sci.*, 2019, **481**, 1139–1147.

83 Q. Ye, J. Jiang, C. Wang, Y. Liu, H. Pan and Y. Shi, *Energy Fuels*, 2012, **26**, 2497–2504.

84 M. M. Gui, Y. X. Yap, S.-P. Chai and A. R. Mohamed, *Int. J. Greenh. Gas Control*, 2013, **14**, 65–73.

85 Z. Zhang, S. Xian, Q. Xia, H. Wang, Z. Li and J. Li, *AIChE J.*, 2013, **59**, 2195–2206.

86 B. Arstad, H. Fjellvåg, K. O. Kongshaug, O. Swang and R. Blom, *Adsorption*, 2008, **14**, 755–762.

87 F. Salles, A. Ghoufi, G. Maurin, R. G. Bell, C. Mellot-Draznieks and G. Férey, *Angew. Chem. Int. Ed.*, 2008, **47**, 8487–8491.

88 Y. Lee, D. Liu, D. Seoung, Z. Liu, C.-C. Kao and T. Vogt, *J. Am. Chem. Soc.*, 2011, **133**, 1674–1677.

89 F. Su, C. Lu, S.-C. Kuo and W. Zeng, *Energy Fuels*, 2010, **24**, 1441–1448.

90 C. Chen, S.-T. Yang, W.-S. Ahn and R. Ryoo, *Chem. Commun.*, 2009, 3627–3629.

91 M. Sevilla, J. B. Parra and A. B. Fuertes, *ACS Appl. Mater. Interfaces*, 2013, **5**, 6360–6368.

92 R.-L. Liu, W.-J. Ji, T. He, Z.-Q. Zhang, J. Zhang and F.-Q. Dang, *Carbon*, 2014, **76**, 84–95.

93 A. Hanif, M. A. Aziz, A. Helal, M. M. Abdelnaby, A. Khan, R. Theravalappil and M. Y. Khan, *ACS Omega*, 2023, **8**, 36228–36236.

94 A. D. Igalavithana, S. W. Choi, J. Shang, A. Hanif, P. D. Dissanayake, D. C. W. Tsang, J.-H. Kwon, K. B. Lee and Y. S. Ok, *Sci. Total Environ.*, 2020, **739**, 139845.

95 P. D. Dissanayake, S. You, A. D. Igalavithana, Y. Xia, A. Bhatnagar, S. Gupta, H. W. Kua, S. Kim, J.-H. Kwon, D. C. W. Tsang and Y. S. Ok, *Renew. Sustain. Energy Rev.*, 2020, **119**, 109582.

96 S. Li, X. Yuan, S. Deng, L. Zhao and K. B. Lee, *Renew. Sustain. Energy Rev.*, 2021, **152**, 111708.

97 M. Bui, C. S. Adjiman, A. Bardow, E. J. Anthony, A. Boston, S. Brown, P. S. Fennell, S. Fuss, A. Galindo, L. A. Hackett, J. P. Hallett, H. J. Herzog, G. Jackson, J. Kemper, S. Krevor, G. C. Maitland, M. Matuszewski, I. S. Metcalfe, C. Petit, G. Puxty, J. Reimer, D. M. Reiner, E. S. Rubin, S. A. Scott, N. Shah, B. Smit, J. P. M. Trusler, P. Webley, J. Wilcox and N. Mac Dowell, *Energy Environ. Sci.*, 2018, **11**, 1062–1176.

98 M. Fajardy and N. Mac Dowell, *Energy Environ. Sci.*, 2018, **11**, 1581–1594.

99 H. Bamdad, K. Hawboldt and S. Macquarrie, *Renew. Sustain. Energy Rev.*, 2017, 1–16.

100 O. A. A. A. Bamisaye, C. O. Eromosele and E. O. Dare, *J. Chem. Soc. Niger.*, 2020, **45**, 804–811.

101 X. Yuan, M. Suvarna, S. Low, P. D. Dissanayake, K. B. Lee, J. Li, X. Wang and Y. S. Ok, *Environ. Sci. Technol.*, 2021, **55**, 11925–11936.

102 A. I. Osman, M. Hefny, M. I. A. Abdel Maksoud, A. M. Elgarahy and D. W. Rooney, *Environ. Chem. Lett.*, 2021, **19**, 797–849.

103 M. Sevilla, P. Valle-Vigón and A. B. Fuertes, *Adv. Funct. Mater.*, 2011, **21**, 2781–2787.

104 J. Xiao, X. Yuan, T. C. Zhang, L. Ouyang and S. Yuan, *Sep. Purif. Technol.*, 2022, **298**, 121602.

105 Y. Li, L. Liu, H. Yu, Y. Zhao, J. Dai, Y. Zhong, Z. Pan and H. Yu, *Sci. Total Environ.*, 2022, **811**, 151384.

106 K. Wiedner, C. Rumpel, C. Steiner, A. Pozzi, R. Maas and B. Glaser, *Biomass Bioenergy*, 2013, **59**, 264–278.

107 Z. Zhang, Z. Zhu, B. Shen and L. Liu, *Energy*, 2019, **171**, 581–598.

108 M. Tripathi, J. N. Sahu and P. Ganesan, *Renew. Sustain. Energy Rev.*, 2016, **55**, 467–481.

109 E. Antunes, M. V Jacob, G. Brodie and P. A. Schneider, *J. Anal. Appl. Pyrolysis*, 2018, **129**, 93–100.

110 T. Kan, V. Strezov and T. J. Evans, *Renew. Sustain. Energy Rev.*, 2016, **57**, 1126–1140.

111 A. Zubrik, M. Matik, S. Hredzák, M. Lovás, Z. Danková, M. Kováčová and J. Briančin, *J. Clean. Prod.*, 2017, **143**, 643–653.

112 H. S. Kambo and A. Dutta, *Renew. Sustain. Energy Rev.*, 2015, **45**, 359–378.

113 M. Rana, K. Subramani, M. Sathish and U. K. Gautam, *Carbon*, 2017, **114**, 679–689.

114 Y. Chen, X. Zhang, W. Chen, H. Yang and H. Chen, *Bioresour. Technol.*, 2017, **246**, 101–109.

115 O. Boujibar, A. Souikny, F. Ghamouss, O. Achak, M. Dahbi and T. Chafik, *J. Environ. Chem. Eng.*, 2018, **6**, 1995–2002.

116 M. Zhu, W. Cai, F. Verpoort and J. Zhou, *Chem. Eng. Res. Des.*, 2019, **146**, 130–140.

117 S. Li, K. Han, J. Li, M. Li and C. Lu, *Microporous Mesoporous Mater.*, 2017, **243**, 291–300.

118 H. M. Coromina, D. A. Walsh and R. Mokaya, *J. Mater. Chem. A*, 2016, **4**, 280–289.

119 M. B. Ahmed, M. A. Hasan Johir, J. L. Zhou, H. H. Ngo, L. D. Nghiem, C. Richardson, M. A. Moni and M. R. Bryant, *J. Clean. Prod.*, 2019, **225**, 405–413.

120 J. Serafin, M. Baca, M. Biegun, E. Mijowska, R. J. Kaleńczuk, J. Sreńscek-Nazzal and B. Michalkiewicz, *Appl. Surf. Sci.*, 2019, **497**, 143722.

121 R. A. Fiuza-Jr, R. C. Andrade and H. M. C. Andrade, *J. Environ. Chem. Eng.*, 2016, **4**, 4229–4236.

122 V. Benedetti, E. Cordioli, F. Patuzzi and M. Baratieri, *J. CO₂ Util.*, 2019, **33**, 46–54.

123 L. Yue, L. Rao, L. Wang, L. Wang, J. Wu, X. Hu, H. DaCosta, J. Yang and M. Fan, *Ind. Eng. Chem. Res.*, 2017, **56**, 14115–14122.

124 J. Serafin, U. Narkiewicz, A. W. Morawski, R. J. Wróbel and B. Michalkiewicz, *J. CO₂ Util.*, 2017, **18**, 73–79.

125 S. Liu, R. Ma, X. Hu, L. Wang, X. Wang, M. Radosz and M. Fan, *Ind. Eng. Chem. Res.*, 2020, **59**, 7046–7053.

126 H. Wei, J. Chen, N. Fu, H. Chen, H. Lin and S. Han, *Electrochim. Acta*, 2018, **266**, 161–169.

127 Z. Geng, Q. Xiao, H. Lv, B. Li, H. Wu, Y. Lu and C. Zhang, *Sci. Rep.*, 2016, **6**, 30049.

128 D. Saha, S. E. Van Bramer, G. Orkoulas, H.-C. Ho, J. Chen and D. K. Henley, *Carbon*, 2017, **121**, 257–266.

129 H. Wei, H. Chen, N. Fu, J. Chen, G. Lan, W. Qian, Y. Liu, H. Lin and S. Han, *Electrochim. Acta*, 2017, **231**, 403–411.

130 B. Chang, W. Shi, H. Yin, S. Zhang and B. Yang, *Chem. Eng. J.*, 2019, **358**, 1507–1518.

131 Y.-J. Heo and S.-J. Park, *Green Chem.*, 2018, **20**, 5224–5234.

132 C. Zhang, W. Song, Q. Ma, L. Xie, X. Zhang and H. Guo, *Energy Fuels*, 2016, **30**, 4181–4190.

133 Z. Rouzitalab, D. Mohammady Maklavany, A. Rashidi and S. Jafarinejad, *J. Environ. Chem. Eng.*, 2018, **6**, 6653–6663.

134 P. Lahijani, M. Mohammadi and A. R. Mohamed, *J. CO₂ Util.*, 2018, **26**, 281–293.

135 X. Kan, X. Chen, W. Chen, J. Mi, J.-Y. Zhang, F. Liu, A. Zheng, K. Huang, L. Shen, C. Au and L. Jiang, *ACS Sustain. Chem. Eng.*, 2019, **7**, 7609–7618.

136 S. Deng, H. Wei, T. Chen, B. Wang, J. Huang and G. Yu, *Chem. Eng. J.*, 2014, **253**, 46–54.

137 X. Ma, Y. Yang, Q. Wu, B. Liu, D. Li, R. Chen, C. Wang, H. Li, Z. Zeng and L. Li, *Fuel*, 2020, **282**, 118727.

138 M. Sevilla and A. B. Fuertes, *Energy Environ. Sci.*, 2011, **4**, 1765–1771.

139 E. Haffner-Staton, N. Balahmar and R. Mokaya, *J. Mater. Chem. A*, 2016, **4**, 13324–13335.

140 G. Singh, K. S. Lakhi, S. Sil, S. V. Bhosale, I. Y. Kim, K. Albahily and A. Vinu, *Carbon*, 2019, **148**, 164–186.

141 O. A. Okon-Akan, O. Abiodun, O. Oluwaseun, O. K. Oladayo, O. Abayomi, A. A. George, E. Opatola, R. F. Orah, E. J. Isukuru, I. C. Ede, O. T. Oluwayomi, J. A. Okolie and I. A. Omotayo, *Clean Technol.*, 2023, **5**, 934–961.

142 F. Sher, S. Z. Iqbal, S. Albazzaz, U. Ali, D. A. Mortari and T. Rashid, *Fuel*, 2020, **282**, 118506.

143 M. M. Bade, A. A. Dubale, D. F. Bebizuh and M. Atlabachew, *ACS Omega*, 2022, **7**, 18770–18779.

144 F. Valdebenito, R. García, K. Cruces, G. Ciudad, G. Chinga-Carrasco and Y. Habibi, *ACS Sustain. Chem. Eng.*, 2018, **6**, 12603–12612.

145 M. S. Khosrowshahi, M. A. Abdol, H. Mashhadimoslem, E. Khakpour, H. B. M. Emrooz, S. Sadeghzadeh and A. Ghaemi, *Sci. Rep.*, 2022, **12**, 8917.

146 H. N. Nguyen, D. A. Khuong and T. Tsubota, *Therm. Sci. Eng. Prog.*, 2024, **49**, 102446.

147 A. E. Creamer, B. Gao and M. Zhang, *Chem. Eng. J.*, 2014, **249**, 174–179.

148 J. M. Martín-Martínez, R. Torregrosa-Maciá and M. C. Mittelmeijer-Hazeleger, *Fuel*, 1995, **74**, 111–114.

149 K. A. Adegoke, S. O. Akinnawo, T. A. Adebusuyi, O. A. Ajala, R. O. Adegoke, N. W. Maxakato and O. S. Bello, *Int. J. Sci. Environ. Technol.*, 2023, **20**, 11615–11644.

150 N. A. Rashidi and S. Yusup, *J. CO₂ Util.*, 2016, **13**, 1–16.

151 W.-J. Liu, H. Jiang, K. Tian, Y.-W. Ding and H.-Q. Yu, *Environ. Sci. Technol.*, 2013, **47**, 9397–9403.

152 A. E. Creamer, B. Gao, A. Zimmerman and W. Harris, *Chem. Eng. J.*, 2018, **334**, 81–88.

153 J. Gopalan, A. Buthiyappan and A. A. Abdul Raman, *J. Ind. Eng. Chem.*, 2022, **113**, 72–95.

154 Q. Li, T. Lu, L. Wang, R. Pang, J. Shao, L. Liu and X. Hu, *Sep. Purif. Technol.*, 2021, **275**, 119204.

155 S. K. Sooriyan and N. Ibrahim, *Biointerface Res. Appl. Chem.*, 2022, **12**, 7972–7982.

156 S. Sumathi, S. Bhatia, K. T. Lee and A. R. Mohamed, *Chem. Eng. J.*, 2010, 1093–1096.

157 V. Viena, *et al.*, *IOP Conf. Ser. Mater. Sci. Eng.*, 2018, 012037, DOI: **10.1088/1757-899X/334/1/012037**.

158 M. M. Meimand and N. Javid, *J. Health Scope*, 2019, 8, DOI: **10.5812/jhealthscope.69158**.

159 J. Shao, J. Zhang, X. Zhang, Y. Feng, H. Zhang and S. Zhang, *Fuel*, 2018, **224**, 138–146.

160 B. Chen and H. Kan, *Environ. Health Prev. Med.*, 2008, **13**, 94–101.

161 F. P. Perera, *Environ. Health Perspect.*, 2017, **125**, 141–148.

162 K. S. Rani, *J. Chem. Pharm. Sci.*, 2014, **2**, 63–67.

163 R. Davarnejad and P. Panahi, *Sep. Purif. Technol.*, 2016, **158**, 286–292.

164 M. B. Yue, B. Sun, Y. Cao, Y. Wang and J. Wang, *Chem.–Eur. J.*, 2008, 3442–3451.

165 D. N. K. Putra Negara, T. G. Tirta Nindhia, I. W. Surata and M. Sucipta, *IOP Conf. Ser.:Mater. Sci. Eng.*, 2017, **201**, 012033.

166 B.-K. Na, K.-K. Koo, H.-M. Eum, H. Lee and H. K. Song, *Korean J. Chem. Eng.*, 2001, **18**, 220–227.

167 S. Hao, J. Zhang, Y. Zhong and W. Zhu, *Adsorption*, 2012, **18**, 423–430.

168 S. Sethupathi, M. J. K. Bashir, Z. A. Akbar and A. R. Mohamed, *Waste Manag. Res.*, 2015, 303–312, DOI: **10.1177/0734242X15576026**.

169 S. Lu, Y. Ji, A. Buekens, Z. Ma, Y. Jin, X. Li and J. Yan, *Waste Manag. Res.*, 2012, **31**, 169–177.

170 W. M. A. W. Daud and W. S. W. Ali, *Bioresour. Technol.*, 2004, **93**, 63–69.

171 J. Guo and A. C. Lua, *J. Colloid Interface Sci.*, 2002, **251**, 242–247.

172 N. S. A. Shukor, *Int. J. Technol.*, 2018, 1121–1131.

173 J. Guo, L. Fan, J. Peng, J. Chen, H. Yin and W. Jiang, *J. Chem. Technol. Biotechnol.*, 2013, 1565–1575, DOI: **10.1002/jctb.4240**.

174 J. Guo and A. C. Lua, *Sep. Purif. Technol.*, 2003, **30**, 265–273.

175 A. C. Lua and T. Yang, *Chem. Eng. J.*, 2009, **155**, 175–183.

176 S. M. Abegunde, K. S. Idowu, O. M. Adejuwon and T. Adeyemi-Adejolu, *Resour. Environ. Sustain.*, 2020, **1**, 100001.

177 R. R. Manory, *Mater. Manuf. Process.*, 1990, **5**, 445–470.

178 V. K. Thakur, D. Vennerberg and M. R. Kessler, *ACS Appl. Mater. Interfaces*, 2014, **6**, 9349–9356.

179 M. G. A. Vieira, A. F. A. Neto, M. L. Gimenes and M. G. C. da Silva, *J. Hazard. Mater.*, 2010, **176**, 109–118.

180 M. Liu and C. Xiao, *E3S Web Conf.*, 2018, **38**, 2–5.

181 M. Kong, L. Huang, L. Li, Z. Zhang, S. Zheng and M. K. Wang, *Appl. Clay Sci.*, 2014, **99**, 207–214.

182 A. Rehman, M. Park and S. Park, *Coatings*, 2019, **9**, 1–22.

183 J. M. Rosas, R. Ruiz-rosas, J. Rodríguez-mirasol and T. Cordero, *Chem. Eng. J.*, 2017, 707–721, DOI: **10.1016/j.cej.2016.08.111**.

184 Y. W. Lee, H. J. Kim, J. W. Park, B. U. Choi, D. K. Choi and J. W. Park, *Carbon*, 2003, **41**, 1881–1888.

185 M. C. Macías-Pérez, *Fuel*, 2007, **86**, 677–683.

186 J. A. Arcibar-Orozco and J. R. Rangel-Mendez, *Chem. Eng. J.*, 2013, **230**, 439–446.

187 Y. Wu, Y. Fan, M. Zhang, Z. Ming, S. Yang, A. Arkin and P. Fang, *Biochem. Eng. J.*, 2016, **105**, 27–35.

188 J. Przepiórski, A. Czyżewski, M. Toyoda, T. Tsumura, R. Pietrzak and A. W. Morawski, *Int. J. Greenh. Gas Control*, 2012, **10**, 164–168.

189 S. Sumathi, S. Bhatia, K. T. Lee and A. R. Mohamed, *Chem. Eng. J.*, 2010, **162**, 194–200.

190 I. Dahlan, K. Teong, A. Harun and A. Rahman, *J. Hazard. Mater.*, 2011, **185**, 1609–1613.

191 H. Yi, Y. Zuo and H. Liu, *Water, Air, Soil Pollut.*, 2014, 1–7, DOI: **10.1007/s11270-014-1965-2**.

192 J. Zhang, J. Shao, D. Huang, Y. Feng, X. Zhang, S. Zhang and H. Chen, *Chem. Eng. J.*, 2020, **385**, 123932.

193 L. Wang, L. Sha, S. Zhang, F. Cao, X. Ren and Y. A. Levendis, *Fuel Process. Technol.*, 2022, 107233, DOI: **10.1016/j.fuproc.2022.107233**.

194 Q. Wang, L. Han, Y. Wang, Z. He, Q. Meng, S. Wang, P. Xiao and X. Jia, *RSC Adv.*, 2022, **12**, 20640–20648.

195 X. Zhang, S. Zhang, J. Zhang, G. Li, H. Zheng, J. Shao, S. Zhang, H. Yang and H. Chen, *Fuel*, 2023, **354**, 129266.

196 X. Zhang, H. Zheng, G. Li, J. Gu, J. Shao, S. Zhang, H. Yang and H. Chen, *J. Anal. Appl. Pyrolysis*, 2021, 105119, DOI: **10.1016/j.jaap.2021.105119**.

197 R. J. Lewis, G. B. Copley, R. J. Lewis and G. B. Copley, *Crit. Rev. Toxicol.*, 2014, 93–123, DOI: **10.3109/10408444.2014.971943**.

198 A. Peluso, N. Gargiulo, P. Aprea, F. Pepe and D. Caputo, *Sep. Purif. Rev.*, 2019, **48**, 78–89.

199 M. C. Castrillon, K. O. Moura, C. A. Alves, M. Bastos-neto, C. S. Azevedo, J. Hofmann, J. Möllmer, W. Einicke and R. Glaser, *Energy Fuel.*, 2016, 9596–9604, DOI: **10.1021/acs.energyfuels.6b01667**.

200 D. Long, Q. Chen, W. Qiao, L. Zhan, X. Liang and L. Ling, *Chem. Commun.*, 2009, 3898–3900.

201 J. Mi, F. Liu, W. Chen, X. Chen, L. Shen, Y. Cao, C. Au, K. Huang, A. Zheng and L. Jiang, *ACS Appl. Mater. Interfaces*, 2019, **11**, 29950–29959.

202 Y. Pan, M. Chen, M. Hu, M. Tian, Y. Zhang and D. Long, *Appl. Catal., B*, 2019, 118266.

203 A. Pudi, M. Rezaei, V. Signorini, M. Peter, M. Giacinti and S. Soheil, *Sep. Purif. Technol.*, 2022, **298**, 121448.

204 D. Somashekara and L. Mulky, *ChemBioEng Rev.*, 2023, **10**, 491–509.

205 Z. Zhang, J. Wang, W. Li, M. Wang, W. Qiao and D. Long, *Carbon*, 2016, **96**, 608–615.

206 P. Zhang, H. Zhu and S. Dai, *ChemCatChem*, 2015, 7, 2788–2805.

207 M. Khabazipour and M. Anbia, *Ind. Eng. Chem. Res.*, 2019, 22133–22164, DOI: 10.1021/acs.iecr.9b03800.

208 K. Kante, C. Nieto-delgado, J. R. Rangel-mendez and T. J. Bandosz, *J. Hazard. Mater.*, 2012, **201–202**, 141–147.

209 T. J. Bandosz, *J. Colloid Interface Sci.*, 2002, **20**, 1–20.

210 M. Seredych and T. J. Bandosz, *Energy Fuel.*, 2008, 850–859.

211 X. Zhang, Y. Tang, S. Qu, J. Da and Z. Hao, *ACS Catal.*, 2015, **5**, 1053–1067.

212 P. Nowicki, P. Skibiszewska and M. Wis, *Adsorption*, 2015, 20–31.

213 H. W. Ou, M. L. Fang, M. S. Chou, H. Y. Chang, T. F. Shiao, M. L. Fang, M. S. Chou, H. Y. Chang and T. F. Shiao, Long-term, *J. Air Waste Manage. Assoc.*, 2020, 641–648, DOI: 10.1080/10962247.2020.1754305.

214 L. Chen, J. Yuan, T. Li, X. Jiang, S. Ma, W. Cen and W. Jiang, *Sci. Total Environ.*, 2021, **768**, 144452.

215 J. Kazmierczak-Razna, P. Nowicki and R. Pietrzak, *Chem. Eng. Res. Des.*, 2016, 346–353, DOI: 10.1016/j.cherd.2016.02.018.

216 J. Kazmierczak-Razna and R. Pietrzak, *Adsorption*, 2016, **22**, 473–480.

217 H. W. Ou, M. L. Fang, M. S. Chou and H. Y. Chang, *J. Air Waste Manage. Assoc.*, 2020, **70**(6), 641–648.

218 G. Shang, G. Shen, L. Liu, Q. Chen and Z. Xu, *Bioresour. Technol.*, 2013, **133**, 495–499.

219 W. Shen, Z. Li and Y. Liu, *Recent Patents Chem. Eng.*, 2010, **1**, 27–40.

220 A. B. Bajaj, H. Jo, S. M. Jo, J. H. Park, K. B. Yi and S. Lee, *Appl. Surf. Sci.*, 2018, 253–257, DOI: 10.1016/j.apsusc.2017.06.280.

221 C. Yang, M. Florent, G. De Falco, H. Fan and T. J. Bandosz, *Chem. Eng. J.*, 2020, **394**, 124906.

222 B. Liu and S. Zuo, *Environ. Prog. Sustain. Energy*, 2022, **41**, e13781.

223 N. M. Nor, L. L. Chung, L. K. Teong and A. R. Mohamed, *Biochem. Pharmacol.*, 2013, **1**, 658–666.

224 A. P. Alekhin, G. M. Boleiko, S. A. Gudkova, A. M. Markeev, A. A. Sigarev, V. F. Toknova, A. G. Kirilenko, R. V Lapshin, E. N. Kozlov and D. V. Tetyukhin, *Nanotechnol. Russ.*, 2010, **5**, 696–708.

225 H. Sawalha, M. Maghalseh, J. Qutaina, K. Junaidi and R. Rene, *Bioengineered*, 2020, **11**, 607–618.

226 Y. Yuan, L. Huang, T. C. Zhang, L. Ouyang and S. Yuan, *Sep. Purif. Technol.*, 2021, **279**, 119686.

227 I. Tole, K. Habermehl-Cwirzen and A. Cwirzen, *Mineral. Petrol.*, 2019, **113**, 449–462.

228 H. Nam, S. Wang and H.-R. Jeong, *Fuel*, 2018, **213**, 186–194.

229 S. Wang, H. Nam and H. Nam, *Environ. Prog. Sustain. Energy*, 2019, **38**, e13241.

230 R. Sitthikhankaew, C. David, A. Suttichai and N. and Laosiripojana, *Sep. Sci. Technol.*, 2014, **49**, 354–366.

231 D. Langhammer, J. Kullgren and L. Österlund, *ACS Catal.*, 2022, **12**, 10472–10481.

232 S. Gyawali, R. T. A. Tirumala, M. Andiappan and A. D. Bristow, *Proc. SPIE*, 2024, **12884**, 128840F.

233 H. J. Choi, S. H. Kwon, W. S. Lee, K. G. Im, T. H. Kim, B. R. Noh, S. Park, S. Oh and K. K. Kim, *Nanomaterials*, 2020, 462, DOI: 10.3390/nano10030462.

234 T. Li, Y. Wu, G. Zhang, C. Guo, X. Zhang, B. Li, X. Zhou, M. Zheng, Y. Xu, S. Gao and L. Huo, *Sens. Actuators, B*, 2024, **399**, 134820.

235 B. Levasseur, C. Petit and T. J. Bandosz, *ACS Appl. Mater. Interfaces*, 2010, **2**, 3606–3613.

236 M. Sun, A. Hanif, T. Wang, Q. Gu and J. Shang, *Sep. Purif. Technol.*, 2023, **314**, 123563.

237 R. Pietrzak, *Energy Fuels*, 2009, **23**, 3617–3624.

238 P. Nowicki, H. Wachowska and R. Pietrzak, *J. Hazard. Mater.*, 2010, **181**, 1088–1094.

239 P. Nowicki, R. Pietrzak and H. Wachowska, *Catal. Today*, 2010, **150**, 107–114.

240 R. Pietrzak, *Bioresour. Technol.*, 2010, **101**, 907–913.

241 P. Nowicki, P. Skibiszewska and R. Pietrzak, *Adsorption*, 2013, **19**, 521–528.

242 S. Bashkova and T. J. Bandosz, *J. Colloid Interface Sci.*, 2009, **333**, 97–103.

243 R. Pietrzak and T. J. Bandosz, *Carbon*, 2007, **45**, 2537–2546.

244 M. Jeguirim, V. Tschamber, J. F. Brilhac and P. Ehrburger, *J. Anal. Appl. Pyrolysis*, 2004, **72**, 171–181.

245 M. Belhachemi, M. Jeguirim, L. Limousy and F. Addoun, *Chem. Eng. J.*, 2014, **253**, 121–129.

246 I. Ghouma, M. Jeguirim, U. Sager, L. Limousy, S. Bennici, E. Däuber, C. Asbach, R. Ligotski, F. Schmidt and A. Ouederni, *Energies*, 2017, 1508, DOI: 10.3390/en10101508.

247 B. Levasseur, E. Gonzalez-Lopez, J. A. Rossin and T. J. Bandosz, *Langmuir*, 2011, **27**, 5354–5365.

248 T. Cheng, Y. Bian, J. Li, X. Ma, L. Yang, L. Zhou and H. Wu, *Fuel*, 2023, **334**, 126452.

249 C. He, J. Cheng, X. Zhang, M. Douthwaite, S. Pattisson and Z. Hao, *Chem. Rev.*, 2019, **119**, 4471–4568.

250 H. Gao, X. Lv, M. Zhang, Q. Li, J. Chen, Z. Hu and H. Jia, *Chem. Eng. J.*, 2022, **434**, 134618.

251 H. Wang, J. Gao, X. Xu, B. Liu, L. Yu, Y. Ren, R. Shi, Z. Zeng and L. Li, *Chem.–Asian J.*, 2021, **16**, 1118–1129.

252 S. A. Halawy, A. I. Osman, N. Mehta, A. Abdelkader, D.-V. N. Vo and D. W. Rooney, *Chemosphere*, 2022, **295**, 133795.

253 X. Ma, H. Lv, L. Yang, Z. Zhang, Z. Sun and H. Wu, *J. Hazard. Mater.*, 2021, **405**, 124193.

254 J. Zhang, J. Shao, X. Zhang, G. Rao, G. Li, H. Yang, S. Zhang and H. Chen, *Chem. Eng. J.*, 2023, **452**, 139003.

255 A. Khan, J. E. Szulejko, P. Samaddar, K.-H. Kim, B. Liu, H. A. Maitlo, X. Yang and Y. S. Ok, *Chem. Eng. J.*, 2019, **361**, 1576–1585.

256 X. Zhang, B. Gao, J. Fang, W. Zou, L. Dong, C. Cao, J. Zhang, Y. Li and H. Wang, *Chemosphere*, 2019, **218**, 680–686.

257 X. Zhang, W. Xiang, B. Wang, J. Fang, W. Zou, F. He, Y. Li, D. C. W. Tsang, Y. S. Ok and B. Gao, *Chemosphere*, 2020, **245**, 125664.

258 H. Rajabi, M. H. Mosleh, P. Mandal, A. Lea-Langton and M. Sedighi, *Chemosphere*, 2021, **268**, 129310.

259 X. Zhang, B. Gao, Y. Zheng, X. Hu, A. E. Creamer, M. D. Annable and Y. Li, *Bioresour. Technol.*, 2017, **245**, 606–614.

260 W. Xiang, X. Zhang, K. Chen, J. Fang, F. He, X. Hu, D. C. W. Tsang, Y. S. Ok and B. Gao, *Chem. Eng. J.*, 2020, **385**, 123842.

261 A. Kumar, E. Singh, A. Khapre, N. Bordoloi and S. Kumar, *Bioresour. Technol.*, 2020, **297**, 122469.

262 Y. Shen and N. Zhang, *Bioresour. Technol.*, 2019, **282**, 294–300.

263 N. R. Abdul Manap, R. Shamsudin, M. N. Maghpor, M. A. Abdul Hamid and A. Jalar, *J. Environ. Chem. Eng.*, 2018, **6**, 970–983.

264 H. Rajabi, M. Hadi Mosleh, T. Prakoso, N. Ghaemi, P. Mandal, A. Lea-Langton and M. Sedighi, *Chemosphere*, 2021, **283**, 131288.

265 X. Zhang, X. Miao, W. Xiang, J. Zhang, C. Cao, H. Wang, X. Hu and B. Gao, *J. Hazard. Mater.*, 2021, **403**, 123540.

266 X. Zhao, X. Zeng, Y. Qin, X. Li, T. Zhu and X. Tang, *Chemosphere*, 2018, **206**, 285–292.

267 Z. Jin, B. Wang, L. Ma, P. Fu, L. Xie, X. Jiang and W. Jiang, *Chem. Eng. J.*, 2020, **385**, 123843.

268 Y. Guo, Y. Li, J. Wang, T. Zhu and M. Ye, *Chem. Eng. J.*, 2014, **236**, 506–512.

269 M. A. Lillo-Ródenas, D. Cazorla-Amorós and A. Linares-Solano, *Carbon*, 2005, **43**, 1758–1767.

270 T. Garcıa, R. Murillo, D. Cazorla-Amoros, A. M. Mastral and A. Linares-Solano, *Carbon*, 2004, **42**, 1683–1689.

271 S. Haydar, M. A. Ferro-Garcıa, J. Rivera-Utrilla and J. P. Joly, *Carbon*, 2003, **41**, 387–395.

272 eR. R. Gil, B. Ruiz, M. S. Lozano, M. J. Martín and E. Fuente, *Chem. Eng. J.*, 2014, **245**, 80–88.

273 C. Wen, T. Liu, D. Wang, Y. Wang, H. Chen, G. Luo, Z. Zhou, C. Li and M. Xu, *Prog. Energy Combust. Sci.*, 2023, **99**, 101098.

274 Z. Li, Y. Li, J. Zhu, Z. Li, Y. Li and J. Zhu, *Materials*, 2021, 3284, DOI: 10.3390/ma14123284.

275 X. Ma, B. Liu, M. Che, Q. Wu, R. Chen, C. Su, X. Xu, Z. Zeng and L. Li, *Sep. Purif. Technol.*, 2021, **269**, 118690.

276 K.-J. Kim, C.-S. Kang, Y.-J. You, M.-C. Chung, M.-W. Woo, W.-J. Jeong, N.-C. Park and H.-G. Ahn, *Catal. Today*, 2006, **111**, 223–228.

277 X. Shen, R. Ou, Y. Lu, A. Yuan, J. Liu, X. Hu, Z. Yang and F. Yang, *ChemistrySelect*, 2020, **5**, 9162–9169.

278 L. Li, S. Liu and J. Liu, *J. Hazard. Mater.*, 2011, **192**, 683–690.

279 K. Zhou, L. Li, X. Ma, Y. Mo, R. Chen, H. Li and H. Li, *RSC Adv.*, 2018, **8**, 2922–2932.

280 J. L. Figueiredo, M. F. R. Pereira, M. M. A. Freitas and J. J. M. Órfão, *Carbon*, 1999, **37**, 1379–1389.

281 W. Shen, Z. Li and Y. Liu, *Recent Patents Chem. Eng.*, 2008, **1**, 27–40.

282 X. Yu, S. Liu, G. Lin, X. Zhu, S. Zhang, R. Qu, C. Zheng and X. Gao, *RSC Adv.*, 2018, **8**, 21541–21550.

283 J. Choma, B. Szczęśniak, A. Kapusta and M. Jaroniec, *Molecules*, 2024, **29**, 5677.

284 S. Sumathi, S. Bhatia, K. T. Lee and A. R. Mohamed, *Sci. China, Ser. E: Technol. Sci.*, 2009, 198–203, DOI: 10.1007/s11431-009-0031-6.

285 S. Sumathi, S. Bhatia, K. T. Lee and A. R. Mohamed, *Chem. Eng. J.*, 2010, **162**, 51–57.

286 C. Zhu, Y. Duan, C.-Y. Wu, Q. Zhou, M. She, T. Yao and J. Zhang, *Fuel*, 2016, **172**, 160–169.

287 S. A. Opatokun, A. Prabhu, A. Al Shoaibi, C. Srinivasakannan and V. Strezov, *Chemosphere*, 2017, **168**, 326–332.

288 L. Gao, C. Li, J. Zhang, X. Du, S. Li, J. Zeng, Y. Yi and G. Zeng, *Chem. Eng. J.*, 2018, **342**, 339–349.

289 Y. Yi, C. Li, L. Zhao, X. Du, L. Gao, J. Chen, Y. Zhai and G. Zeng, *Environ. Sci. Pollut. Res.*, 2018, **25**, 4761–4775.

290 Y. Qin, C. Wang, X. Sun, Y. Ma, X. Song, F. Wang, K. Li and P. Ning, *Fuel*, 2021, **293**, 120391.

291 X. Zhang, K. Ren, Y. Wang, B. Shen, F. Shen and Y. Shang, *Energy Fuels*, 2021, **35**, 15969–15977.

292 A. A. Abdulrasheed, A. A. Jalil, S. Triwahyono, M. A. A. Zaini, Y. Gambo and M. Ibrahim, *Renew. Sustain. Energy Rev.*, 2018, **94**, 1067–1085.

293 G. Li, B. Shen, Y. Li, B. Zhao, F. Wang, C. He, Y. Wang and M. Zhang, *J. Hazard. Mater.*, 2015, **298**, 162–169.

294 H. Li, J. Zhang, Y. Cao, C. Liu, F. Li, Y. Song, J. Hu and Y. Wang, *Fuel Process. Technol.*, 2020, **207**, 106478.

295 S. Sumathi, S. Bhatia, K. T. Lee and A. R. Mohamed, *Energy Fuel.*, 2010, **24**, 427–431.

296 S. Wang, H. Nam, T. B. Gebreegziabher and H. Nam, *Eng. Rep.*, 2020, **2**, e12083.

297 A. S. González, M. G. Plaza, F. Rubiera and C. Pevida, *Chem. Eng. J.*, 2013, **230**, 456–465.

298 E. Atanes, A. Nieto-Márquez, A. Cambra, M. C. Ruiz-Pérez and F. Fernández-Martínez, *Chem. Eng. J.*, 2012, **211**, 60–67.

299 F. L. Braghiroli, H. Bouafif and A. Koubaa, *Ind. Crops Prod.*, 2019, **138**, 111456.

300 N. Iberahim, S. Sethupathi, C. L. Goh, M. J. K. Bashir and W. Ahmad, *J. Environ. Manage.*, 2019, **248**, 109302.

301 N. Iberahim, S. Sethupathi, M. J. K. Bashir, R. Kanthasamy and T. Ahmad, *Sci. Total Environ.*, 2022, **805**, 150421.

302 M. G. Plaza, A. S. González, J. J. Pis, F. Rubiera and C. Pevida, *Appl. Energy*, 2014, **114**, 551–562.

303 M.-V. Nguyen and B.-K. Lee, *Process Saf. Environ. Prot.*, 2016, **104**, 490–498.

304 W. Hao, E. Björkman, M. Lilliestråle and N. Hedin, *Appl. Energy*, 2013, **112**, 526–532.

305 H. Wei, S. Deng, B. Hu, Z. Chen, B. Wang, J. Huang and G. Yu, *ChemSusChem*, 2012, **5**, 2354–2360.

306 P. Murge, S. Dinda and S. Roy, *Energy Fuel.*, 2018, **32**, 10786–10795.

307 A. E. Creamer, B. Gao and S. Wang, *Chem. Eng. J.*, 2016, **283**, 826–832.

308 W. Gao, T. Zhou and Q. Wang, *Chem. Eng. J.*, 2018, **336**, 710–720.

309 C. Chen, J. Kim, D.-A. Yang and W.-S. Ahn, *Chem. Eng. J.*, 2011, **168**, 1134–1139.

310 M. Kandiah, M. H. Nilsen, S. Usseglio, S. Jakobsen, U. Olsbye, M. Tilset, C. Larabi, E. A. Quadrelli, F. Bonino and K. P. Lillerud, *Chem. Mater.*, 2010, **22**, 6632–6640.

311 S. Xiang, Y. He, Z. Zhang, H. Wu, W. Zhou, R. Krishna and B. Chen, *Nat. Commun.*, 2012, 954, DOI: **10.1038/ncomms1956**.

312 H.-J. Kim and J.-H. Lee, *Sens. Actuators, B*, 2014, **192**, 607–627.

313 A. Mirzaei, S. G. Leonardi and G. Neri, *Ceram. Int.*, 2016, **42**, 15119–15141.

314 D. M. D'Alessandro, B. Smit and J. R. Long, *Angew. Chem. Int. Ed.*, 2010, **49**, 6058–6082.

315 D. Jiang, H. Li, S. Wang, X. Cheng, P. Bartocci and F. Fantozzi, *Fuel*, 2023, 125948, DOI: **10.1016/j.fuel.2022.125948**.

316 M. Rahimi, M. H. Abbaspour-Fard, A. Rohani, O. Yuksel Orhan and X. Li, *Ind. Eng. Chem. Res.*, 2022, **61**, 10670–10688.

317 R. Rahamathullah, D. S. Zakaria, S. K. M. Rozi, H. N. A. Halim, F. I. A. Razak and S. Sapari, *Biomass Convers. Biorefin.*, 2024, 1–13, DOI: **10.1007/s13399-024-05343-5**.

318 M. Ahmadi, F. Bahmanzadegan, M. Qasemnazhand, A. Ghaemi and H. Ramezanipour Penchah, *Sci. Rep.*, 2024, 13595, DOI: **10.1038/s41598-024-64503-9**.

319 C. S. Allen, F. Ghamouss, O. Boujibar and P. J. F. Harris, *Proc. R. Soc. A Math. Phys. Eng. Sci.*, 2022, **478**, 20210580.

320 M. Qasemnazhand, F. Khoeini and M. Badakhshan, *Mater. Today Chem.*, 2023, **28**, 101383.

321 L. Deng, J. Shi, Y. Zhao, D. Feng, W. Zhang, Y. Yu and S. Sun, *Chem. Eng. J.*, 2024, 153403, DOI: **10.1016/j.cej.2024.153403**.

322 M. Su, W. Peng, Z. Ding, Y. Zhou, H. Gao, Q. Jiang and C. Yu, *Bioelectrochemistry*, 2024, **160**, 108776.

323 X. Yang, D. Jiang, X. Cheng, C. Yuan, S. Wang, Z. He and S. Esakkimuthu, *Biomass Bioenergy*, 2022, 106519, DOI: **10.1016/j.biombioe.2022.106519**.

324 F. Raganati, F. Miccio and P. Ammendola, *Energy Fuel.*, 2021, **35**, 12845–12868.

325 W. Yang, Z. Wang and Y. Liu, *Energy Fuels*, 2020, **34**, 13473–13490.